NASA Technical Paper 1512

Application of the Concept of Dynamic Trim Control to Automatic Landing of Carrier Aircraft

G. Allan Smith and George Meyer

APRIL 1980

NASA

NASA Technical Paper 1512

Application of the Concept of Dynamic Trim Control to Automatic Landing of Carrier Aircraft

G. Allan Smith and George Meyer
Ames Research Center
Moffett Field, California

NOMENCLATURE

A_{as_c} smooth-commanded direction cosine rotation matrix from space axes to aircraft axes

$A_{as_{rc}}$ rough-commanded direction cosine rotation matrix from space axes to aircraft axes

$\hat{A}_{as}$ measured direction cosine rotation matrix from space axes to aircraft axes

C_{D_c} commanded drag coefficient

$\bar{C}_{D_c}$ commanded drag coefficient before limiting

C_{L_c} commanded lift coefficient

$\bar{C}_{L_c}$ commanded lift coefficient before limiting

C_{ℓ_c} commanded rolling-moment coefficient

C_{m_c} commanded pitching-moment coefficient

C_{n_c} commanded yawing-moment coefficient

C_{T_c} commanded thrust coefficient

f_{cc} closed-loop commanded specific force vector

f_{oc} open-loop commanded specific force vector

f_{tc} total commanded specific force vector

$\bar{q}$ dynamic pressure

R_c smooth-commanded aircraft position vector

$\hat{R}$ measured aircraft position vector

T time from start of simulation run

V_c smooth-commanded aircraft velocity vector

$\dot{V}_c$ total commanded aircraft acceleration vector

$\hat{V}$ measured aircraft velocity vector

α_c commanded angle of attack

Γ_c commanded vertical flightpath angle

ϕ_c commanded roll angle

ψ_c commanded horizontal flightpath angle

$\hat{\omega}$ measured aircraft angular velocity vector

ω_c smooth-commanded aircraft angular velocity vector

$\dot{\omega}_c$ total commanded aircraft angular acceleration vector

$\dot{\omega}_{oc}$ open-loop commanded aircraft angular acceleration vector

$\dot{\omega}_{cc}$ closed-loop commanded aircraft angular acceleration vector

Acronym

TAFCOS total aircraft flight-control system

APPLICATION OF THE CONCEPT OF DYNAMIC TRIM CONTROL

TO AUTOMATIC LANDING OF CARRIER AIRCRAFT

G. Allan Smith and George Meyer

Ames Research Center

SUMMARY

The availability of the airborne digital computer has made possible the practical implementation of the concept of a balanced feed-forward and feedback automatic aircraft flightpath-control system. The concept is explained and simulation results are presented. The essential nonlinear force and moment characteristics of the aircraft are collected in tabular form as dynamic trim maps and inverted to give a feed-forward command signal path which, in series with the actual aircraft, provides essentially an identity transfer function. With perfect modeling and no disturbances this would provide perfect trajectory control. Feedback loops are closed around this linear path to compensate for disturbances and imperfect modeling. Simulation results and a flight test have shown that only a small fraction of the total drive signal is required from the feedback while the major portion is provided by the feed-forward control.

This concept has several advantages. It allows a straightforward design for aircraft with highly nonlinear characteristics since conventional linear techniques can be employed to design the feedback loops around the linearized feed-forward path. The use of the complete aircraft characteristics in the feed-forward path allows an integrated design so that total aerodynamic and propulsive forces and moments are combined in a natural way and aid, rather than partially offset, each other as often occurs in conventional designs. The explicit aircraft aerodynamic characteristics available in the feed-forward signal path allow direct limiting of commanded angle of attack and various accelerations and rates so that a smooth executable trajectory is commanded regardless of excessive or inadvertent commands from an air-traffic-control system or other input. Required digital computer speed and memory is substantially less than that required for conventional designs of comparable capability.

Simulation results are presented for an application to automatic landing on an aircraft carrier.

INTRODUCTION

Precise flightpath control is required over the approach trajectory to land an aircraft on an aircraft carrier in heavy seas. The touchdown point is restricted to a small area on a deck that is pitching and heaving due to wave action. Furthermore, the flightpath is continually disturbed by severe atmospheric turbulence generated in part by the carrier superstructure. Landing

the aircraft is particularly difficult at night and is generally acknowledged to be the most difficult piloting task encountered in routine operations.

In an attempt to improve landing performance, the Navy has developed an automatic carrier-landing system. The system is based on a conventional autopilot that is controlled by attitude signals sent by radio link from the carrier and generated from path errors determined by a carrier-based radar. Although the system is operational for a few types of aircraft, it has performance deficiencies in strong turbulence and significant touchdown point dispersion. The alternative automatic-control-system design concept presented in this report has shown potential for improving landing performance.

This new design concept was developed at Ames Research Center over the past 4 years. The theoretical basis for the system is presented in reference 1. This report will explain the system structure developed to apply the concept to the carrier-landing problem and present results of simulation studies of an automatic carrier-landing system based on the new principles.

The concept provides for control of the aircraft trajectory directly by commanding the aerodynamic and propulsive forces required rather than by a conventional autopilot that commands aircraft attitude to minimize trajectory errors. In addition, the dynamic trim concept allows a single configuration to function over the complete flight envelope without the gain scheduling or configuration switching that is used in conventional systems based on perturbations about a number of different static trim points. The concept is termed a "total aircraft flight-control system," or TAFCOS. TAFCOS is essentially an open-loop, feed-forward system that commands the proper instantaneous thrust, angle of attack, and roll angle dynamic trim conditions to achieve the forces required to follow the desired trajectory. The dynamic trim conditions are determined by an inversion of the aircraft nonlinear force characteristics to calculate the required angle of attack and throttle setting, while the commanded roll angle is determined from the required normal and lateral force coefficients. The angle of attack is combined with roll angle and flightpath angles to give the commanded attitude. This feed-forward design is completed by inversion of the aircraft nonlinear moment characteristics to determine the control surface angles.

The concept of open-loop control for a completely calibrated system can provide any desired response that is within the physical capability of the system. On the other hand, the value of feedback to deal with uncalibrated systems or systems with uncertainties and disturbances is well established. Therefore the basic open-loop design of TAFCOS is supplemented by feedback loops that compensate for lack of knowledge of the aircraft characteristics and for imperfect wind estimation, and provide control in the presence of disturbances. TAFCOS is a balanced system that employs an open-loop controller with as much a priori information as feasible about the aircraft force and moment characteristics; it uses feedback to provide tight control in the face of limited knowledge of plant characteristics, measurement inaccuracies, and disturbance inputs.

Advances in avionics technology have produced airborne digital computers of the type needed to carry out the calculations required for TAFCOS.

2

Extensive two-dimensional tables of the aircraft force and moment characteristics are used for the inversion calculations, and numerous matrix multiplications are required to transform the force and moment vectors between various coordinate systems. Computational feasibility of the concept has recently been demonstrated by a successful flight test of TAFCOS in a STOL aircraft (ref. 2). A Sperry 1819A airborne digital computer was used. Only a small portion of the computer capacity was required.

During the past 3 years several simulations of the current operational Navy automatic carrier-landing system have been carried out on the piloted simulators at Ames Research Center. They were conducted jointly by Ames Research Center, the Naval Air Test Center, and the Naval Air Development Center to investigate pilot acceptance of various system modifications designed to improve touchdown point dispersion under turbulent conditions (ref. 3). The same computer simulation model of the A-7E aircraft used by the Navy for these simulations was used to represent the aircraft in the TAFCOS simulations that are the subject of this report. The model includes the nonlinear aerodynamic force and moment equations and nonlinear effects of the engine, including hysteresis in the throttle actuator.

The simulations presented here were carried out to demonstrate that the TAFCOS concept provides substantially improved performance for the carrier landing task. The results are presented in four sections to show the critical responses that must be examined to evaluate automatic control-system performance. The first results show all the important variables for a tip-over and landing maneuver without atmospheric turbulence. This allows the attitude and thrust control interaction to be clearly observed and establishes a performance reference for the task of tracking the moving deck. The next results show the performance for a landing with atmospheric turbulence.

The quality of an automatic control system is established by both its ability to regulate to a reference flightpath in the presence of input disturbances and to respond to maneuver commands. Therefore, the final two sections of results show the system response to a series of severe gust inputs and response to a sequence of maneuver commands that include altitude changes and lateral flightpath control.

AUTOMATIC CARRIER-LANDING TASK

The automatic carrier-landing situation is illustrated in figure 1. The carrier normally heads into the wind at a speed such that the relative wind is parallel to the deck at about 30 knots. The aircraft is first directed to a marshall point or to a holding pattern. Individual aircraft are then cleared to the approach course at 2-min intervals. For the A-7E aircraft considered in this simulation study, the aircraft is commanded to hold a steady velocity, with respect to the wind of 129 knots, which is 99 knots with respect to the carrier.

For this simulation a level-approach course is commanded at an elevation of 152.4 m (500 ft) above the carrier-deck reference until a 3.5° glide slope

3

to the ideal touchdown point is intercepted. The ideal touchdown point is located 70 m (230 ft) aft of the carrier center of pitch. The aircraft must touch down within ±18.3 m (±60 ft) longitudinally and ±4.6 m (±15 ft) laterally of that point.

The carrier is equipped with a tracking radar that determines the aircraft position with respect to the carrier. A shipboard inertial platform measures the instantaneous elevation of the ideal touchdown point due to deck pitch and heave with respect to the undisturbed carrier deck reference position. As shown in figure 1, after tip-over, the aircraft is commanded to descend on the glide slope until 12 sec before touchdown. At that time the aircraft is commanded to follow the instantaneous displaced position of the touchdown point.

An approach that misses the required touchdown area or an arresting wire is termed a bolter and the aircraft is commanded to follow a recovery path back to the reference altitude of 152.4 m (500 ft) before making another attempt.

The most critical portion of the landing sequence is the final 12 sec, during which time the aircraft is commanded to follow the instantaneous vertical position of the touchdown point. For this simulation, the deck motion was taken as the sum of two sinusoidal displacements due to heave and pitch, the former at a frequency of 0.1 Hz and an amplitude of ±1.2 m (±4 ft), and the latter at a frequency of 0.096 Hz and an amplitude of ±1°, which is ±1.2 m (±4 ft) vertical displacement at the 70.1-m (230-ft) distance from the center of pitch. This can produce a maximum touchdown point excursion of ±2.4 m (±8 ft). Also, during the final portion of the run, strong atmospheric turbulence, called burble, is encountered in the carrier wake. This turbulence is caused by the interaction of the carrier superstructure with the wind; it was modeled as a combination of vertical and horizontal gust patterns in time and space as a function of carrier deck attitude plus random superimposed turbulence. Peak total turbulence was about ±1.8 m/sec (±6 ft/sec).

The primary concern in this simulation was to investigate aircraft landing-point dispersion due to the effects of pitch and heave deck motion and atmospheric turbulence. Therefore, 160 landing simulation runs were made with various random turbulence patterns and with different deck motion component phases at touchdown.

It should be noted that a carrier landing is accomplished by flying a direct path to the deck without any landing flare.

For the currently operational Navy automatic carrier-landing system the aircraft is under manual control during a holding pattern, or after a missed approach during wave-off. However, TAFCOS has the potential for automatic control during such situations, so simulation runs were made of additional trajectories that incorporated lateral maneuvers, altitude changes, and severe gusts. These runs included maneuver commands and disturbances that illustrate the system response over a much wider flight envelope than the conventional carrier approach path.

An important part of any automatic trajectory-control system is the instrumentation required to measure the aircraft position with respect to the commanded trajectory. The current Navy system uses a ship-mounted tracking radar in conjunction with a beacon transponder on the aircraft. Such a system was therefore simulated for TAFCOS; it included the usual loss of radar information when the aircraft is within about 150 m (492 ft) of touchdown. Of course, TAFCOS receives the radar position information by data link from the carrier and processes it in the airborne digital computer. This is in contrast to the operational system, which processes the radar data in a shipborne computer and sends aircraft attitude commands to the approaching vehicle. The radar position and the velocity and acceleration data used by TAFCOS were corrupted by appropriate noise inputs.

AUTOMATIC CONTROL SYSTEM

The command structure of TAFCOS is entirely different from that of a conventional control system. It employs dynamic trim maps which represent an inversion of the nonlinear six-degree-of-freedom equations of the aircraft. The trim maps take the form of extensive two-dimensional tables of force and moment data. They represent a calibration of the aircraft so that trajectory commands can be processed in an open-loop fashion to yield surface and thrust controls. Closed-loop state feedback is employed to balance trim map inaccuracies and measurement uncertainties.

Figures 2 and 3 will be used to describe the configuration and functions of TAFCOS. They illustrate the signal flow paths that will be traced to show what operations are carried out by the system. The details of how these operations are accomplished are presented in appendix A. Many of the quantities in figures 2 and 3 are vectors which, for calculation, are resolved into components in appropriate coordinate systems. For example, the trajectory is presented in an inertial frame, the major aerodynamic forces act in a frame determined by the aircraft velocity with respect to the air mass, and the aircraft control surfaces and engine thrust are expressed in an aircraft body reference frame. Therefore, a characteristic of TAFCOS is the repeated resolution of forces, moments, accelerations, velocities, and positions from one reference frame to another using matrix transformation methods. Figure 2 illustrates only the open-loop elements and does not include the closed-loop feedback employed in the complete system. Figure 2 will be used for a brief explanation of the fundamental concept of TAFCOS without consideration of many secondary, although important, details that are treated more completely in the discussion of figure 3 and in appendix A.

The desired trajectory in figure 2 enters the system as a series of straight, circular, or helical arc geometric segments described by their length, orientation, and airspeed. Angles of climb or descent for all segments, radii, and arc lengths for circular and helical sections are given. From this geometric-data input the trajectory command sequencer produces a consistent commanded dynamic sequence of trajectory position, velocity, and acceleration vectors in inertial space coordinates. These dynamic commands

are rough in the sense that they may require instantaneous changes in velocity, direction, and, sometimes, position at the segment junctions. The trajectory is defined in space relative to the carrier and at a commanded airspeed.

The trajectory command generator smooths and limits these rough commands to be consistent with the desired aircraft response. The trajectory command generator also performs a coordinate system rotation so that the desired trajectory commands in inertial space axes are transformed to relative wind velocity axes. The output vector $\dot{V}_c$ is a smooth executable commanded acceleration. Smooth-commanded velocity components are combined with estimated steady wind to calculate commanded flightpath angles, Γ_c and ψ_c.

In the coefficient development section, $\dot{V}_c$ is multiplied by aircraft mass to give the force required to carry out the desired trajectory. The force is then divided by dynamic pressure and wing area to give the total lift and drag coefficients. These total commanded coefficients, which include engine thrust forces as well as aerodynamic forces, are sent to the force trim map. Furthermore, the ratio of the lateral to the normal commanded force coefficient gives the tangent of the commanded roll angle ϕ_c. Figure 4 is a graphical representation of the force trim map which is seen to be a series of lift drag polars for the aircraft, shifted by the effect of engine thrust as indicated by the thrust coefficient C_{T_c}. Inputs to the trim map are the commanded lift and drag coefficients C_{L_c} and C_{D_c}. The trim map outputs are the corresponding commanded angle of attack α_c and thrust coefficient C_{T_c} calculated by the digital computer, which carries out an interpolation of the trim-map data stored in tabular form. This is a dynamic trim map in the sense that angle of attack and thrust are calculated for any vector acceleration, not just for a conventional trimmed flightpath. A very convenient feature of the trim map is the ease with which it allows commands to be limited to selected values of α_c and C_{T_c}. For this simulation, commanded angle of attack was limited to between $-2°$ and $+16°$ and commanded thrust coefficient to between 0.01 and 0.7. This permits commands over almost the entire flight envelope but prevents commands that approach stall conditions. The effect of this limiting is clearly seen in figure 8(e) of the results.

In figure 2, one output of the trim map, commanded thrust coefficient, C_{T_c}, is converted to commanded thrust and sent to an engine thrust table where the digital computer performs an inverse interpolation to calculate the commanded throttle angle. The other output of the trim map, commanded angle of attack α_c, is combined with commanded roll angle and horizontal and vertical flightpath angles to give the commanded aircraft attitude.

A procedure generally similar to that followed in the trajectory portion of the system is then employed in the attitude control section. The attitude command generator provides a smooth executable angular acceleration vector command $\dot{\omega}_c$. This angular acceleration vector is multiplied by the aircraft inertia matrix to give the torques required to carry out the desired attitude variations. These torques are then expressed in terms of moment coefficients. The moment trim map in figure 2 inverts the aircraft torque equations to yield the control surface angles needed to generate the commanded angular acceleration vector.

6

When the basic feed-forward control of figure 2 is implemented with reasonably accurate trim maps, the aircraft follows the commanded acceleration $\dot{V}_c$ quite well. The output response is essentially linearly proportional to the input command. Thus, it can be considered to be a linear acceleration command system and linear theory can be used to select the feedback gains used for the actual complete control system (ref. 4).

The basic open-loop concept of figure 2 is augmented in the complete TAFCOS configuration by the addition of feedback loops as shown in figure 3. Figure 3 shows the underlying structure of figure 2 with additional symbolism as well as the closed-loop position and attitude feedback. Only the new additions and certain details previously ignored will be discussed in connection with figure 3.

The commanded acceleration $\dot{V}_c$ in figure 2 includes a component to balance the acceleration of gravity so it is more accurately a specific force or the total force per unit mass required to follow the trajectory under the influence of gravity. The symbol f_{tc} is therefore introduced to indicate commanded specific force in figure 3.

In the trajectory regulator of figure 3 the smooth commanded position R_c is compared with the measured position $\hat{R}$ and the smooth commanded velocity V_c is compared with the measured velocity $\hat{V}$. The resulting error signals are combined with appropriate gains and limits to give a closed-loop specific force command f_{cc}. This perturbation command from the trajectory regulator is added to the open-loop command f_{oc} to form the total specific force command f_{tc}. For most maneuvers, f_{cc} is only about 20% of f_{oc}. This means that the major burden of control is borne by the open loop.

The trajectory command generator and the trajectory regulator are the principal parts of the system where gain and limit adjustments are made to achieve satisfactory performance, which is characterized by smooth and accurate response to trajectory commands, properly coordinated and suitably limited control-surface and engine-thrust responses to disturbance inputs, and well-executed capture of the initial trajectory and transition between trajectory segments.

As previously noted, the force trim map for this application expresses the lift and drag coefficients as functions of angle of attack and thrust. For a different application, a three-dimensional trim map was developed with flap angle as a third parameter and a three-parameter interpolation routine was used in the airborne digital computer (ref. 5). For attitude commands, TAFCOS manipulates angles by constructing the corresponding direction cosine matrices that represent the angular rotation about the appropriate axis (ref. 6). The required angle of attack α_c and roll angle ϕ_c are combined with commanded flightpath angles Γ_c and ψ_c by multiplication of their direction cosine matrices to give the rough commanded aircraft attitude matrix $A_{as_{rc}}$ which serves as the input to the attitude command generator. The attitude command generator provides a smooth commanded attitude matrix A_{as_c}, a smooth commanded angular velocity vector ω_c, and a smooth commanded open-loop angular acceleration vector $\dot{\omega}_{oc}$. The attitude regulator compares the commanded and measured

attitudes and angular velocities to form error signals which are combined with suitable gains and limits to give a closed-loop perturbation angular acceleration command $\dot{\omega}_{cc}$. This is added to the open-loop command $\dot{\omega}_{oc}$ to give the total angular acceleration command vector $\dot{\omega}_c$.

The moment trim map in figure 3 is functionally similar to the force trim map. It accepts commanded moment coefficients as inputs and provides the commanded control surface positions necessary to achieve the corresponding angular accelerations. These commanded surface deflections are the final output of the airborne digital computer. They are sent to conventional control-surface servos which produce the actual deflections as influenced by servo lags and by surface rate and deflection limits. Additional details of the TAFCOS structure are discussed in appendix A in connection with figure 10 which is a further expansion of figure 3.

In summary, TAFCOS is an aerodynamically oriented computational flight control system that fully incorporates the limitations and nonlinearities of the force and moment characteristics, including the propulsion system, so that it is possible to maintain desired stall margins and limits on attitude response rates and control deflections, and yet exploit the aircraft capabilities over its full practical flight envelope.

SIMULATION RESULTS

Simulation runs were carried out on a general purpose digital computer (IBM 360/67). The results appear as time-history plots of significant variables as measured during the approach to the carrier. Measurements are taken in a right-handed orthogonal coordinate system with origin at the undisturbed center of pitch of the carrier. The carrier is on a straight course with a 30-knot wind over the deck which is aligned with the X axis of the inertial space coordinate system as defined in appendix B. The carrier heave and pitch motions are the same as those used for the Navy simulations mentioned previously; sinusoidal heave and pitch that produce a maximum vertical excursion of the touchdown point of about ±2.4 m (±8 ft).

The results are arranged in four groups. The first group includes figures 5(a-h) which show results for a tip-over and landing with carrier deck motion but no atmospheric turbulence or other disturbances. This portrays the upper bound of performance level, allows a comparison of smooth variables, and illustrates theoretical design considerations.

The second group includes figures 6(a-f) and 7 which show results for a tip-over and landing with carrier deck motion following, atmospheric turbulence, radar noise, and throttle hysteresis to give a realistic simulation. One hundred and sixty of these runs with different disturbance statistics were made to collect data on touchdown dispersion. Results from a typical run are presented in the figures.

The third group includes figures 8(a-f) which show results for a straight and level run with no atmospheric turbulence but with a series of sharp, severe gusts to show how TAFCOS responds to disturbance inputs.

The fourth group includes figures 9(a-f) which show results for a modified racetrack course with large altitude changes. There is no atmospheric turbulence, but a steady 30-knot wind is imposed. These curves show how TAFCOS responds to a range of lateral and vertical commands at a commanded airspeed of 129 knots for a varying wind orientation to the flightpath.

Carrier Approach with No Disturbances

The performance of the A-7E aircraft with the TAFCOS automatic carrier landing system for a simplified standard touchdown run with no atmospheric turbulence is shown in figures 5(a-h). For figures 5(a-e), no hysteresis is included in the throttle actuator, and radar-range information is used all the way to touchdown. Moreover, the phase of the carrier sinusoidal deck motion is such that the touchdown occurs at the peak of touchdown point displacement from its undisturbed position. These runs thus establish the best system performance; they will be compared with other runs that include more realistic operating conditions. The aircraft is moving in the direction of the positive X and Z axes toward the carrier at the origin. Thus the aircraft position coordinates are generally negative in both the X and Z axes.

Figure 5(a) consists of time histories of the trajectory variables in the vertical channel. Tip-over occurs at 8 sec where the actual vertical position and velocity show a very smooth transition. To provide anticipation, the rough position and velocity commands jump from the level-flight trajectory to a glide slope of 3.5°. A section of the initial vertical-position curves, plotted to expanded time and altitude scales, is presented to show how effectively the trajectory command generator smooths the rough-position command. The smooth position, velocity, and acceleration commands are very closely followed by the actual aircraft response. It will be noted that although no rough-commanded vertical acceleration is provided at tip-over, the trajectory command generator does provide a smooth tip-over acceleration command. It is interesting to note that the actual acceleration closely follows the smooth command, except for a slight initial acceleration at tip-over that is in the opposite direction; and is characteristic of the nonminimum phase, right-half plane zeroes of the aircraft transfer function.

Figure 5(b) shows the carrier deck motion and the deck motion following commands that are superimposed on the rough-commanded glide-slope trajectory during the final 12 sec before touchdown. Because these quantities are measured by the ship inertial platform they can be transmitted by radio link to the aircraft until touchdown. It will be noted that these signals are attenuated during the first 2 sec so that they build up slowly to their final values and do not jump abruptly. It will also be observed that touchdown occurs at the peak of carrier motion. One of the most important curves in figure 5(c) is the throttle (power lever angle) which shows, except at tip-over, a very smooth response consistent with the acceleration requirements of the aircraft longitudinal axis. The other variables of figure 5(c) show

satisfactory transient response at tip-over and recovery to steady values before taking on sinusoidal variations during the deck motion following just before touchdown. For this run the aircraft passed over the carrier ramp with a clearance of 5.2 m (17.1 ft) and landed 0.61 cm (0.02 ft) beyond the ideal touchdown point.

TAFCOS performance is illustrated by the various error measurements of figure 5(d). The first six curves show time histories of position, velocity, and acceleration errors in the vertical channel. The rough errors are between actual and rough-commanded quantities; the smooth errors are between actual and smooth commanded quantities. The smooth vertical position error indicates how well the aircraft follows the smoothed command, which is the actual input to the vehicle control system. It will be seen that the aircraft tracking of the smoothed input is extremely good. Maximum smooth position, velocity, and acceleration errors are only 0.15 m (0.5 ft), 0.15 m/sec (0.5 ft/sec), and 0.03 g respectively. On the other hand, rough state errors are much greater as the aircraft cannot perform the step changes at tip-over. These curves emphasize the two problems of trajectory control: first, to provide a smooth command signal that is consistent with aircraft capability, and second to design a control system that can closely follow the smooth command to yield a small error. Figure 5(d) also shows errors in the longitudinal channel which relate generally to the engine thrust curve of figure 5(c).

The curves of figure 5(e) display internal signals to indicate the proportion of feed-forward and feedback signals that make up the input to the trim map. As shown in figure 3, the open-loop feed-forward signal f_{oc} is added to the closed-loop feedback signal f_{cc} to form the specific force-command input to the trim map f_{tc}. These signals, which are in velocity axes appropriate for entry to the trim map, are shown in the curves of figure 5(e). The feed-forward signal f_{oc} has two components: a portion that represents the feed-forward acceleration required to follow the flightpath dynamics and a portion needed to sustain flight in the presence of gravity. The gravity term is the major portion of the feed-forward signal for the vertical axes; it should be noted when considering the relative importance of the feed-forward and feedback signals. Thus, considering only the variation of the signals it is seen that the feed-forward signal is over 90% of the total. The curves of figure 5(e) show that for small maneuvers with no atmospheric turbulence, most of the control is provided by the feed-forward signals. The differences between the trim map and the actual aircraft model show up in the transient activity of the first 6 sec of flight where integrators build up to take care of the bias effects.

Figure 5(f) displays second-order effects that were not included in the landing run of figures 5(a-e). The A-7E model has almost 1° of hysteresis in the throttle actuator, and radar signal information is lost at 150 m (492 ft) before touchdown. These effects were observable only in the thrust and in some of the longitudinal variables. The touchdown error increased only by 20 cm (0.66 ft) when these second-order effects were included.

One other factor that influences touchdown point error is the phase of the deck motion at touchdown. Errors are minimum when the touchdown height is

near maximum or minimum. Figure 5(g) is a summary plot of the data for 16 runs of touchdown error as a function of touchdown phase for the condition of no disturbances. The deck motion phase is seen to produce a substantial touchdown error, because on the 3.5° glide slope an error of 0.3 m (1 ft) vertically results in a horizontal error of 5 m (16 ft).

Because a distinguishing characteristic of TAFCOS is the calculation of the lift and drag coefficients required to follow the trajectory, it is important to compare the commanded coefficients with the values actually achieved. A direct comparison of the time histories of the coefficients may be seen in figure 5(h). The actual lift coefficient follows the commanded coefficient very closely except during the initialization of the first 6 sec and at the start of tip-over, when the characteristic aircraft response starts in the opposite direction. The drag coefficient likewise follows closely except for the abrupt command at tip-over. The variations of commanded lift and drag coefficients in figure 5(h) cover only a small part of the trim map that was shown in figure 4 and from which it can be seen that the corresponding commanded angle of attack varies from 9° to 14° while commanded thrust coefficient varies from 0.04 to 0.23. A much greater area of the trim map is covered during the gust response runs, as displayed in figures 8(d-f).

Carrier Approach with Atmospheric Turbulence

The previous touchdown runs without disturbances are valuable for understanding and analysis of system performance, but in actual service the aircraft must operate in an environment of ship-induced and random atmospheric turbulence. Therefore, a series of 160 simulated landings with disturbances was made to collect statistical data on touchdown dispersion. Performance curves for a representative run are presented in figures 6(a-f), and a summary of touchdown dispersion for the entire series of runs is shown in figure 7 and in table 1. To provide a comparison with the previous Navy simulation tests at Ames Research Center, the same turbulence and other disturbances were used for these TAFCOS simulations. In addition to the usual random wind gusts encountered when flying within a few hundred feet of the ocean, a strong pattern of atmospheric turbulence extends behind the carrier for about 1/2 mile. This atmospheric turbulence, shown in figure 6(e), is generated by the bulk of the carrier, as it moves through the air at speeds approaching 30 knots. A major component of this carrier-wake turbulence or burble is due to the vertical motion of the carrier in response to wave action. This deck motion, which was transmitted to the aircraft for tracking during the final approach, was the same as previously shown in figure 5(b). Throttle hysteresis was included in all of these runs and its effects can be observed in figure 6(b). Radar was inoperative within 150 m (492 ft) of touchdown.

Most of the quantities shown in figures 6(a-f) were also shown for the tip-over run without turbulence in figures 5(a-h). It will be observed that the rough and smooth feed-forward commands (6(a)) are nearly the same as before. As open-loop commands, they are not dependent on the aircraft response to turbulence except through the effect of airspeed. It should be recalled that the basic trajectory commands specify position along the

trajectory at a commanded airspeed. This effect can be observed by noting that the rough-commanded forward velocity relative to the deck in figure 6(a) is no longer constant. The effects of disturbances are evident in the velocity and acceleration curves of figure 6(a) and in the aircraft variables of figure 6(b). Of course, the response to disturbances increases the trajectory errors. It can be seen from figure 6(c) that the smooth error ordinate scales for the vertical channel are two or more times greater than for figure 5(d) and that while the errors in figure 5(d) were only at tip-over and during deck motion following, they occurred throughout the entire run of figure 6(c).

In the presence of turbulence, lateral response of the aircraft becomes significant. As illustrated in figure 6(d), the greatest lateral position and velocity responses occur a few seconds before touchdown when strong burble effects are encountered. The total specific force command f_{tc} used to compute the commanded aerodynamic coefficients contains a component from the closed-loop command f_{cc} which depends on measured position $\hat{R}$ and measured velocity $\hat{V}$; hence, f_{tc} includes the effects of turbulence. The effects of turbulence are evident in the commanded thrust coefficient shown in figure 6(b) and in the commanded lift and drag coefficients shown in figure 6(f). Considerably more variation is observed in the actual lift and drag coefficients that directly reflect the total turbulence.

A summary plot of touchdown errors for the entire series of 160 runs is shown in figure 7. Runs were made at 16 different values of carrier deck motion phase at touchdown — about every 22.5° — as shown by the abscissa of figure 7. For each carrier deck motion phase, runs were made with a set of 10 different turbulence inputs. The same turbulence process operated but with a different random number sequence so that roughly the same turbulence variations as shown in the top three curves of figure 6(e) were encountered, but different peak values of turbulence near touchdown caused a variation of touchdown errors. Each point in figure 7 represents the touchdown error for one run. The mean error was 3.9 m (+13 ft) (landed long) and the standard deviation was 6.7 m (22 ft). This is about half the 12.4-m (40.6-ft) standard deviation that resulted from a series of runs in an earlier simulation at Ames Research Center in which an operational Navy system was used with the same disturbances (ref. 3). It should be noted that on only six runs were the landings beyond the 18.3-m (60-ft) limit and none landed more than 18.3 m (60 ft) short. There were no ramp strikes as the minimum ramp clearance was 3 m (10 ft), the mean was 4.9 m (16 ft); and the standard deviation was 0.9 m (3 ft).

Gust Responses

The two essential functions of any aircraft control system are to maintain the commanded trajectory in spite of external disturbances and respond to commands that modify the trajectory. These capabilities have already been presented for the turbulence disturbances and path commands of a standard carrier approach. The responses of TAFCOS to much more severe disturbances and to a wider range of vertical and lateral commands are presented in the simulation results of this section and the next. For the gust responses of this section the aircraft has the same system configuration as for the carrier landing. No

gains or limits were altered but throttle hysteresis was eliminated. The aircraft is commanded to hold an airspeed of 129 knots for a straight and level path at an altitude of 152 m (500 ft). Measurements are made with respect to a coordinate system fixed to the Earth. A steady headwind of 30 knots is assumed. The gust run for which trajectory variables are displayed in figure 8(a) was a series of sharp step gusts. This does not represent a realistic situation but was chosen to give a concise picture from which the general characteristics of the aircraft response could be obtained. Time-history plots of system variables for step gusts of 25 knots sustained for 5 sec from six different directions are shown in figures 8(a-c). This simulation was accomplished in a single run of 150 sec.

A 25-knot step gust is a severe disturbance for an aircraft with airspeed of only 129 knots; thus, large attitude, flightpath, and thrust corrections were required to maintain airspeed and the commanded altitude. However, the corrections were generally smooth and nonoscillatory and aircraft angular rates and control surface rates were moderate. The throttle and engine power, which show characteristic time delays, are very responsive.

The trajectory variables are shown in figure 8(a) and the aircraft controls and angular responses are shown in figure 8(b). Time histories of the lift and drag coefficients are presented in figure 8(c). Figures 8(d-f) show the effect of limiting on the coefficients.

The first 55 sec of figures 8(a-c) show the response to the down and up gusts. There is a somewhat greater trajectory disturbance from the up gust. Also the disturbance in forward velocity and airspeed is considerably greater. The throttle is driven to its lower limit of 22° and the angle of attack excursion is greater.

The tailwind and headwind gust responses, displayed between 55 and 105 sec, show about the same trajectory disturbances in each direction (figs. 8(a-c)). The step in airspeed can be observed as the step gusts are applied and removed. It will be observed that the actual lift and drag coefficients follow the limited commands. This contrasts with the situation for the up and down gusts where the actual lift coefficient shows a sharp spike, not in response to a command but as a result of the sharp gust which gives an instantaneous change of angle of attack. It should be noted that the attitude and engine-thrust responses are consistent; that is, they do not act against each other by starting in one direction and then reversing one or more times during the transient, as can frequently be observed in conventional attitude and engine thrust control systems. The tailwind at 55 sec reduces dynamic pressure (fig. 8(c)) so lift is lost and altitude drops (fig. 8(a)). An increase is then commanded in angle of attack and throttle (fig. 8(b)), so that groundspeed (fig. 8(a)) increases and airspeed (fig. 8(a)) recovers almost half its commanded value in 5 sec. Vertical velocity (fig. 8(a)) is brought almost to zero, and flightpath angle (fig. 8(b)) recovers about half its value before the gust abruptly ends at 60 sec. This condition suddenly leaves the aircraft at about 15 knots above commanded airspeed, so the throttle is quickly reduced to its minimum at 22° and the attitude and airspeed reach their normal values before the headwind gust strikes at 80 sec.

13

The response to lateral gusts between 105 and 150 sec in figures 8(a-c) shows almost complete symmetry in the two directions. It will be noted that there is some horizontal stabilizer response although there had been no aileron or rudder response to the longitudinal disturbances.

The curves of figures 8(d-f) show the effect of trim map perimeter limiting on the lift and drag coefficients. They are plots of lift against drag coefficients for a single 150-sec run to the same scales as the force trim map of figure 4 and with the trim map perimeter superimposed. Figure 8(d) shows the coefficients $\bar{C}_{L_C}$ and $\bar{C}_{D_C}$ that exist before the limiter in figure 10 of appendix A. It is seen that because of the severe disturbances of this run, values of angle of attack and thrust coefficient are occasionally called for that are outside the boundary of the trim map. Figure 8(e) is a plot of the commanded values C_{L_C} and C_{D_C} that emerged from the limiter and were sent to the trim map. The limits were set to the perimeter of the trim map except that in order to provide an angle-of-attack margin, a limit of 16° for α_c was imposed. It is seen that the curve stays within the limits. Figure 8(f) shows the actual coefficients C_L and C_D that were achieved by the aircraft. They follow the limited commands of figure 8(e), except for sharp transients when the aircraft responded to gusts. The development of these curves as a function of time can be visualized by comparison with the corresponding time history plots of figure 8(c). The limiting to desired performance margins is quite straightforward for TAFCOS but would be very difficult for a conventional system.

Maneuver Command Responses

The simulation results presented in this section demonstrate the capability of TAFCOS to respond to a complicated set of maneuver commands. They roughly correspond to a trajectory that might be required after a carrier landing wave-off or during a holding-pattern situation. A flightpath of about 6-min duration over a modified racetrack course, including an altitude change of 305 m (1000 ft), was used as shown in figure 9(a). The control system gains and limits remained the same as for the carrier landing, but throttle hysteresis was suppressed. Measurements were made with respect to a coordinate system fixed to Earth. A steady wind of 30 knots in the negative inertial X-axis direction was assumed so that for a constant commanded airspeed of 129 knots the ground speed varied from 99 knots to 159 knots. The trajectory consists of a series of straight, circular, and helical segments. The input commands to the trajectory time sequencer are shown in table 2. They do not quite command a closed trajectory, as can be seen by the gap between start and finish in figure 9(a). The trajectory consists of 14 segments at a constant commanded airspeed. Each line of table 2 gives the flightpath commands for one segment. They are converted by the trajectory command sequencer into rough trajectory commands. The initial position of each segment is noted by the corresponding number along the path in figure 9(a), which is a plot of the trajectory actually flown. In an actual flight situation the basic trajectory data could be supplied by an air-traffic-control system or entered by the pilot as long as the next segment was entered more than 2 sec before the end of the current segment. This is necessary as the path segment initialization, discussed in appendix A, operates by having the rough command jump to the new trajectory

2 sec before the start of the new segment, in the same way that the rough commands were shown to jump for the tip-over maneuver.

This is a fundamental characteristic of TAFCOS which allows simple rough path segments to be specified with abrupt changes of path angle as in the first section of sketch (a).

SEGMENT 1   SEGMENT 1   SEGMENT 1

SEGMENT 2   SEGMENT 2   SEGMENT 2

GEOMETRIC SEGMENT   ROUGH-COMMANDED   SMOOTH-COMMANDED
JUNCTION   JUNCTION   JUNCTION
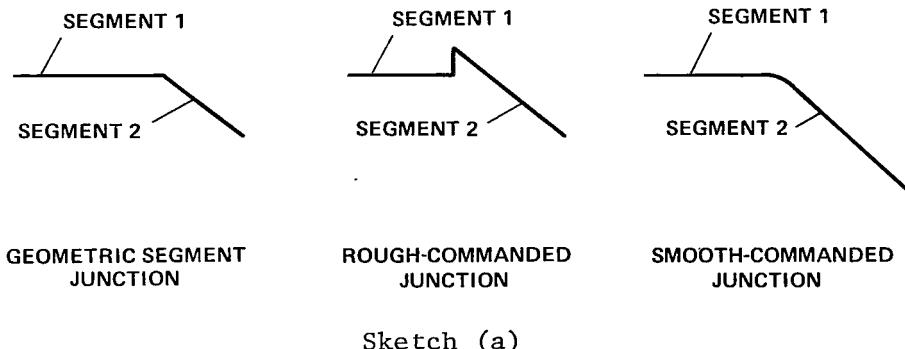
Sketch (a)

The trajectory command sequencer then modifies the segment junction by introducing a more abrupt discontinuity sooner to provide anticipation, as shown in the second section of the sketch (a). This more severe discontinuity, but with anticipation, is then smoothed by the filter action of the trajectory command generator to give the smooth command shown in the third section of the sketch. This final smooth command can be followed quite closely by the aircraft and the anticipation gives a smoothly flared-transition between segments.

The constant wind makes this trajectory a demanding test; however, it was successfully completed, as shown by the performance curves of figures 9(b-d). The trajectory variables of figure 9(b) show that the trajectory is smoothly followed. There are small disturbances in the vertical velocity, and the airspeed shows variations up to 6 knots as turns are made with respect to the steady wind. It should be noted that the ground speed varies by ±30 knots when flying either directly with or against the wind.

The variables of figures 9(c and d) show the effects of path changes with respect to the wind. The control surfaces have well-damped response, as shown in figure 9d. The spoilers are connected to the ailerons but do not deflect until the aileron exceeds 3°. The heading angle (fig. 9(c)) is restricted to ±180°. The jump at about 100 sec does not represent a discontinuity to the system since angles are manipulated by direction cosine matrices so all internal operations are smooth.

The rough error curves of figure 9(e) show a substantial sustained error between the executed trajectory and the rough commanded trajectory during path segment 10. Segment 10 is a downwind turn of 180° between about 200 and 250 sec. The rough errors reach 213 m (700 ft) for the inertial X axis and 122 m (400 ft) for the inertial Y axis. For the other segments of the trajectory, the rough errors are only the usual jump discontinuities at the start

15

of a new segment. The smooth errors are less than 2 m (6.5 ft) in segment 10 and less than 0.6 m (2 ft) for the other segments, so the aircraft is following the smooth-commanded trajectory quite closely.

An explanation of the large rough errors in the horizontal plane for segment 10 will point out how effectively acceleration limits can be applied to the TAFCOS configuration. If the rough-commanded horizontal trajectory is plotted over the executed trajectory of figure 9(a) the scale is such that no difference can be detected. When the rough-commanded and the executed trajectories are plotted for segment 10 to the enlarged scale of the top curve of figure 9(f), however, it can be seen that the executed trajectory does not follow as tight a turn as the rough-commanded so that the large errors of figure 9(e) result. This can be explained by the final three curves of figure 9(f), which are time histories of the rough-commanded, smooth-commanded, and actual accelerations for the inertial Y axis. The turn of segment 10 is with a smaller radius (914 m (3,000 ft)) than for the previous turn (1524 m (5,000 ft)) and although airspeed is essentially constant over the entire trajectory, the 30-knot tailwind gives an inertial velocity of 159 knots at the start of the segment-10 turn. These conditions require a radial acceleration of 7.3 m/sec^2 (24 ft/sec^2) which is the peak value of the rough-commanded acceleration in figure 9(f). However, internal limits (L3 and L4 of fig. 11) were set to allow only 5.8 m/sec^2 (19 ft/sec^2) of smooth-commanded acceleration as shown in the smooth-commanded acceleration curve of figure 9(f). The actual acceleration then followed this smooth command very closely. At the end of segment 10 the wind has become a headwind and inertial velocity is only 99 knots. Rough-commanded radial acceleration is only 2.9 m/sec^2 (9.5 ft/sec^2) so no limiting takes place. Similarly, the ground speed has been reduced to 129 knots halfway through the turn so the rough-commanded acceleration in the inertial X axis is only 4.8 m/sec^2 (15.8 ft/sec^2) and no limiting results. The limits considered here are limits on commanded acceleration; they are discussed in appendix A. (They are not the angle of attack limits mentioned in connection with the discussion of the force trim map.)

PRACTICAL IMPLEMENTATION PROBLEMS

The simulation of the automatic carrier landing problem using the TAFCOS open-loop dynamic trim control concept yielded very promising performance results. There are several practical problem areas that must be considered, however, before any particular application could realistically be undertaken.

One of the most important questions concerns the amount of airborne digital computer capacity required. A very good estimate of required computer capacity for an aircraft installation has recently become available (ref. 2). The TAFCOS concept was applied to a commercial aircraft, the deHavilland Twin Otter. A successful flight test was completed using essentially the modified racetrack course discussed in the section of results. The airborne installation used a Sperry 1819A airborne digital computer which has been in flight service for 10 years. The TAFCOS installation required only 3000 words of memory or about 10% of the 32,000 words available. The airborne computer operated at a rate of 20 Hz. The higher frequency rotational dynamics were

16

calculated every cycle and the lower frequency trajectory variables were cal-
culated every fifth cycle. The TAFCOS calculations used only 10 msec of com-
puting time per cycle out of an available 50 msec. It was found that the
required computer capacity was quite reasonable and substantially less than
that required for a conventional control system with the usual modes of atti-
tude hold, turn coordination, glide-slope capture, glide-slope tracking, flare,
and automatic landing.

The simulation results presented in this report were obtained from an
IBM 360-67 digital computer and did not simulate the word length or internal
structure that would be found in an airborne computer; consequently, some per-
formance differences might be expected due to quantization effects and internal
computer dynamics.

Another important question is how to provide the best data for the trim
map. This simulation relied on wind-tunnel data for the aircraft character-
istics, but supplementing and correcting those data from flight test results
would seem desirable. On the other hand, the differences between the trim map
for this simulation and the aircraft model used for generating the actual state
variables were largely compensated by integral control.

A question for the carrier landing is whether to track the deck during the
final approach or to predict the deck position several seconds ahead and aim
for that point. A brief study of this problem that showed promise for a pre-
diction technique was reported in reference 7. The TAFCOS framework is well
suited to use of a prediction scheme.

Finally, the question of system reliability is of utmost importance. The
TAFCOS framework appears to be convenient for reliability analysis and self-
checking procedures that would utilize its aircraft-response data.

CONCLUDING REMARKS

The theoretical basis for a new design concept for computational flight
control of aircraft has recently been developed at Ames Research Center. This
report presented the application of the concept to the problem of automatic
carrier landing. The implementation of the concept was explained by tracing
the operations in the signal flow path for the system. Simulation results were
shown for the carrier approach and landing. Further results for extreme dis-
turbances and a wide range of maneuver commands were also presented.

The concept employs a balance of feed-forward and feedback signals. It
is essentially an aerodynamically based control system that takes full advan-
tage of a priori knowledge of the aircraft force and moment characteristics
stored as dynamic trim maps, and utilized by an airborne digital computer to
calculate the angle of attack and thrust coefficient required to follow a
trajectory.

It was found that the feed-forward signal was about 80% of the total signal for most maneuvers and only 20% was needed from the feedback loops. The simulation results showed very smooth response to the carrier approach and landing commands. The deck motion was closely followed with moderate control activity, even for large vertical excursions of the touchdown point. The simulation showed that the digital computer requirements could be easily met by currently available computers. The TAFCOS configuration allowed straight-forward use of limits to control-commanded accelerations and angle of attack so that only executable trajectories would be commanded regardless of initial path errors, extreme discontinuities at path segment junctions, or severe external disturbances.

It is concluded that the TAFCOS concept potentially has the ability to achieve a substantial improvement in landing-point dispersion for the automatic carrier-landing task. It also appears that it would be readily adaptable for control of the aircraft over a much wider range of trajectory commands.

Ames Research Center
    National Aeronautics and Space Administration
        Moffett Field, California 94035, October 2, 1979

18

DETAILED SIGNAL FLOW OF TAFCOS SIMULATION

NOMENCLATURE

A	system matrix — perturbation model
A_{as}	direction cosine matrix representing rotation from the space axis system to the aircraft axis system
A_{as_c}	direction cosine matrix representing smooth commanded rotation from space axis system to aircraft axis system
$A_{as_{rc}}$	direction cosine matrix representing rough commanded rotation from space axis system to aircraft axis system
$\hat{A}_{as}$	estimated value of A_{as}
A_{vs}	direction cosine matrix representing rotation from the space axis system to the smooth-commanded velocity axis system
$A_{vs_{rc}}$	direction cosine matrix representing rotation from space axes to rough commanded velocity axis system
Ail	aileron deflection
Ail_c	commanded aileron deflection
b	wing span
$\bar{c}$	mean aerodynamic chord
C_{D_c}	commanded drag coefficient
C_{L_c}	commanded lift coefficient
C_{ℓ_c}	commanded rolling-moment coefficient
C_{m_c}	commanded pitching-moment coefficient
C_{n_c}	commanded yawing-moment coefficient
C_{T_c}	commanded thrust coefficient
$\bar{C}_{D_c}$	commanded drag coefficient before limiting
$\bar{C}_{L_c}$	commanded lift coefficient before limiting

$C(1)$	force coefficient along No. 1 velocity axis
$C(2)$	force coefficient along No. 2 velocity axis
$C(3)$	force coefficient along No. 3 velocity axis
$E_1(\phi_c)$	elementary direction cosine matrix representing a rotation through the angle ϕ_c about the No. 1 axis
$E_2(\alpha_c)$	elementary direction cosine matrix representing a rotation through the angle α_c about the No. 2 axis
$E_2(\Gamma_c)$	elementary direction cosine matrix representing a rotation through the angle Γ_c about the No. 2 axis
$E_3(\psi_c)$	elementary direction cosine matrix representing a rotation through the angle ψ_c about the No. 3 axis
$E_3(-\beta_c)$	elementary direction cosine matrix representing a rotation through the angle $-\beta_c$ about the No. 3 axis
f_c	output of force generation servo
f_{cc}	closed-loop commanded specific force vector
f_e	specific force error vector
f_{oc}	open-loop commanded specific force vector and input to force generation servo
f_{pc}	total commanded specific force vector before addition of integral term
f_{tc}	total commanded specific force vector
$\hat{f}$	estimated specific force vector
$\dot{f}_c$	time derivative of f_c
$\ddot{f}_c$	second time derivative of f_c
$f_c(2)_{max}$	maximum permissible value of $f_c(2)$
$\dot{f}_c(2)_{max}$	maximum permissible value of $\dot{f}_c(2)$
$\ddot{f}_c(2)_{max}$	maximum permissible value of $\ddot{f}_c(2)$
g	acceleration of gravity
$G1, G2, \ldots$	gains (three components)

I	identity matrix — three by three
I_{12}	identity matrix — twelve by twelve
J	aircraft inertia matrix
L1,L2,...	limits (three component)
M	aircraft mass
PLA	power lever angle
PLA_c	commanded power lever angle
$\hat{p}$	estimated aircraft roll rate
$Q(A) = \frac{1}{2}\begin{vmatrix} A_{23} - A_{32} \\ A_{31} - A_{13} \\ A_{12} - A_{21} \end{vmatrix}$	the column vector function of the rotational matrix A
$\hat{q}$	estimated aircraft pitching rate
$\bar{q}$	dynamic pressure
R	aircraft position vector
R_c	smooth-commanded aircraft position vector
R_e	aircraft position vector error between rough and smooth commands
R_{ep}	aircraft position vector error between estimated and smooth command
R_r	rough-commanded aircraft position vector
Rud	rudder deflection
Rud_c	commanded rudder deflection
$\hat{R}$	estimated aircraft position vector
$\hat{r}$	estimated aircraft yawing rate
S	wing area
Splr	spoiler deflection
$Splr_c$	commanded spoiler deflection
Stab	stabilizer deflection

$Stab_c$ commanded stabilizer deflection

$S(\omega)$ $= \begin{vmatrix} 0 & \omega(3) & -\omega(2) \\ -\omega(3) & 0 & \omega(1) \\ \omega(2) & -\omega(1) & 0 \end{vmatrix}$ the skew symmetric matrix function of the angular velocity vector ω

s Laplace variable

V aircraft velocity vector

V_c smooth-commanded aircraft velocity vector

V_e aircraft velocity-vector error between rough and smooth commands

V_{ep} aircraft velocity-vector error between estimated and smooth commands

V_r rough-commanded aircraft velocity vector

V_{rw} commanded velocity vector with respect to the airmass

$\hat{V}$ estimated aircraft velocity vector

$\dot{V}$ aircraft acceleration vector

$\dot{V}_c$ smooth-commanded aircraft acceleration vector in space or velocity axes as appropriate

$\dot{V}_p$ perturbation acceleration command within trajectory command generator

$\dot{V}_r$ rough-commanded aircraft acceleration vector

$\dot{V}_t$ total acceleration command within trajectory command generator

$\hat{\dot{V}}$ estimated aircraft acceleration vector

$\hat{W}$ estimated steady wind vector

α_c commanded angle of attack

β_c commanded sideslip angle

Γ_c commanded vertical flightpath angle

Γ_{rc} rough-commanded vertical flightpath angle

Δ_{fc} output of force generation servo — perturbation model

ζ_{1f} damping ratio of perturbation model, channel one force servo

ζ_{1t} damping ratio of perturbation model, channel one translational response

ζ_{2f}	damping ratio of perturbation model, channel two force servo
ζ_{2t}	damping ratio of perturbation model, channel two translational response
ϕ	aircraft roll angle
ϕ_c	commanded roll angle
ϕ_{max}	roll angle limit
$\dot{\phi}_{max}$	roll angle rate limit
$\ddot{\phi}_{max}$	roll angle acceleration limit
ψ_c	commanded horizontal flightpath angle
ψ_{rc}	rough-commanded horizontal flightpath angle
ω	aircraft angular velocity vector
$\hat{\omega}$	estimated aircraft angular velocity vector
ω_c	smooth-commanded aircraft angular velocity vector
$\dot{\omega}_c$	total aircraft commanded angular acceleration vector
$\dot{\omega}_{cc}$	closed-loop commanded aircraft angular acceleration vector
ω_f	angular frequency in open loop frequency response
$\dot{\omega}_{oc}$	open-loop commanded aircraft angular acceleration vector
ω_{rc}	rough-commanded aircraft angular velocity vector
ω_{1f}	natural frequency of perturbation model, channel one force servo
ω_{1t}	natural frequency of perturbation model, channel one translational response
ω_{2f}	natural frequency of perturbation model, channel two force servo
ω_{2t}	natural frequency of perturbation model, channel two translational response

Subscripts

c	commanded
e	error
ep	perturbation error
p	perturbation

23

t	total
cc	closed-loop commanded
oc	open-loop commanded
r	rough
rc	rough commanded
tc	total commanded

Other Notations:

•	time derivative
^	estimated
—	aerodynamic quantities $\bar{q}$, $\bar{c}$
t	transpose of an orthogonal matrix, hence also inverse
——	solid line denotes 3 × 1 column vector diagram connection
===	double line denotes 3 × 3 matrix diagram connection

INTRODUCTION

The TAFCOS implementation depends essentially on the airborne digital computer. Thus, a complete understanding of all the details that were necessary for the simulations would require a careful examination of the digital computer source programs. Most of the important considerations, however, including some that were not covered in the body of this report, can be explained by a study of figure 10, which is a diagram of the information flow between the major operational elements of the simulation computer program. It will be seen that figure 10 has the same basic configuration as figure 3 with the addition of several new elements to bring out details. The following discussion will trace the information flow in figure 10, commenting primarily on the new elements and explaining how the functions of the major elements previously described in the body of the report were implemented.

Aircraft, Control Servos, Sensors and State Estimation

The aircraft block, the control servo block, the dynamic lag block, and the sensor block are not part of the airborne digital computer. The equations implemented in the aircraft block represent the complete aircraft as used for the simulation of TAFCOS and include a number of secondary aerodynamic effects and engine response characteristics that were not taken into account when constructing the trim maps for TAFCOS. The actual aircraft state and trajectory

variables are measured by various sensors and processed by a state estimation system. Data from airborne and shipboard sensors are utilized by such a system. The inputs to TAFCOS are then the hatted quantities from the estimation system; they include an estimate of the steady wind velocity vector $\hat{W}$ and the aircraft velocity vector with respect to the carrier $\hat{V}$, all expressed in the carrier-centered inertial coordinate system defined in appendix B.

Trajectory Command Sequencer and Segment Initialization

The trajectory command sequencer contains the desired trajectory geometry that describes the aircraft flightpath as a series of straight line, circular, and helical segments. This can be prestored information, as in the case of the carrier landing where the tip-over the glide-slope geometry is standardized, or it could be entered a segment at a time, either by the pilot or by radio link from an air-traffic-control system. The trajectory command sequencer uses the desired airspeed and estimated winds $\hat{W}$ to calculate an inertial acceleration $\dot{V}_r$ which is required to hold airspeed and follow the flightpath. This acceleration is integrated to provide commanded velocity V_r and position R_r. The acceleration command vector is limited to acceptable values, thus, although the desired geometric trajectory relative to the carrier is commanded, the ground speed and touchdown time may vary due to winds while airspeed remains constant. For any desired trajectory, anticipation of the next segment is introduced near the end of each segment. Estimated position $\hat{R}$ and velocity $\hat{V}$ are compared with commanded quantities at the initialization of each segment to correct accumulated errors. Therefore, there may be small but abrupt changes in command introduced at the start of each trajectory segment. The outputs of the trajectory command sequencer are the rough commanded position R_r, velocity V_r, and acceleration $\dot{V}_r$, vectors which include the carrier deck motion components during the final 12 sec of the trajectory.

Trajectory Command Generator

From the preceding discussion of the trajectory command sequencer, it is apparent that although the path segments are intended to be flyable the transitions, possibly discontinuous, are in general not executable. The purpose of the trajectory command generator is to generate a smooth, flyable transition or capture maneuver. The trajectory command generator employs a four-integrator filter on each of three axes to provide smoothing. Information concerning the proximity of the flight envelope limits is used to ensure the flyability of the commanded trajectory.

A conceptual block diagram of the trajectory command generator is shown in figure 11. The nomenclature of figures 10-15 generally follows that previously employed. Amplitude limits are denoted by the symbol $\underline{}$; integrations are indicated by the symbol $\int$. The symbol $\sqrt{\Sigma(\cdot)^2}$ indicates the square root of the sum of the squares of the components of the vector input; that is, its magnitude; $|V_c|$ also indicates magnitude. The rate limit allows its output to change at no more than a specified maximum rate. Figure 11 is really a three-channel vector diagram that represents three scalar diagrams. The

25

variables are three-component vectors, such as R_r and V_c. Rotational transformations from the inertial space coordinate system to the rough-commanded relative velocity axis system are indicated by $A_{vs_{rc}}$. It should also be noted that the No. 1 axis of the relative velocity axis system is along the direction of the rough commanded relative velocity $V_{r-\hat{W}}$ and that the No. 2 axis is horizontal. The inverse transformation is $A_{vs_{rc}}^t$. Gains are indicated as G1, G2, etc. The inputs to the trajectory command generator are rough position R_r, rough velocity V_r, and rough acceleration $\dot{V}_r$ commands, each of which has three components.

The structure of the trajectory command generator is that of a three-channel servomechanism in which the plant is a simplified model of the aircraft. The state space has dimension 12 and is defined by the outputs of the four integrators in three axes. The commanded position of the aircraft is defined in inertial coordinates by R_c; the velocity is defined in inertial coordinates by V_c. The remaining six dimensions are used to model the force generation process. The total specific force f_c is expressed in the rough relative velocity axis system defined by the axis transformation $A_{vs_{rc}}$ and the final three dimensions define $\dot{f}_c$. The first channel is identified with engine thrust and is primarily associated with the aircraft longitudinal axis. The second channel is identified with roll and lateral translational response. The third channel is identified with pitch and translational response normal to the flightpath.

The sources of the dynamics in the force generation process are the attitude and power control systems. A correspondence can be established between limits that are to be imposed on engine power, attitude, angular velocity, and angular acceleration, and the equivalent limits on the force dynamics. For example, a useful approximate link between the lateral force $f_c(2)$ and the roll angle ϕ is simply $f_c(2) = g\phi$, where g is the acceleration of gravity. This equation, and its derivatives with maximum limiting values of the variables, yields the following relations:

$$f_c(2)_{max} = g\phi_{max}$$

$$\dot{f}_c(2)_{max} = g\dot{\phi}_{max}$$

$$\ddot{f}_c(2)_{max} = g\ddot{\phi}_{max}$$

The limiting angular acceleration $\ddot{\phi}_{max}$ is related by the moment generating process to the aileron and spoiler limits which are given, thus establishing a value for $\ddot{f}_c(2)_{max}$. Similarly acceptable maximum values of roll rate $\dot{\phi}_{max}$ and roll angle ϕ_{max} establish values for $\dot{f}_c(2)_{max}$ and $f_c(2)_{max}$, respectively. Limits on the other two axes can be similarly established by associating the No. 1 axis with engine thrust and the No. 3 axis with vertical plane maneuvers.

The limits L5 and L6 in figure 11 are contingency limits on the error values R_e and V_e in space coordinates to cope with unusual cases in which extremely large errors could result from faulty commands calling for a trajectory hundreds or thousands of feet from the present position. They permit

such errors to be reduced gradually as the aircraft responds by a prolonged transition with acceptable values of various rates and angles. The remaining amplitude limits — L1, L2, L3, and L4 — act on quantities in the rough relative velocity axis system and can be adjusted along with the gains and rate limit to ensure that the desired limits on f_c and its derivatives will not be exceeded.

The force generation process is represented as a simple servo with f_{oc} as input and f_c as output and is designed in such a way that regardless of the behavior of the driving signal $\dot{V}_t$ the resulting evolution of the force is consistent with aircraft limitations. In figure 11, rough- and smooth-commanded position R_r, R_c, rough- and smooth-commanded velocity V_r, V_c, and rough- and smooth-commanded acceleration $\dot{V}_r$, $\dot{V}_c$ are in inertial coordinates; the force variables are in the rough relative velocity axis system. The rough acceleration command $\dot{V}_r$ has the perturbation component $\dot{V}_p$ added to give the total acceleration command $\dot{V}_t$. The addition of a force command to overcome gravity yields the specific force f_{oc} as input to the force generating servo. In the steady state, f_c will equal f_{oc} because of the unity negative feedback. The gains G3 and G4 are chosen to give a desired natural frequency and damping ratio to the dynamic buildup of f_c. This commanded specific force f_c is then resolved to inertial axes and the counter gravity force removed to give the total commanded path acceleration $\dot{V}_c$ in inertial coordinates. Simple integration then gives velocity V_c and one more integration gives position R_c.

It might be expected that the specific force f_c would serve as the input to the trim map; however, f_{oc} is used as the open-loop specific force command because it provides the required dynamic anticipation of f_c while being equal to it in the steady state.

Open-loop excitation of the trajectory command generator is provided by the acceleration command from the trajectory command sequencer $\dot{V}_r$. In addition, regulation feedback $\dot{V}_p$ is provided to force the trajectory command generator to follow the trajectory from the sequencer asymptotically. Several limits are included, as shown in figure 11, to ensure stable, well-behaved regulation for large initial errors.

The trajectory command generator provides the open-loop specific force command f_{oc}, which is combined with the closed-loop specific force command from the trajectory regulator and sent to the force trim map section further down the hierarchy of the control logic, where it is converted to corresponding attitude and power commands. Additional outputs of the trajectory command generator are R_c and V_c; they describe the reference trajectory and are sent to the trajectory perturbation regulator for comparison with the corresponding measured quantities and subsequent regulator action to reduce trajectory errors. Since TAFCOS is primarily a feed-forward system that relies only partially on feedback, the regulator is properly a perturbation regulator.

The following paragraphs provide a more detailed explanation of how the gains in figure 11 were chosen by using linear control theory. Because figure 11 is a vector block diagram that represents three channels, the variables are three-component vectors; that is:

$$R_r = \begin{vmatrix} R_{r1} \\ R_{r2} \\ R_{r3} \end{vmatrix}$$

and the gains were chosen to be three by three diagonal matrices; that is:

$$G_1 = \begin{vmatrix} G_{11} & 0 & 0 \\ 0 & G_{12} & 0 \\ 0 & 0 & G_{13} \end{vmatrix}$$

The direction cosine matrix $A_{rs_{rc}}$ in figure 11 represents a rotation from inertial axes to the rough-commanded relative velocity axes system whose first axis is lined up with the direction of the rough-commanded relative-velocity $V_r - \hat{W}$ and whose second axis is horizontal. This matrix differs slightly from A_{vs} in figure 13 which represents a rotation from inertial axes to the smooth-commanded relative-velocity axis system whose first axis is lined up with the direction of the smooth-commanded relative velocity $V_c - \hat{W}$ and whose second axis is horizontal. This distinction is necessary to avoid an internal feedback loop (fig. 11) that would arise if V_c, which is computed in the loop, were used instead of V_r.

The perturbation model of the command generator for a linear analysis is shown in sketch (b). The symbol Δf_c is introduced instead of $\dot{V}_c$ because the addition and subtraction of the constant gravity term has been ignored.
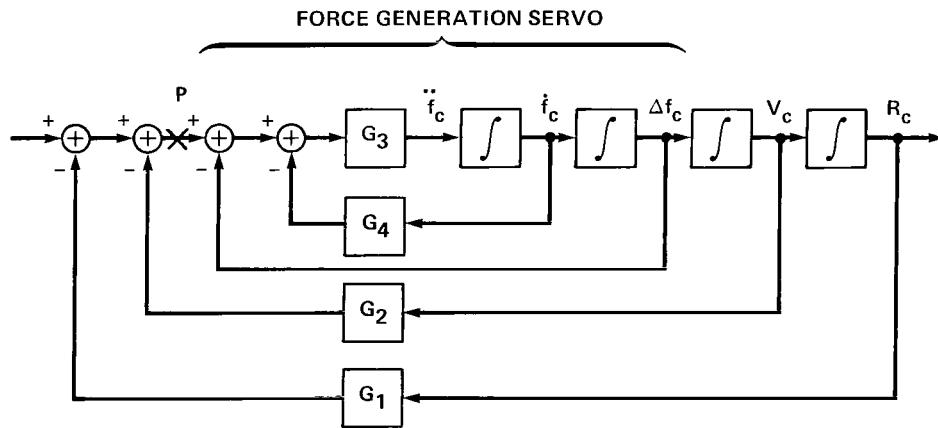
Sketch (b)

The integrator outputs are chosen as the state variables of this twelve-dimensional system. The unforced state equations — in vector matrix form — are:

$$
\begin{vmatrix} \dot{R}_c \\ \dot{V}_c \\ \Delta \dot{f}_c \\ \ddot{f}_c \end{vmatrix} = \begin{vmatrix} 0 & I & 0 & 0 \\ 0 & 0 & I & 0 \\ 0 & 0 & 0 & I \\ -G_1 G_3 & -G_2 G_3 & -G_3 & -G_4 G_3 \end{vmatrix} \begin{vmatrix} R_c \\ V_c \\ \Delta f_c \\ \dot{f}_c \end{vmatrix}
$$

where I is the three-by-three identity matrix and the other quantities are vectors and matrices as previously defined. The characteristic equation of the system is $\det(sI_{12} - A) = 0$, where A is the system matrix and I_{12} is the twelve-by-twelve identity matrix. This leads to the determinant equation

$$
\begin{vmatrix} Is & -I & 0 & 0 \\ 0 & Is & -I & 0 \\ 0 & 0 & Is & -I \\ G_3 G_1 & G_3 G_2 & G_3 & (Is + G_3 G_4) \end{vmatrix} = 0
$$

which yields

$$Is^4 + G_3 G_4 s^3 + G_3 s^2 + G_3 G_2 s + G_3 G_1 = 0$$

This vector equation represents a three-axis decoupled system because the gain matrices are diagonal. Thus, each of the corresponding scalar equations represents a single channel.

The roots of the scalar characteristic equation are the poles of the transfer function for the corresponding channel. The gains for the various channels in sketch (b) can be determined by any of the conventional pole placement techniques. The following discussion explains in detail how they were determined for the second channel. The force generation servo represented essentially by the first two integrators was specified to have a second-order response with natural frequency $\omega_{2f} = 2.85$ rad/sec and damping ratio $\zeta_{2f} = 0.75$. The lateral translational response generally associated with the last two integrators was specified to have a second-order response with natural frequency $\omega_{2t} = 0.67$ rad/sec and damping ratio $\zeta_{2t} = 0.71$. This leads to a desired transfer function that is a cascade of two second-order systems. The denominator of this transfer function then determines the characteristic equation:

$$(s^2 + 2\zeta_{2f}\omega_{2f}s + \omega_{2f}^2)(s^2 + 2\zeta_{2t}\omega_{2t}s + \omega_{2t}^2) = 0$$

When this desired characteristic equation is set equal to the characteristic equation of sketch (b) we have:

$$s^4 + s^3(2\zeta_{2f}\omega_{2f} + 2\zeta_{2t}\omega_{2t}) + s^2(4\zeta_{2f}\zeta_{2t}\omega_{2f}\omega_{2t} + \omega_{2f}^2 + \omega_{2t}^2)$$

$$+ s(2\zeta_{2f}\omega_{2f}\omega_{2t}^2 + 2\zeta_{2t}\omega_{2t}\omega_{2f}^2) + \omega_{2f}^2\omega_{2t}^2 = s^4 + s^3 G_3 G_4 + s^2 G_3 + s G_3 G_2 + G_3 G_1$$

A direct matching of the coefficients gives the gains $G_1 = 0.29$, $G_2 = 0.76$, $G_3 = 12.6$, $G_4 = 0.41$.

The same gains were also used for the third channel. For the first channel, which is identified with the slower engine thrust response, the desired parameters were taken as $\omega_{1f} = 1.52$, $\zeta_{1f} = 0.75$, $\omega_{1t} = 0.53$, $\zeta_{1t} = 0.73$; these parameters yield the gains: $G_1 = 0.15$, $G_2 = 0.56$, $G_3 = 4.9$, and $G_4 = 0.7$. It is apparent that all of the techniques of modern control theory and optimization could be used at this point in the trajectory command generator design to give specified dynamics for each channel. One interesting feature of sketch (b) is the inclusion of the gain G_3 in the direct path. This prevents the representation from being exactly the controller canonical form, but permits unity feedback to close the force generator servo loop. This gives a direct physical representation for convenient numerical checking during system tests and observation of limiting behavior.

The design described above was examined by classical servomechanism analysis. The loop was opened at point P in sketch (b) to give the servo configuration of sketch (c) which has an open-loop transfer function of

$$\frac{Q}{P} = \frac{G_3(G_1 + G_2 s)}{s^2(s^2 + G_3 G_4 s + G_3)}$$
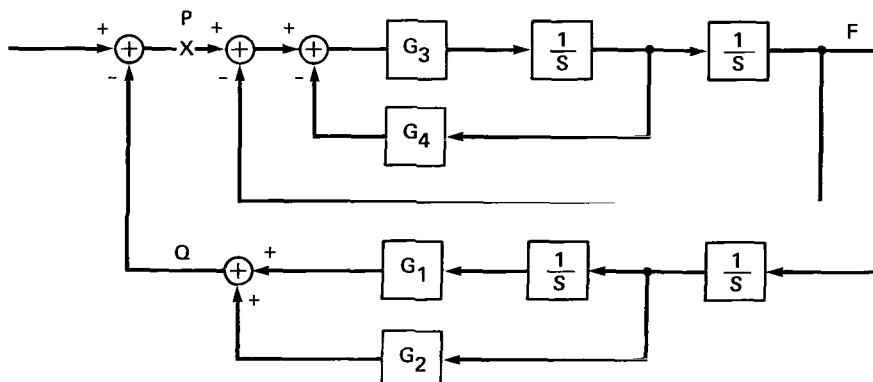
Sketch (c)

This open-loop transfer function, of course, has different roots and poles than the specified closed loop. The amplitude ratios and phases of the open-loop frequency response and of its factors are shown in figure 12 plotted against the logarithm of angular frequency ω_f. Curve A is the amplitude ratio of the force servo factor

$$\frac{F}{P} = \frac{G_3}{s^2 + G_3 G_4 s + G_3} = \frac{1}{1 + G_4 s + (s^2/G_3)}$$

with break point at $\omega_f = 3.55$. In figure 12, curve B is the corresponding phase; curve C is the amplitude ratio of the remaining factor

$$\frac{Q}{F} = \frac{G_1}{s^2}\left(1 + \frac{G_2}{G_1} s\right)$$

with break point at $\omega_f = 0.377$. The corresponding phase is curve D. The total open-loop amplitude ratio from P to Q is curve E and the corresponding phase is curve F. It can be seen that this yields a very satisfactory Bode plot with a phase margin of 46° and a gain margin of 16 dB.

Time domain responses were then investigated on the simulation and iterated to give the most satisfactory transient performance. The final gains thus selected are those used for the example calculations; this accounts for the three-figure precision.

Trajectory Perturbation Regulator

The trajectory command generator discussed in the preceding section provides an open-loop control and the corresponding reference trajectory. Because the aircraft equations of motion and the environment are never represented in every detail, a closed-loop feedback is needed to regulate the errors caused by deviation of the real process from the model used in the command generator. The purpose of the trajectory regulator is to provide control of the trajectory errors. The structure of the regulator is shown in figure 13. The structure of figure 13 is quite similar to the first section of figure 11. Note that the position and velocity error signals are formed by a comparison of smooth commands R_c and V_c, from the trajectory command generator, with measured values $\hat{R}$ and $\hat{V}$, rather than by comparison of rough and smooth commands. Figure 13 also includes an integrator section that was not shown in figure 10. The trajectory errors in position, $R_{ep} = -\hat{R} + R_c$, and velocity, $V_{ep} = -\hat{V} + V_c$, which are in inertial coordinates, are transformed into velocity axes, passed through limits and gains, and then combined to form a closed-loop corrective perturbation specific force command f_{cc} which is added to the open-loop command f_{oc} from the trajectory command generator. The gains and limits, applied in the velocity axis system, are designed by assuming the same model of the force generation process that was used in the trajectory command generator. In addition to the position plus (velocity) feedback, integral feedback is used as shown in the figure. This loop is applied to the force generation process, and it unloads the corrective acceleration f_{cc}. The effect of integral control of the error ($f_e = f_{pc} - \hat{f}$) is limited by L9 to 0.1 g. The estimated

specific force $\hat{f}$ is obtained from the accelerometer package. Consequently, slow errors in the a priori model of the force generation process resulting in acceleration errors up to 0.1 g will cause no trajectory offsets. The resulting specific force f_{tc} representing open-loop command plus closed-loop perturbation is next expressed in coefficient form.

Force Coefficient Development

The total commanded specific force vector f_{tc} in figure 10 is in relative velocity axes. It is multiplied by $M/\bar{q}S$ to provide force coefficients C(1), C(2), and C(3). The drag acts along the negative No. 1 axis in this system so the commanded drag coefficient before limiting $\bar{C}_{D_c}$ is merely the negative of the No. 1 force coefficient. The total lift coefficient before limiting as defined in reference 2 is due to all forces perpendicular to the drag. Therefore $\bar{C}_{L_c}$ is $\sqrt{C(2)^2 + C(3)^2}$. Also, the commanded roll angle ϕ_c is calculated as the arc tangent of the ratio of the second and third force coefficients. At this point in figure 10 the commanded lift and drag coefficients before limiting $\bar{C}_{L_c}$ and $\bar{C}_{D_c}$ have been generated in response to the open-loop commands supplemented by the closed-loop commands so that for severe atmospheric disturbances they may be beyond the aircraft capability. Therefore, at this point they are conveniently limited to the perimeter of the force trim map of figure 4, or to some sub-envelope based on desired stall margin, to give the limited commanded coefficients C_{L_c} and C_{D_c} which are then sent to the trim map. The operation of these limits can be seen dramatically in figure 8(e) compared to figure 8(d).

Force Trim Map and Thrust Calculations

The aircraft model for this simulation represents only the landing configuration; hence, no effects of changing flaps are included. Thus, the simple two-dimensional trim map of figure 4 could be developed. Furthermore, the trim map includes only the major aerodynamic forces due to the angle of attack and stabilizer. Other secondary aerodynamic lift, drag, and side forces, used in the complete aircraft model, are neglected for the force trim map but could be included if more complete open-loop control fidelity was desired. Some of them are in fact included in the moment trim map calculations. As noted in the body of the report, a three-dimensional trim map to include flap angle configuration changes was developed for another application.

The commanded thrust coefficient C_{T_c} from the force trim map is multiplied by $\bar{q}S$ to give the total required thrust. The digital computer then interpolates a table of thrust vs power-lever angle to determine the required throttle setting. This commanded power-lever angle PLA_c is then modified by a dynamic lag and hysteresis to simulate the action of the throttle actuator that is used in the A-7E aircraft.

In a different application, in which engine response time and different nonlinear processes that occur during thrust buildup and decay were particularly important, a thrust perturbation regulator was developed that used

measured values of engine speed feedback to provide a closed-loop perturbation command similar to the action of the trajectory perturbation and the attitude perturbation regulators.

Angle and Angular Rate Calculations

As explained in appendix B, the rough-commanded aircraft attitude matrix $A_{as_{rc}}$ is constructed as the product of five elementary direction cosine matrices

$$A_{as_{rc}} = E_2(\alpha_c) E_3(-\beta_c) E_1(\phi_c) E_2(\Gamma_c) E_3(\psi_c)$$

The commanded flightpath angles ψ_c and Γ_c are computed from the components of the commanded velocity with respect to the steady wind. The estimated steady wind is $\hat{W}$ and the commanded inertial velocity is V_c so that the vector relative velocity is $V_{rw} = V_c - \hat{W}$ and the commanded flightpath angles are computed as:

$$\psi_c = \tan^{-1} \frac{-V_{rw}(2)}{V_{rw}(1)}$$

$$\Gamma_c = \tan^{-1} \frac{-V_{rw}(3)}{\sqrt{V_{rw}(1)^2 + V_{rw}(2)^2}}$$

If desired for a particular trajectory, a commanded angle of sideslip β_c can be generated by the trajectory command sequencer. The rough commanded angular rate vector ω_{rc} is shown in appendix B to be:

$$\omega_{rc} = \begin{vmatrix} \dfrac{-\dot{V}_c(2)}{|V_c|} \tan \Gamma_c \\[3mm] \dfrac{-\dot{V}_c(3)}{|V_c|} \\[3mm] \dfrac{\dot{V}_c(2)}{|V_c|} \end{vmatrix}$$

where $\dot{V}_c$ is the smooth-commanded acceleration vector expressed in velocity axes for this particular calculation and $|V_c|$ is the magnitude of the smooth-commanded velocity vector.

Attitude Command Generator and Perturbation Regulator

The variables in the attitude command generator and perturbation regulator include vectors and matrices. The details of the implementation can be seen from figure 14. They are manipulated and integrated in much the same way as described in the detailed discussion of figure 15 in appendix B.

Commanded Moment Coefficients and Moment Trim Map

The commanded moment vector is first obtained from the commanded angular acceleration $\dot{\omega}_c$ by matrix multiplication by the inertial matrix J. Then the moment coefficients are obtained by dividing the pitching torque component by $\bar{q}S\bar{c}$ and the roll and yaw torque components by $\bar{q}sb$. The moment trim map involves both tabular interpolations and algebraic equation solutions. For the lateral response, the roll and yaw torque contributions due to commanded angle of attack, roll, and yaw rates are calculated from tabular data. The remaining portion of the torques required to produce the commanded roll and yaw accelerations can be expressed in two simultaneous linear algebraic equations in the lateral controls; the equations are solved for the required rudder, and lateral stick deflection. The aileron and spoiler are then given as functions of the lateral stick. The pitching torque contribution due to the commanded angle of attack, aileron and spoiler deflections, and commanded pitch rate is then calculated using tabular data. It is subtracted from the total required pitching torque to find the torque contribution needed from the horizontal stabilizer. A table of torque vs commanded angle of attack for various stabilizer deflections is then interpolated to find the required stabilizer deflection.

This completes the description of the calculations carried out for the simulation of TAFCOS. These calculations must be carried out by the airborne digital computer 20 times per second. To provide insight into the system, and for convenience and flexibility in the simulation, a number of special subroutines were employed to execute vector and matrix computations and for one- and two-dimensional table interpolations as well as for recording computer output. However, when the TAFCOS concept was flight tested, the airborne computer requirements were reduced to a minimum. Matrix calculation subroutines were replaced by efficient in-line coding, tabular data were replaced by piecewise linear analytic expressions, and slow and fast loops were employed.

34

APPENDIX B

MATHEMATICAL DETAIL

NOMENCLATURE

$A = \begin{vmatrix} a_{11} & a_{12} & a_{13} \\ a_{21} & a_{22} & a_{23} \\ a_{31} & a_{32} & a_{33} \end{vmatrix}$ direction cosine matrix representation of a rotational transformation

A_{as} direction cosine matrix representing rotation from space to body axes

$A_{as_{rc}}$ direction cosine matrix representing the rotation from space to rough commanded aircraft body axes

A_{vs} direction cosine matrix representing the rotation from space to velocity axes

$\dot{A} = \frac{dA}{dt}$ time derivative of the matrix A

$A_{as}^{-1} = A_{as}^{t}$ inverse and transpose of the orthogonal matrix A_{as}

a_{11}, a_{32}, etc.   cosine of angle between axes of two coordinate systems as indicated by the subscripts

$E_x(y)$ elementary direction cosine matrix representing a rotation through the angle y about the axis x. For example:

$$E_2(\alpha) = \begin{vmatrix} \cos \alpha & 0 & -\sin \alpha \\ 0 & 1 & 0 \\ \sin \alpha & 0 & \cos \alpha \end{vmatrix}$$

h_a angular momentum vector of the aircraft in body axes represented as:

$$\begin{vmatrix} h_a(1) \\ h_a(2) \\ h_a(3) \end{vmatrix}$$

h_s angular momentum vector of the aircraft in space axes

I the identity matrix 3×3

J_a matrix representation of the inertia operator of the aircraft in body axes 3×3

35

J_a^{-1} inverse of the matrix J_a

J_s matrix representation of the inertia operator of the aircraft in space axes

M_a total torque vector acting on the aircraft in body axes

M_s total torque vector acting on the aircraft in space axes

$S(\omega) = \begin{vmatrix} 0 & \omega(3) & -\omega(2) \\ -\omega(3) & 0 & \omega(1) \\ \omega(2) & -\omega(1) & 0 \end{vmatrix}$ the skew symmetric matrix function of the vector ω

V_c smooth-commanded velocity vector in velocity axes

V_r rough-commanded velocity vector in space axes

$\dot{V}_c$ smooth-commanded acceleration vector in velocity axes

$\dot{V}_r$ rough-commanded acceleration vector in space axes

$|V_c|$ magnitude of V_c

α angle of attack

α_c commanded angle of attack

β sideslip angle

β_c commanded sideslip angle

Γ vertical flightpath angle

Γ_c commanded vertical flightpath angle

Φ Euler angle about No. 1 axis

ϕ roll angle

ϕ_c commanded roll angle

Ψ Euler angle about No. 3 axis

ψ horizontal flightpath angle

ψ_c commanded horizontal flightpath angle

ω angular velocity vector associated with the rotational matrix $\dot{A}$ represented as: $\begin{vmatrix} \omega(1) \\ \omega(2) \\ \omega(3) \end{vmatrix}$

36

Θ Euler angle about the No. 2 axis

ω_a angular velocity vector of aircraft axis system (associated with $\dot{A}_{as}$) expressed in aircraft body axis system

ω_c smooth-commanded angular velocity vector (associated with $\dot{A}_{as_c}$) in body axes

ω_{rc} rough-commanded angular velocity vector (associated with $\dot{A}_{vs}$) in velocity axes

Subscripts

a   aircraft body axis system

c   commanded

r   rough

s   space axis system

v   velocity axis system

Other Notations

$\cdot$ time derivative

-1 inverse of a matrix

COORDINATE SYSTEMS

TAFCOS requires the definition of several coordinate systems. All are right-handed, three-axis orthogonal systems. Vectors are expressed by their three components in the appropriate system. Sketch (d) illustrates the chain of coordinate systems that transforms quantities from inertial space coordinates to aircraft body axes. The inertial space axis system is centered at the

Sketch (d)
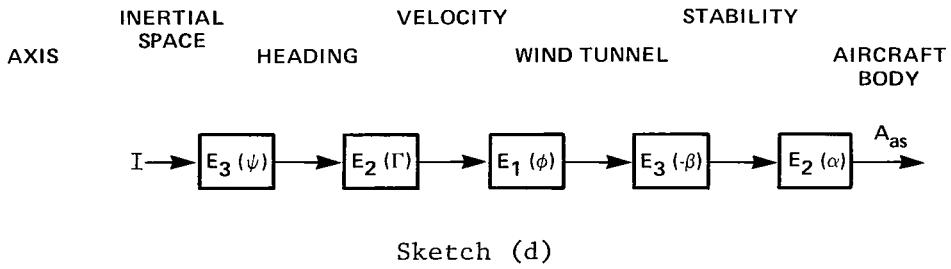
carrier's undisturbed center of pitch with its first axis along the carrier deck and its third axis downward. For the short times involved in the landing, the carrier velocity has been assumed to be constant over a flat nonrotating Earth with the steady wind along the deck; hence, this is an inertial system. The aircraft velocity vector with respect to relative wind is along the first axis of the velocity axis system. The velocity axis system thus results from a rotation of the space axis system about its third axis through the horizontal flightpath angle ψ followed by a rotation about its second axis through the vertical flightpath angle Γ. The next rotation about the No. 1 velocity axis through the roll angle ϕ defines what has been called the wind-tunnel axis system. Rotation about its third axis through the sideslip angle (negative β) leads to the stability axis system, and a final rotation about its second axis through the angle of attack α defines the aircraft body axis system. It should be noted that this series of five rotations achieves the same aircraft body axis orientation as the three conventional rotations through the Euler angles Ψ, Θ, and Φ. Three of these axis systems are used extensively. The space axis system (s) is used for basic trajectory definition and for differentiation when inertial accelerations are involved. The velocity axis system (v) is particularly important because the aircraft center of gravity is fixed at the origin and the relative velocity vector is aligned along the No. 1 axis. The aircraft lift and drag are easily expressed in this system. The aircraft body axis system (a) is used for developing forces and torques due to the engine and control surfaces and for body rate calculations. The coordinates of a vector are transformed from one of these coordinate systems to another by multiplication by the direction cosine matrix between the systems. The first subscript of the rotation matrix symbol A represents the final system, and the second subscript represents the initial system. For example A_{vs} is the rotation matrix from space to velocity axes. The rotation from space to aircraft body axes is $A_{as} = E_2(\alpha)E_3(-\beta)E_1(\phi)E_2(\Gamma)E_3(\psi)$. It should be noted that this does not represent the rotation of a vector. The vector remains fixed but is represented in various coordinate systems which are rotated with respect to each other.

The Skew Symmetric Matrix Function of a Vector

The vector cross product $\omega \times v$ where ω and v are three-component vectors is equivalent to the matrix product $-S(\omega)v$ where $S(\omega)$ is the skew symmetric matrix

$$S(\omega) = \begin{vmatrix} 0 & \omega_3 & -\omega_2 \\ -\omega_3 & 0 & \omega_1 \\ \omega_2 & -\omega_1 & 0 \end{vmatrix}$$

This can be shown by forming the vector cross product and comparing term-by-term with the matrix product. The skew symmetric matrix function $S(\omega)$ is in some sense the matrix equivalent of the vector ω and is used in relations where both three component vectors and three-by-three matrices are involved. The skew symmetric matrix function of the angular velocity vector appears in figures 14 and 15.

38

The Vector Function of a Matrix

Let the rotation matrix A be

$$A = \begin{vmatrix} a_{11} & a_{12} & a_{13} \\ a_{21} & a_{22} & a_{23} \\ a_{31} & a_{32} & a_{33} \end{vmatrix} .$$

Then the vector function of A is defined as

$$Q(A) = \frac{1}{2} \begin{vmatrix} a_{23} - a_{32} \\ a_{31} - a_{13} \\ a_{12} - a_{21} \end{vmatrix}$$

In some sense $Q(A)$ is the vector equivalent of the matrix A as can be seen by noting that under appropriate conditions the Q and S functions cancel. In general $Q(S(\omega)) = \omega$ and for a skew symmetric matrix A, $S(Q(A)) = A$. The vector function of a rotational matrix $Q(A)$ appears in figure 14 where it is used to convert a matrix representing an angular error into a vector that can be added to another vector representing an angular velocity error to form a total error vector.

Angular Rate Calculations

The time derivative of a direction cosine matrix A is: $\dot{A} = S(\omega)A$ where $S(\omega)$ is the skew symmetric matrix

$$S(\omega) = \begin{vmatrix} 0 & \omega(3) & -\omega(2) \\ -\omega(3) & 0 & \omega(1) \\ \omega(2) & -\omega(1) & 0 \end{vmatrix}$$

whose elements are the components of the angular velocity vector associated with the rotation, that is:

$$\omega = \begin{vmatrix} \omega(1) \\ \omega(2) \\ \omega(3) \end{vmatrix}$$

The rough-commanded aircraft orientation matrix ($A_{as_{rc}}$) is the input to the attitude command generator in figures 2, 3, and 10. It is desirable to supplement this open-loop commanded attitude by the corresponding open-loop commanded attitude rate.

This would strictly be the angular velocity vector associated with $\dot{A}_{as_{rc}}$. This in turn depends on the time derivatives of all five angles involved in

the transformation. However, only the major components were implemented for this application. Hence, only the time derivatives of ψ_c and Γ_c were used to command open-loop attitude rate. The commanded flightpath angles ψ_c and Γ_c, which define the orientation of the relative velocity axis system, may change over a wide range during an extended period of time as the flightpath is described. Thus, their time derivatives can maintain substantial, slowly changing values. Furthermore, these commanded angles are computed from the components of the commanded aircraft velocity with respect to steady wind and hence are noise free. On the other hand, commanded angle of attack α_c changes rapidly to initiate maneuvers, contains a noise component due to feedback from the trajectory regulator, and has zero average rate of change over relatively short periods. Commanded sideslip β_c, which would be needed for crabbing and decrabbing, was not used in these simulations and in any event would have only short duration, nonzero values of time derivative. Commanded roll angle ϕ_c about the velocity axis likewise is characterized by rapid changes of short duration. The angular velocity vector of the velocity axis system is given in terms of the angle rates $\dot{\psi}_c$ and $\dot{\Gamma}_c$ as:

$$\omega_{rc} = \begin{vmatrix} -\dot{\psi}_c \sin \Gamma_c \\ \dot{\Gamma}_c \\ \dot{\psi}_c \cos \Gamma_c \end{vmatrix}$$

Now ψ_c and Γ_c are the flightpath angles generated to command the aircraft center of gravity to follow the trajectory. The trajectory has been defined in terms of the corresponding accelerations. The rough commanded acceleration $\dot{V}_r$ (fig. 10) is expressed in space axes at the input to the trajectory command generator and produces the smooth commanded acceleration $\dot{V}_c$ in velocity axes. The flightpath angle rates $\dot{\Gamma}_c$ and $\dot{\psi}_c$ depend on components of this acceleration that are perpendicular to the velocity vector and on the magnitude of the velocity $|V_c|$:

$$\dot{\Gamma}_c = -\frac{\dot{V}_c(3)}{|V_c|} \qquad \dot{\psi}_c = \frac{\dot{V}_c(2)}{|V_c| \cos \Gamma_c}$$

Substituting these values into the expression for ω_{rc} gives the rough commanded open-loop angular velocity, which is used as an input to the attitude command generator in figure 10.

The Matrix Form of the Rotational Dynamic Equation

The rotational dynamic portion of the aircraft simulation represented in the aircraft block at the extreme right end of figure 3 uses a matrix formulation of the dynamic equation derived below. Let M_s and M_a be the total torque — aerodynamic and propulsive — expressed in the inertial frame and the body frame respectively. Let h_s and h_a be the angular momentum vector in space and body coordinates. Let J_s and J_a be the inertia matrix in space and body axes. Let ω_a be the angular velocity vector of the body axes with respect to the space axes expressed in body axes coordinates and let A_{as}

40

be the rotation matrix from the space axes to the body axes. Note that the vector quantities are all three-element column vectors; that is,

$$h_a = \begin{pmatrix} h_{a1} \\ h_{a2} \\ h_{a3} \end{pmatrix}$$

and the matrices are three-by-three arrays. Now

$$M_a = A_{as}M_s$$
$$h_a = A_{as}h_s$$
$$\dot{A}_{as} = S(\omega_a)A_{as}$$

from a preceding section of this appendix. Also by neglecting spinning rotors we have

$$h_a = J_a\omega_a$$

and because J_a is constant in the body frame

$$\dot{h}_a = J_a\dot{\omega}_a$$

Furthermore, the basic dynamic relation in inertial axes is

$$\dot{h}_s = M_s$$

The relation using the easily available quantities M_a and $\dot{h}_a$ may now be found by the following manipulations:

$$h_a = A_{as}h_s$$
$$\dot{h}_a = \dot{A}_{as}h_s + A_{as}\dot{h}_s = J_a\dot{\omega}_a$$

then

$$\dot{\omega}_a = J_a^{-1}[S(\omega_a)A_{as}A_{as}^{-1}h_a + A_{as}M_s]$$

$$\dot{\omega}_a = J_a^{-1}[S(\omega_a)h_a + M_a] = J_a^{-1}[M_a + S(\omega_a)J_a\omega_a]$$

A block diagram of this expression is included in the first section of figure 15.

The final portion of figure 15 illustrates how the angular velocity vector ω_a is integrated to obtain the aircraft attitude expressed as the direction cosine matrix A_{as}. The vector ω_a is first used to construct the skew symmetric matrix function $S(\omega_a)$. Then the relation for the derivative of a direction cosine matrix $\dot{A}_{as} = S(\omega_a)A_{as}$ is implemented by the matrix

multiplication indicated. This is followed by a straightforward integration to give A_{as}. The Gram-Schmidt orthogonalization is then required, otherwise cumulative computer round-off error would soon lead to a nonorthogonal matrix in which individual elements exceed unity. Angles are treated throughout the system by manipulation of their direction cosine matrices. This completes the aircraft rotational dynamics. However, for purposes of angular readout during the simulation, a computer routine has been developed (ref.8) that further displays the Euler angles corresponding to the direction cosine matrix A_{as}:

$$A_{as} = E_1(\Phi)E_2(\Theta)E_3(\Psi)$$

REFERENCES

1. Meyer, G.; and Cicolani, L. S.: A Formal Structure for Advanced Automatic Flight-Control Systems. NASA TN D-7940, 1975.

2. Wehrend, W.; and Meyer, G.: DHC-6 Flight Tests of the Total Automatic Flight Control System (TAFCOS) Concept. NASA TP-1513. (In preparation)

3. Smith, G. Allan; McNeill, Walter E.; and Huff, Richard B.: A Comparison of Restructured Designs for the Automatic Carrier Landing System. Proceedings of Flight Control Systems Criteria Symposium, U.S. Naval Post Graduate School, July 1978.

4. Smith, G. Allan; and Meyer, George: Total Aircraft Flight-Control System — Balanced Open- and Closed-Loop Control With Dynamic Trim Maps. Proceedings of the Third Digital Avionics Systems Conference, Ft. Worth, Texas, Nov. 1979, IEEE Catalog No. 79CH1518-0.

5. Cicolani, L. S.; Sridhar, B.; and Meyer, George: Configuration Management and Automatic Control of an Augmentor Wing Aircraft with Vectored Thrust. NASA TP-1222, 1979.

6. Meyer, G.: On the Use of Euler's Theorem on Rotations for the Synthesis of Attitude Control Systems. NASA TN D-3643, 1966.

7. Sidar, M.; and Doolin, B. F.: On the Feasibility of Real-Time Predictions of Aircraft Carrier Motion at Sea. NASA TM X-62454, 1975.

8. Meyer, G.; Lee, H. Q.; and Wehrend, W. R., Jr.: A Method for Expanding a Direction Cosine Matrix into an Euler Sequence of Rotations. NASA TM X-1384, 1967.

TABLE 1.- SUMMARY OF 160 SIMULATED APPROACHES WITH TURBULENCE.

Condition	Dispersion
Maximum deck displacement due to pitch and heave	2.4 m (8 ft)
Mean touchdown error (long)	3.9 m (13 ft)
Standard deviation of touchdown error	6.7 m (22 ft)
Mean ramp clearance	4.9 m (16 ft)
Standard deviation of ramp clearance	0.9 m (3 ft)
Touchdowns beyond allowable area	6
Touchdowns short of allowable area	0

TABLE 2.- CLOSED TRAJECTORY PARAMETERS.

Segment number	Trajectory type		Climb angle, deg	Path length		Duration, deg	Radius	
				m	ft		m	ft
1	Straight	level	---	512	1680	---	---	---
2	Straight	climb	3	349	1146	---	---	---
3	Helical		3			90	1524	5000
4	Straight	↓	3	914	3000	---	---	---
5	Helical		3	---	---	64	1524	5000
6	Circular	level	---	---	---	71	1524	5000
7	Straight			1755	5760	---	---	---
8	Circular			---	---	45	1524	5000
9	Straight			3947	12950	---	---	---
10	Circular			---	---	180	914	3000
11	Straight	↓	↓	628	2060	---	---	---
12	↓	descend	-6	2509	8230			
13		descend	-0.9	1161	3810			
14	↓	level	---	610	2000	↓	↓	↓

MARSHAL
POINT

DESCENT

APPROACH
COURSE

CHECKOFF

RADAR
LOCKON

TIPOVER

DECK MOTION
FOLLOWING
12 sec

WAVEOFF
CONTROL
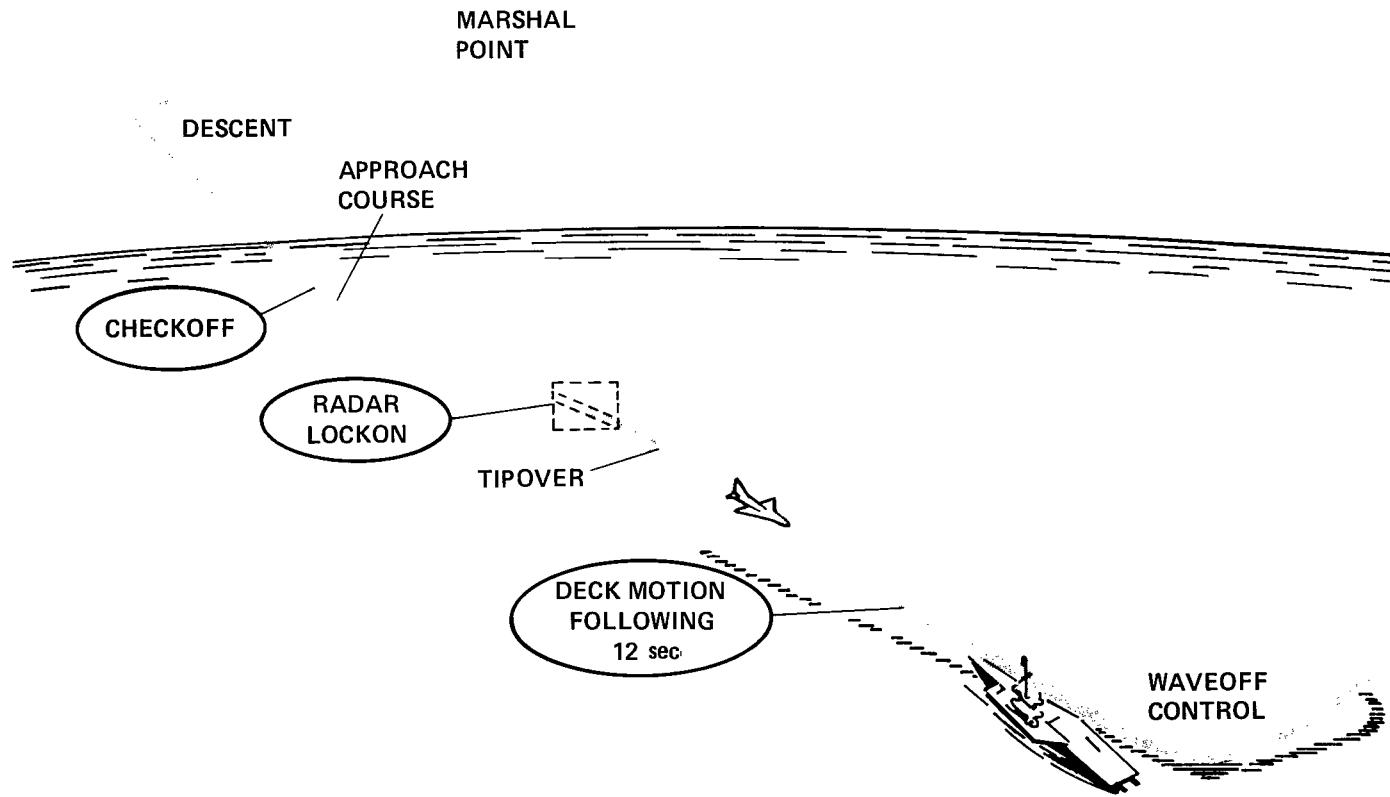
Figure 1.- Aircraft carrier landing situation.

COMMANDED ROLL ANGLE

ROUGH-COMMANDED TRAJECTORY
SMOOTH-COMMANDED ACCELERATION
COMMANDED LIFT AND DRAG COEFFICIENTS
COMMANDED ALPHA
COMMANDED ATTITUDE
ϕ_c
COMMANDED ANGULAR ACCELERATION
COMMANDED MOMENT COEFFICIENTS

COMMANDED AILERON
COMMANDED SPOILERS
COMMANDED RUDDER
COMMANDED STABILIZER

| DESIRED TRAJECTORY SEGMENTS | TRAJECTORY COMMAND SEQUENCER | TRAJECTORY COMMAND GENERATOR | COEFFICIENT DEVELOPMENT | FORCE TRIM MAP (INVERT LIFT AND DRAG TABLES) | ATTITUDE COMMAND GENERATOR | COEFFICIENT DEVELOPMENT | MOMENT TRIM MAP (INVERT MOMENT TABLES) | AIRCRAFT |

$\dot{V}_c$
c_{L_c}
c_{D_c}
α_c
$\dot{\omega}_c$

COMMANDED FLIGHTPATH ANGLES
Γ_c ψ_c

COMMANDED THRUST COEFFICIENT
c_{T_c}

| ENGINE THRUST TABLE (INVERTED) |

COMMANDED THROTTLE ANGLE

Figure 2.- Basic open-loop feed-forward control concept.

FEEDBACK LOOPS
$\hat{R}$
$\hat{V}$
$\hat{A}_{as}$
$\hat{\omega}$

COMMANDED ATTITUDE

| TRAJECTORY REGULATOR | | ATTITUDE REGULATOR | |

f_{cc}
COMMANDED ROLL ANGLE ϕ_c
$\dot{\omega}_{cc}$

ROUGH-COMMANDED TRAJECTORY
COMMANDED SPECIFIC FORCE
COMMANDED LIFT AND DRAG COEFFICIENTS
COMMANDED ALPHA
COMMANDED ANGULAR ACCELERATION
COMMANDED MOMENT COEFFICIENTS

COMMANDED AILERON
COMMANDED SPOILERS
COMMANDED RUDDER
COMMANDED STABILIZER

R_c V_c
A_{as_c} ω_c

| DESIRED TRAJECTORY SEGMENTS | TRAJECTORY COMMAND SEQUENCER | TRAJECTORY COMMAND GENERATOR | COEFFICIENT DEVELOPMENT | FORCE TRIM MAP (INVERT LIFT AND DRAG TABLES) | ATTITUDE COMMAND GENERATOR | COEFFICIENT DEVELOPMENT | MOMENT TRIM MAP (INVERT MOMENT TABLES) | AIRCRAFT |

f_{oc}
f_{tc}
c_{L_c}
c_{D_c}
α_c
$A_{as_{rc}}$
$\dot{\omega}_{oc}$
$\dot{\omega}_c$
c_{ℓ_c}
c_{m_c}
c_{n_c}

COMMANDED FLIGHTPATH ANGLES
Γ_c ψ_c

COMMANDED THRUST COEFFICIENT
c_{T_c}

| ENGINE THRUST TABLE (INVERTED) |

COMMANDED THROTTLE ANGLE

Figure 3.- Total aircraft flight-control system (TAFCOS).
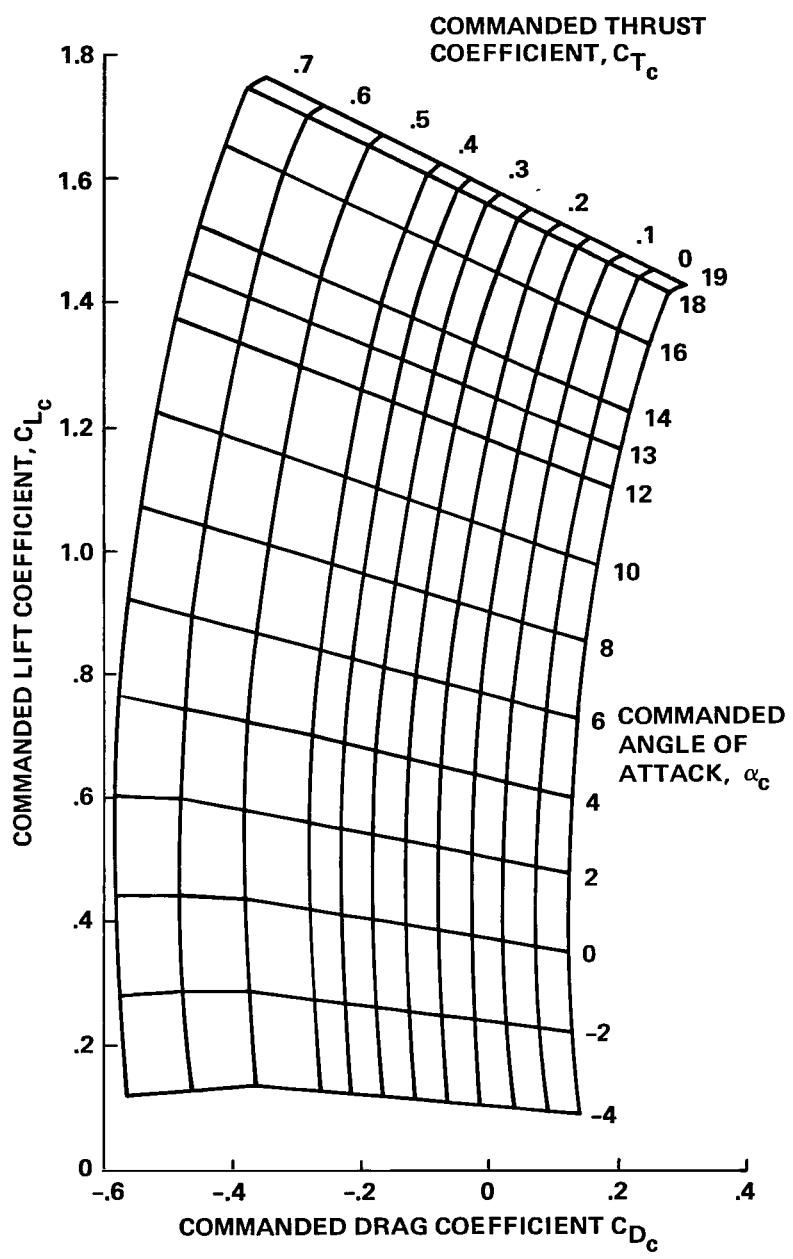
Figure 4.- Force trim map.
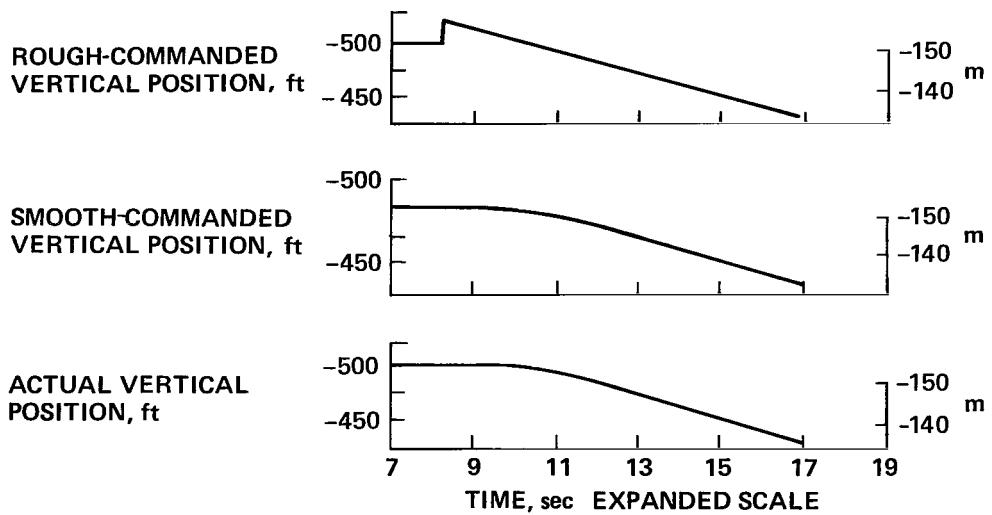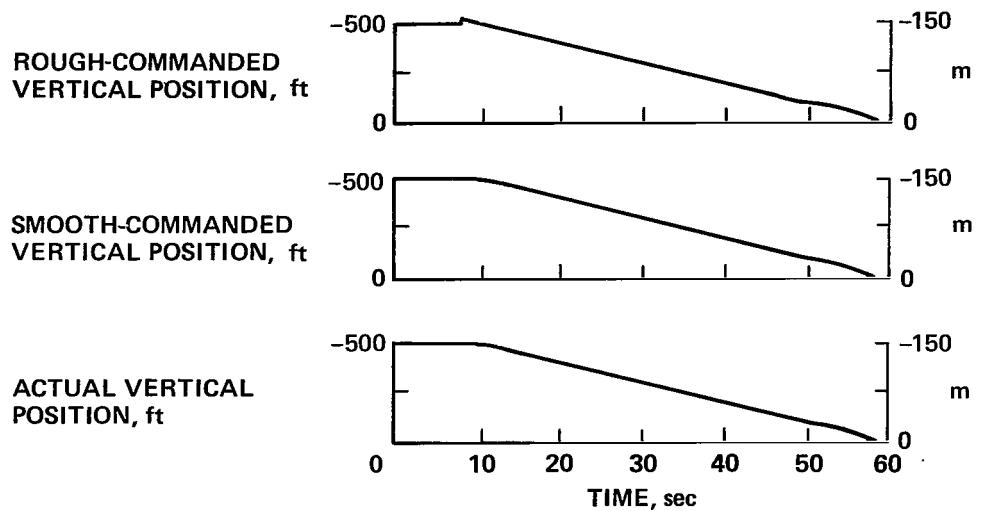
(a) Trajectory variables.

Figure 5.- Tip-over run without turbulence.
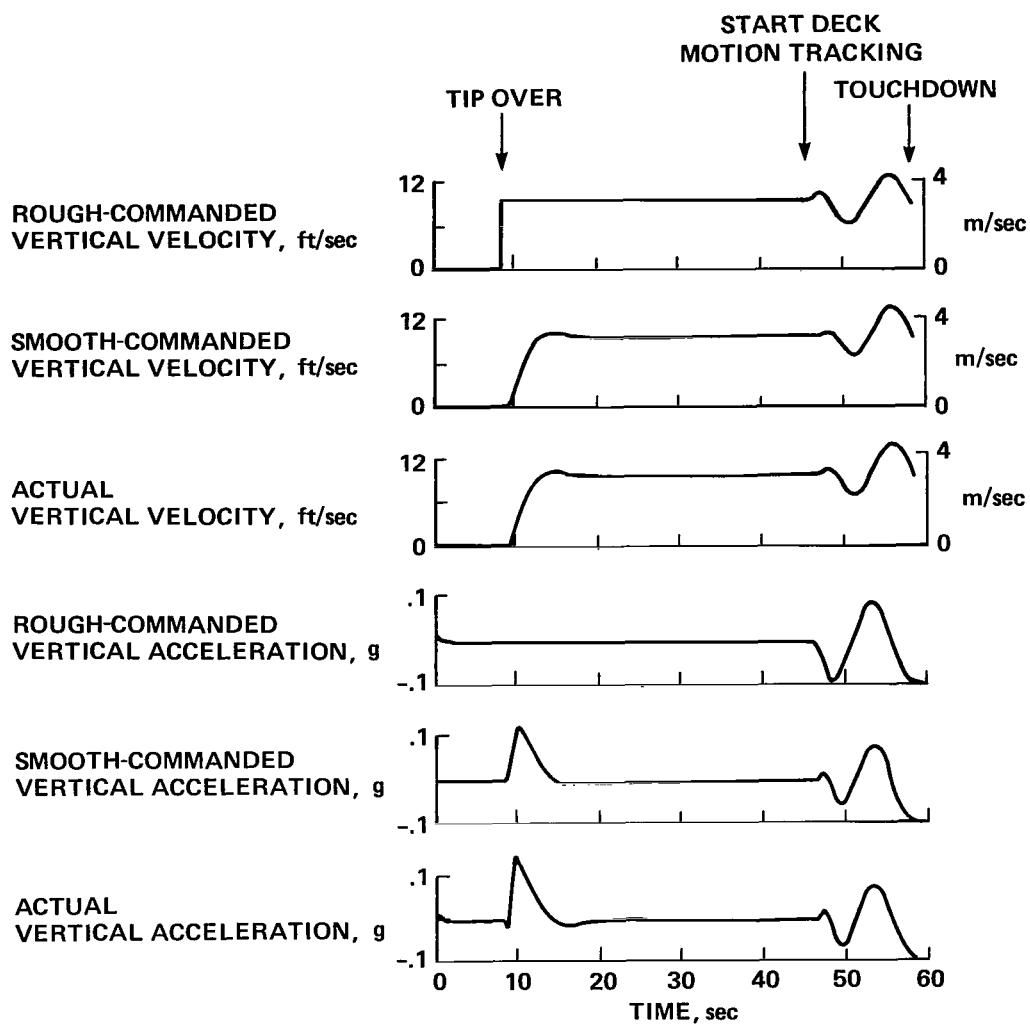
(a) Trajectory variables – Concluded.

Figure 5.– Tip-over run without turbulence – Continued.
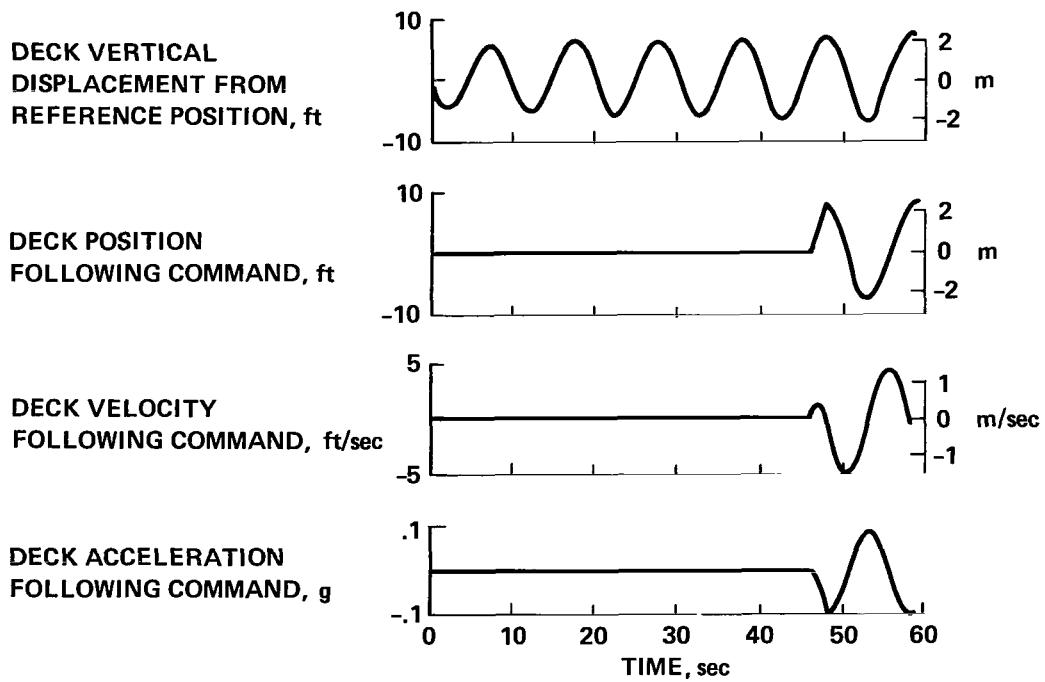
(b) Vertical deck motion variables.

Figure 5.- Tip-over run without turbulence - Continued.
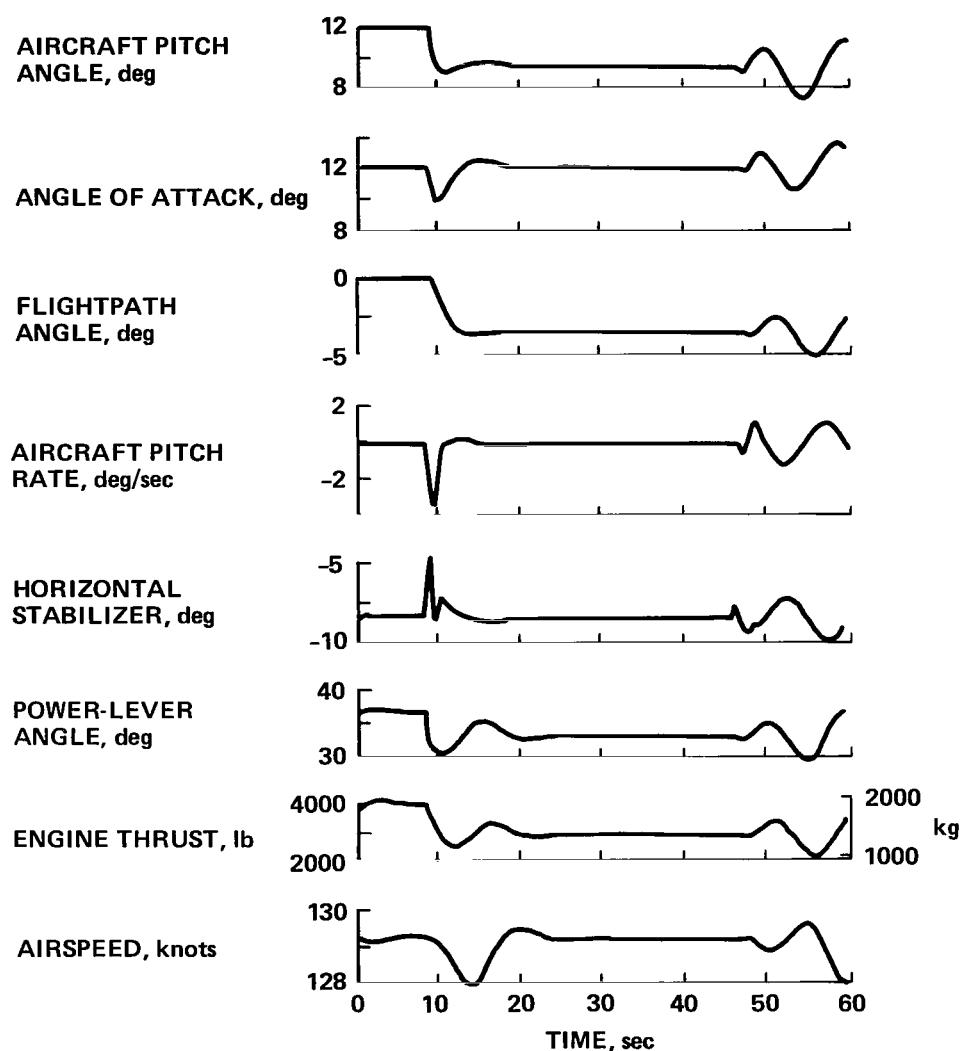
(c) Aircraft variables.

Figure 5.- Tip-over run without turbulence - Continued.
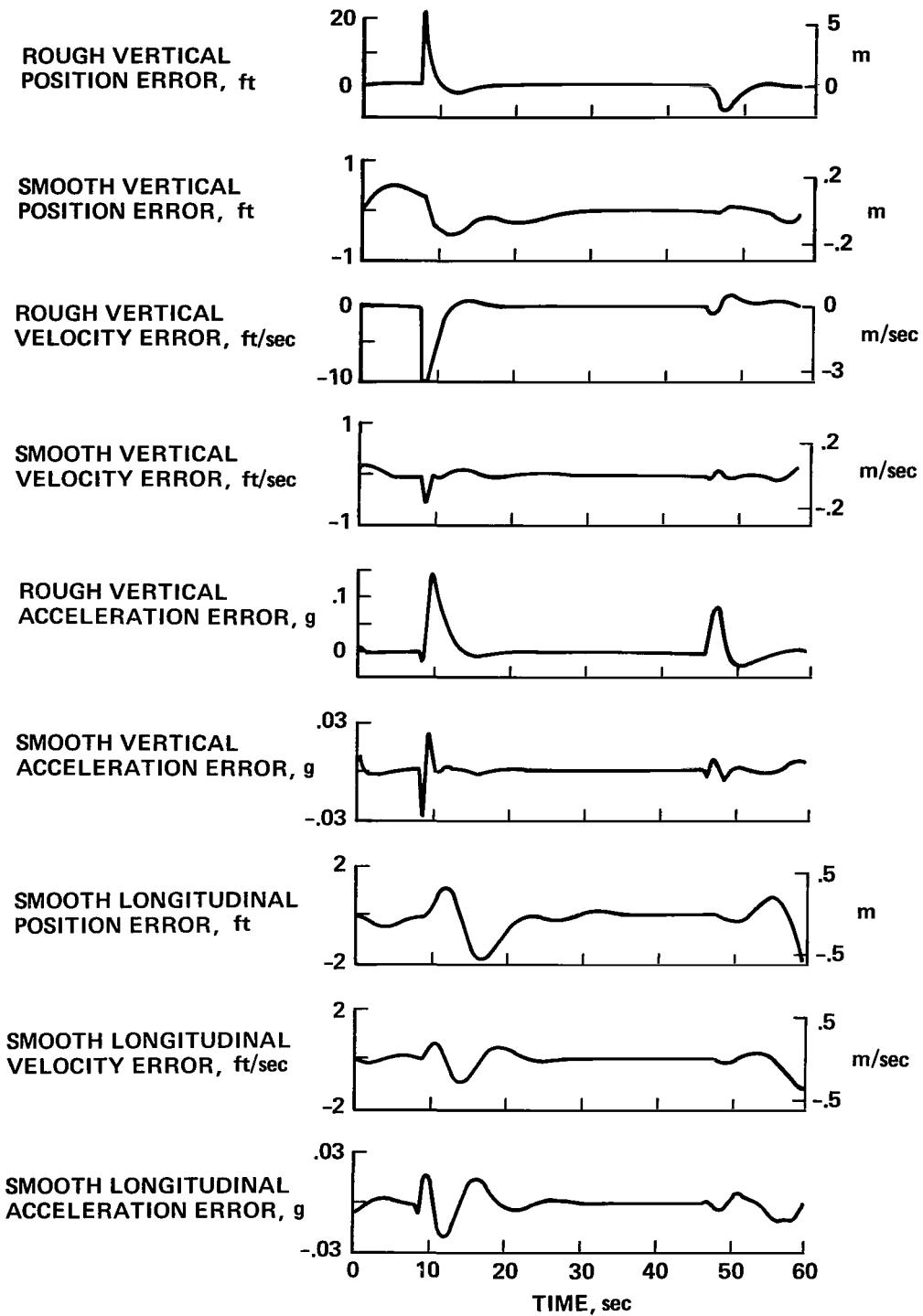
(d) Trajectory errors.

Figure 5.- Tip-over run without turbulence - Continued.

VERTICAL FEED FORWARD SPECIFIC FORCE SIGNAL f_{oc}, g

VERTICAL FEEDBACK SPECIFIC FORCE SIGNAL f_{cc}, g

VERTICAL TOTAL SPECIFIC FORCE SIGNAL f_{tc}, g

LONGITUDINAL FEED FORWARD SPECIFIC FORCE SIGNAL f_{oc}, g

LONGITUDINAL FEEDBACK SPECIFIC FORCE SIGNAL f_{cc}, g

LONGITUDINAL TOTAL SPECIFIC FORCE SIGNAL f_{tc}, g

TIME, sec
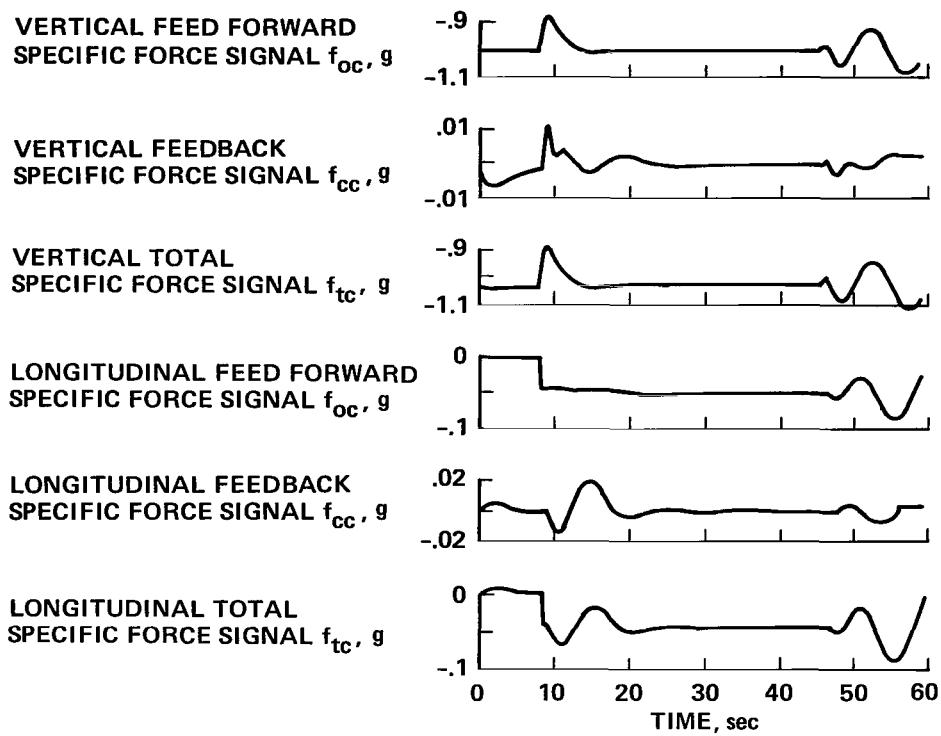
(e) Internal feed-forward and feedback signals.

Figure 5.- Tip-over run without turbulence – Continued.

53

POWER-LEVER ANGLE, deg

ENGINE THRUST, lb

FORWARD VELOCITY WITH RESPECT TO DECK, knots

FORWARD ACCELERATION WITH RESPECT TO DECK, g

AIRSPEED, knots

TIME, sec
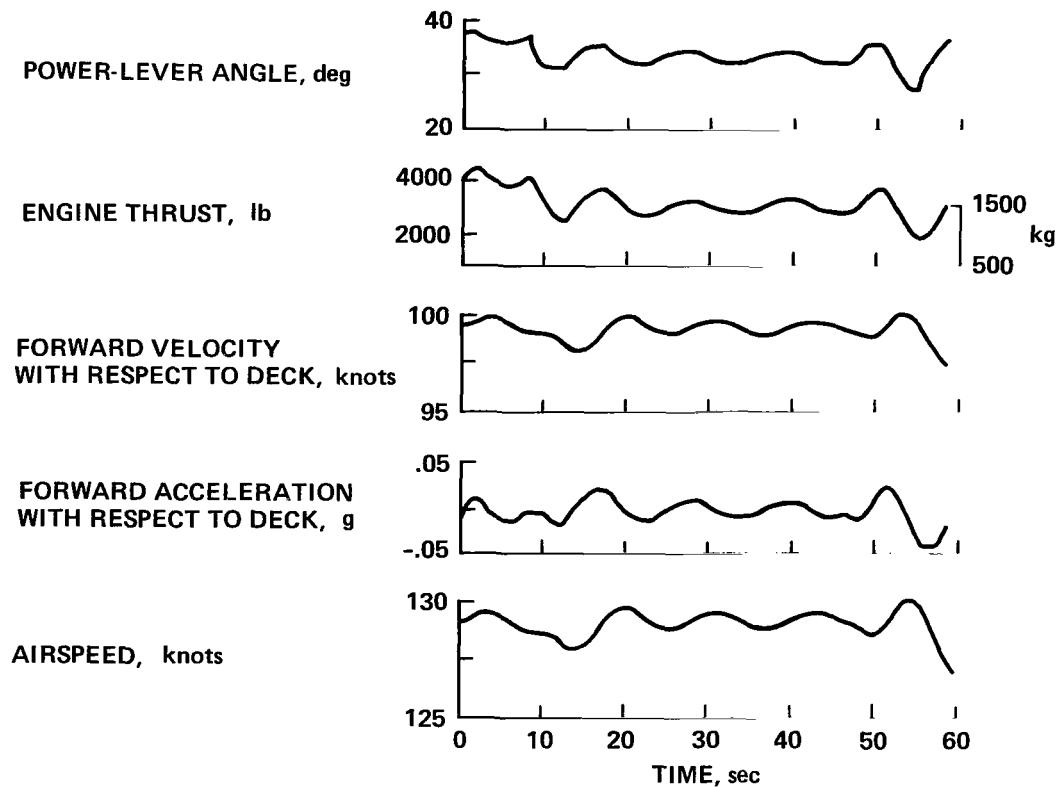
(f) Radar signal lost at 150 m (493 ft) before touchdown, throttle hysteresis included. Plots of major variables that were noticeably affected.

Figure 5.- Tip-over run without turbulence - Continued.
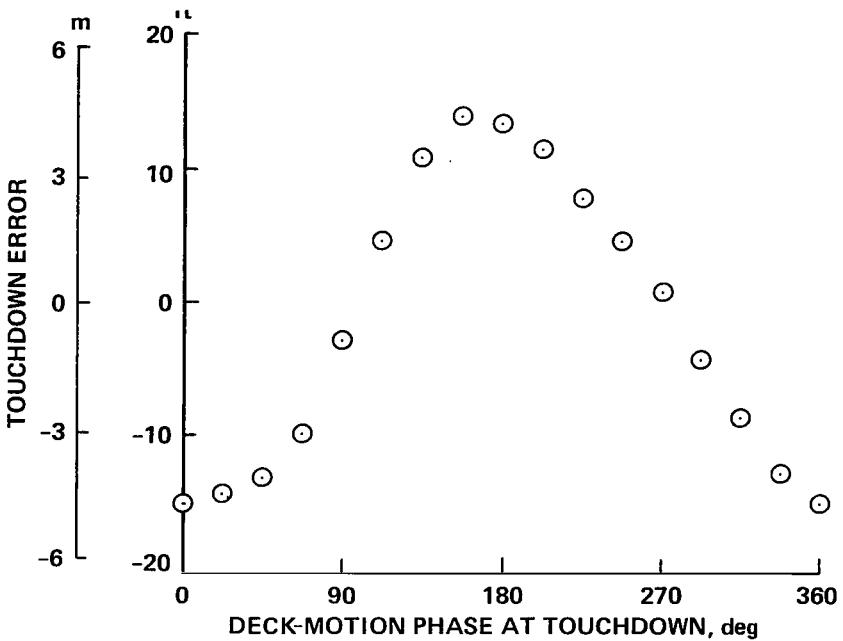
(g) Touchdown error as a function of deck-motion phase.
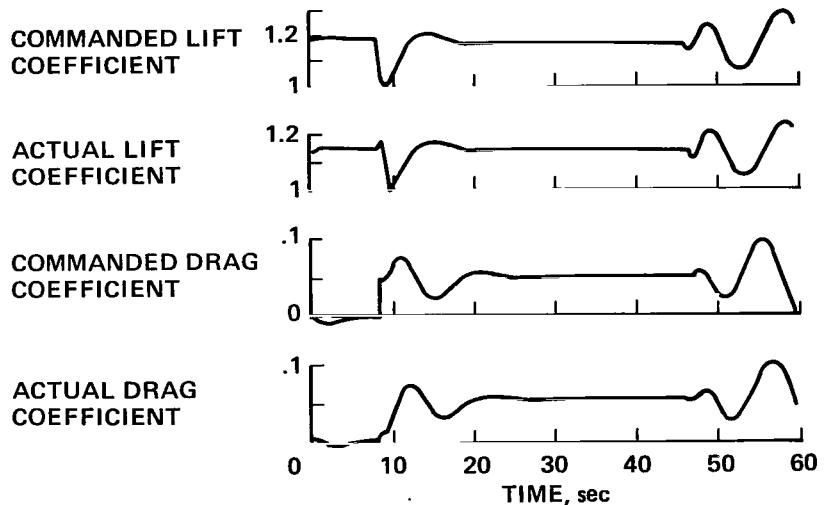
(h) Commanded and actual lift and drag coefficients.

Figure 5.- Tip-over run without turbulence - Concluded.
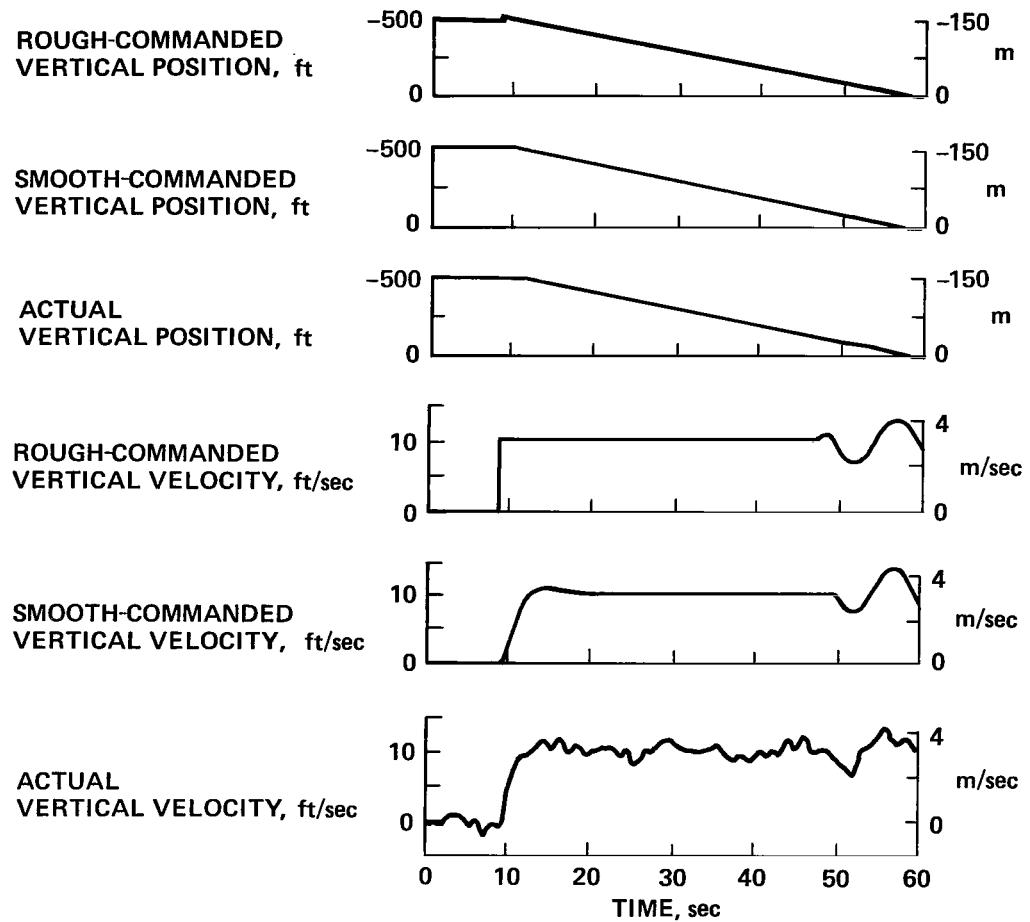
(a) Trajectory variables.

Figure 6.- Tip-over run with turbulence.
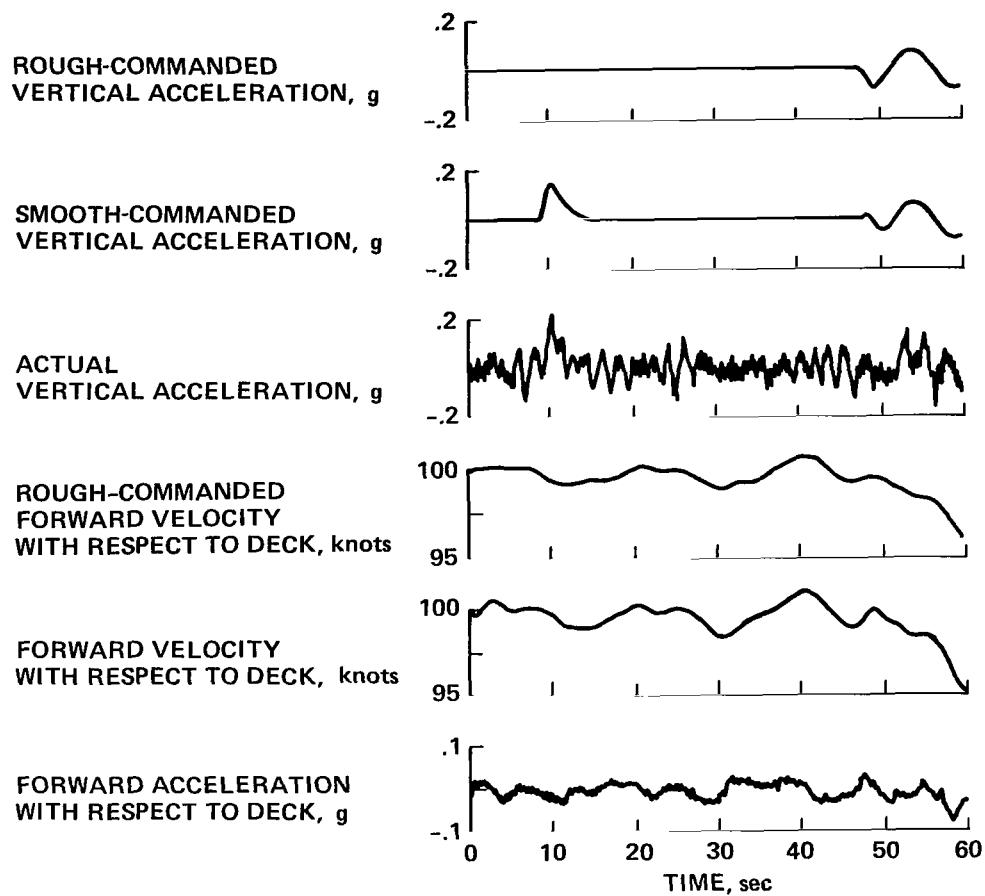
(a) Trajectory variables – Concluded.

Figure 6.– Tip-over run with turbulence – Continued.
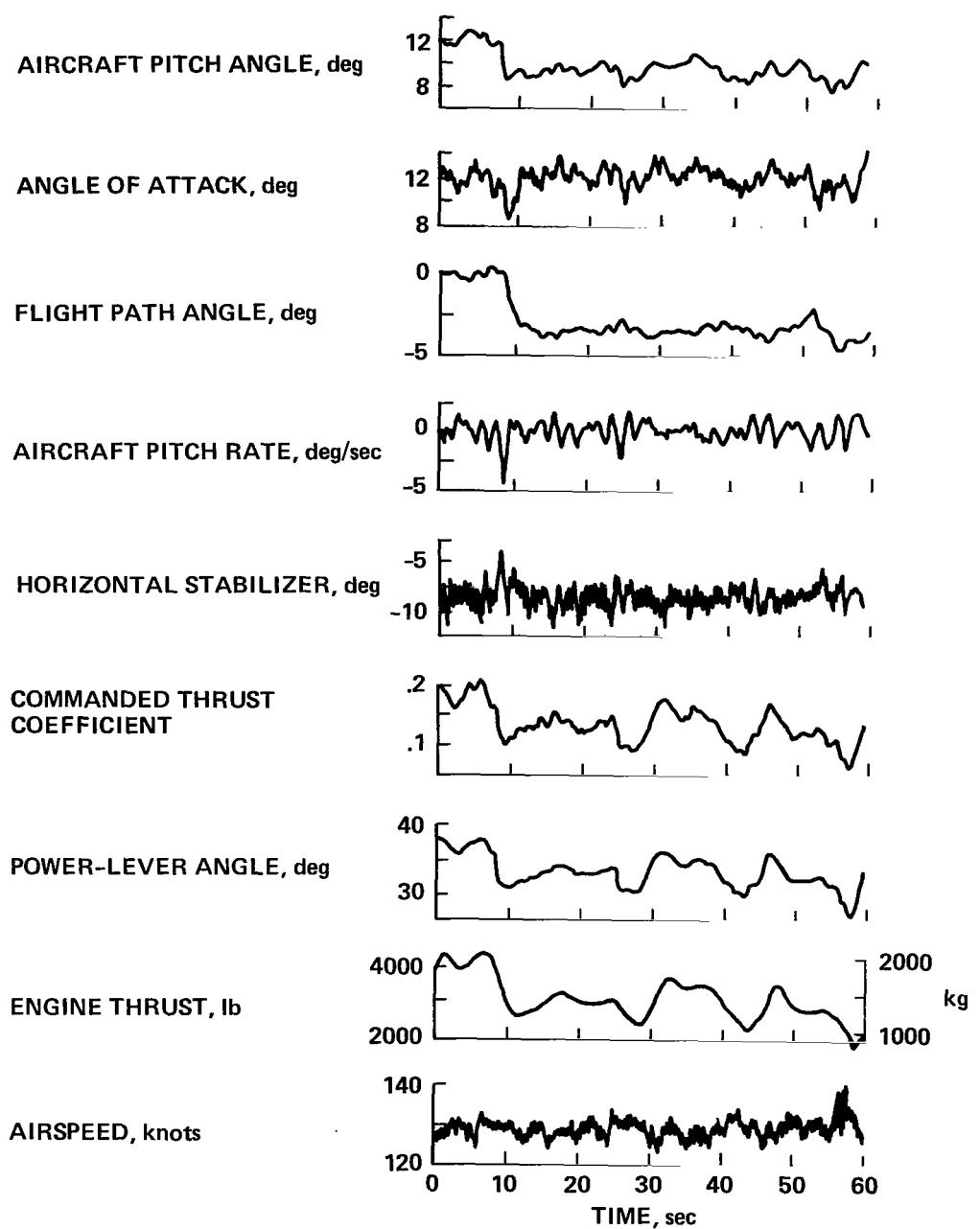
(b) Aircraft variables.

Figure 6.– Tip-over run with turbulence – Continued.
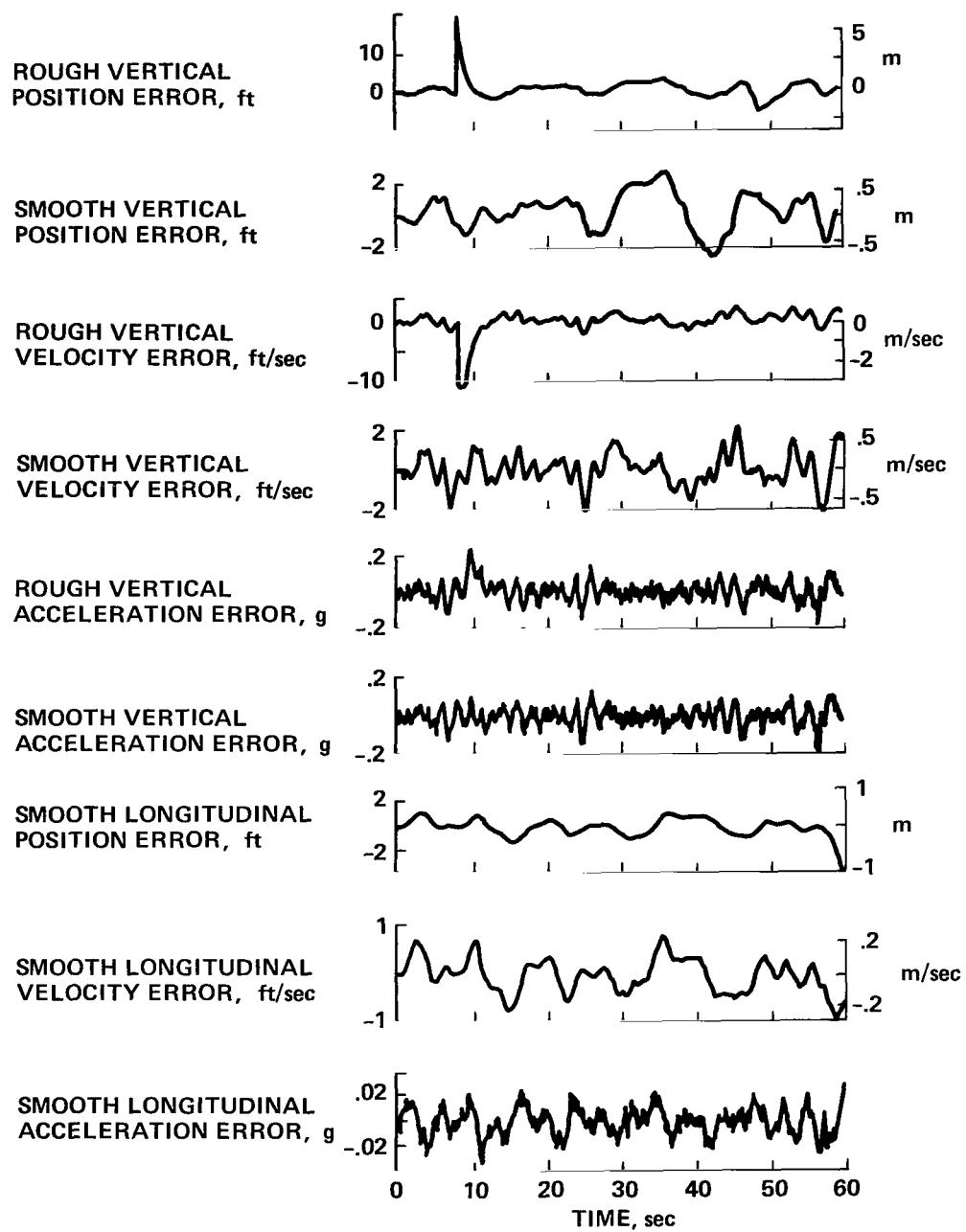
(c) Trajectory errors.

Figure 6.– Tip-over run with turbulence – Continued.
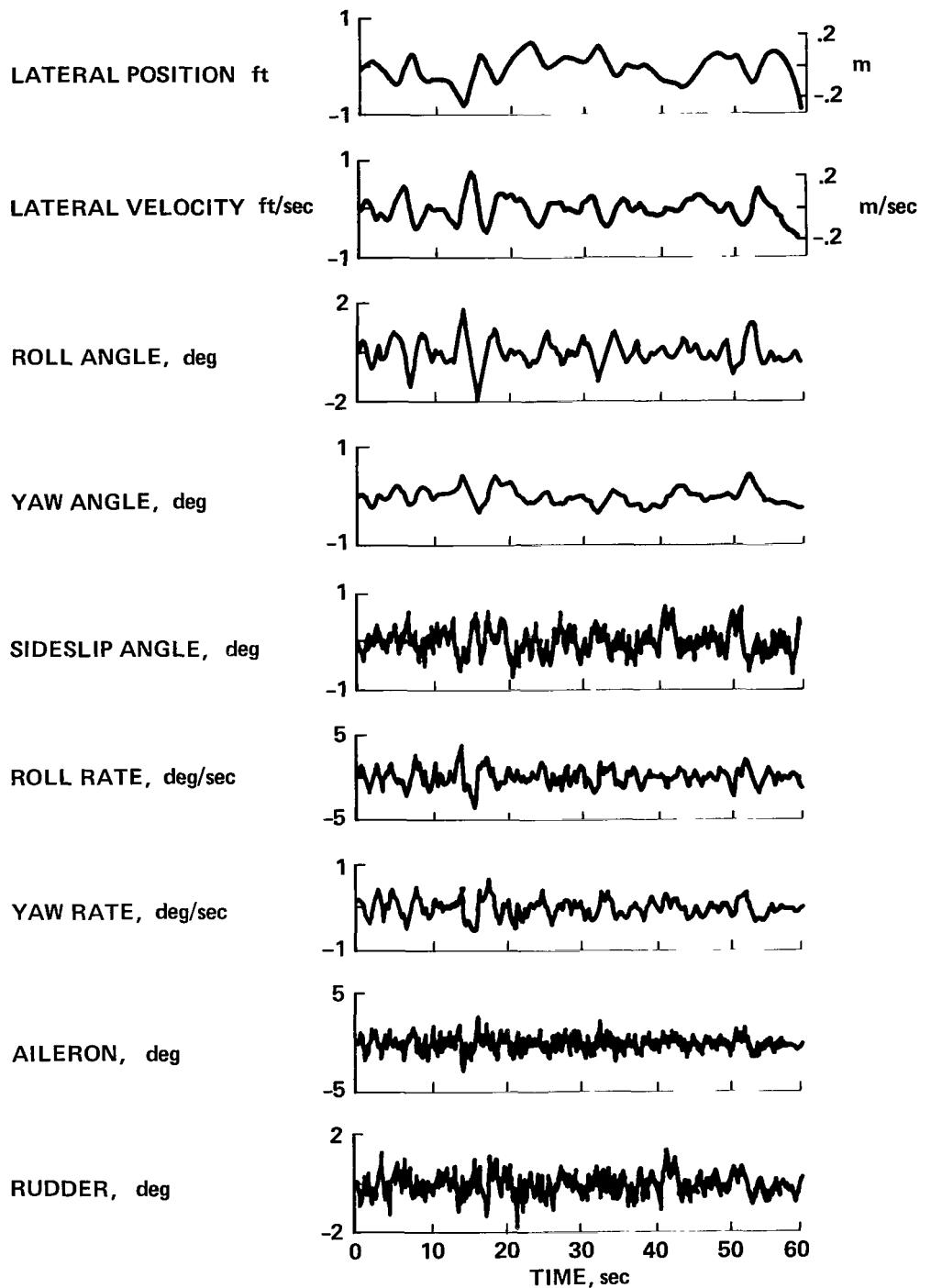
(d) Lateral variables.

Figure 6.- Tip-over run with turbulence - Continued.

LONGITUDINAL TURBULENCE, ft/sec

LATERAL TURBULENCE, ft/sec

VERTICAL TURBULENCE, ft/sec

VERTICAL RADAR ERROR, ft

HORIZONTAL RADAR ERROR, ft
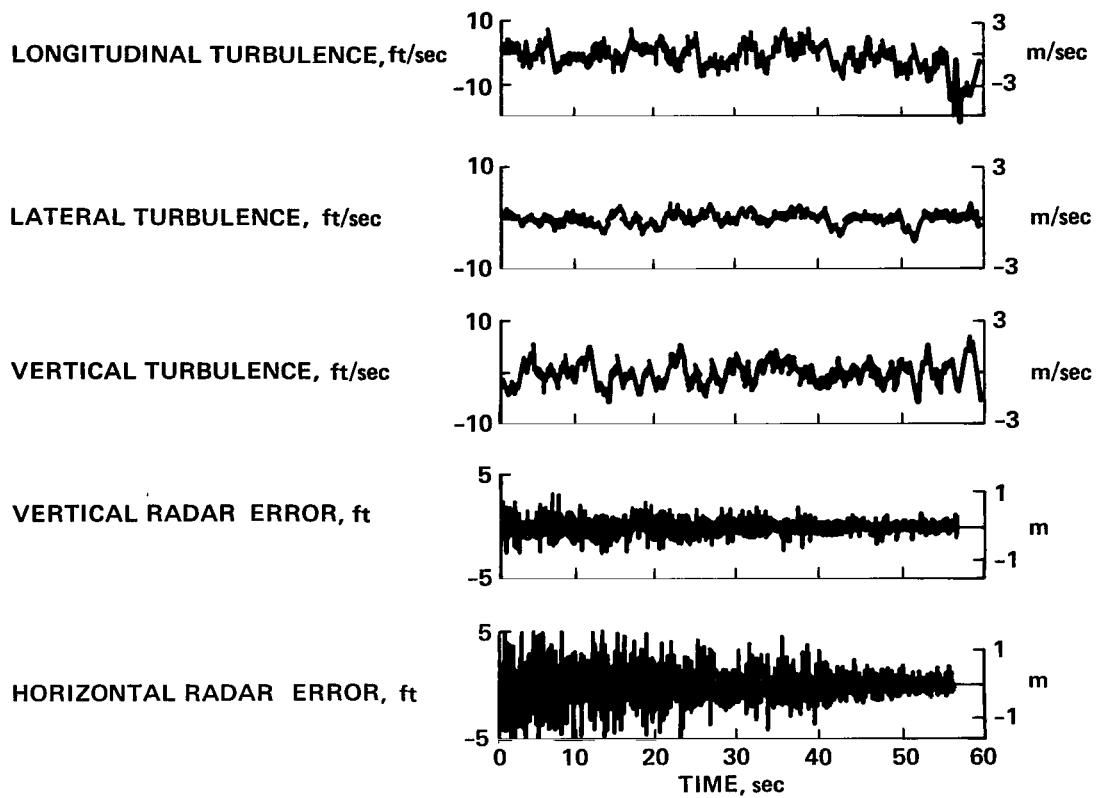
(e) Turbulence and radar noise inputs.

COMMANDED DRAG COEFFICIENT

ACTUAL DRAG COEFFICIENT

COMMANDED LIFT COEFFICIENT

ACTUAL LIFT COEFFICIENT
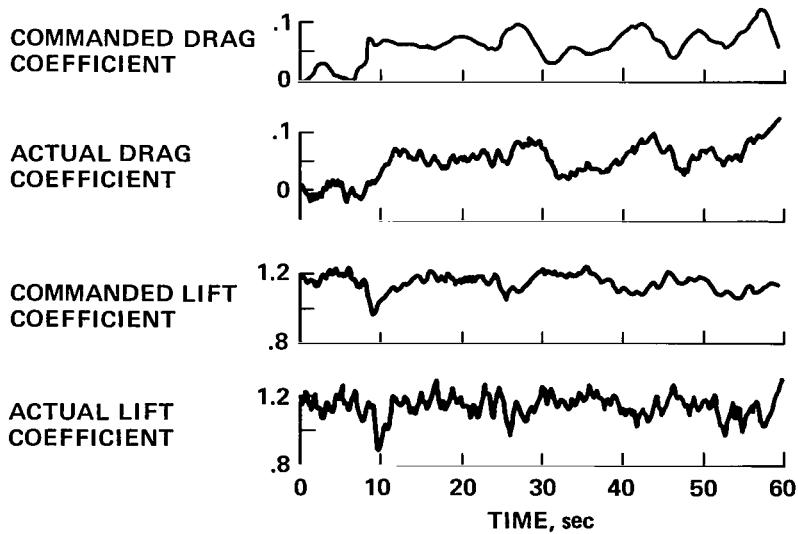
(f) Commanded and actual lift and drag coefficients.

Figure 6.- Tip-over run with turbulence - Concluded.

61
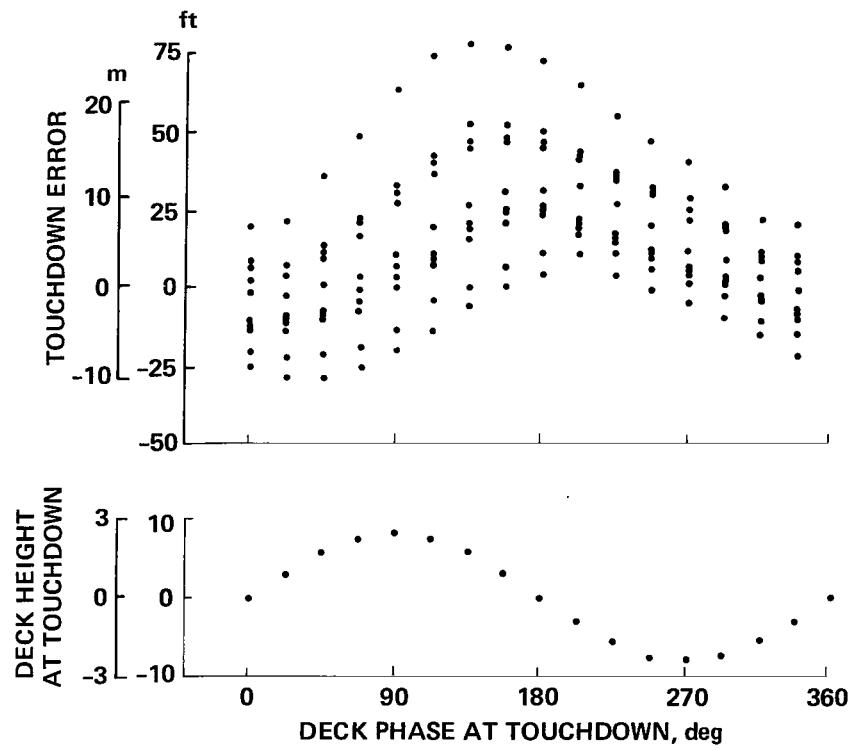
Figure 7.- Landing position errors for 160 runs with turbulence.
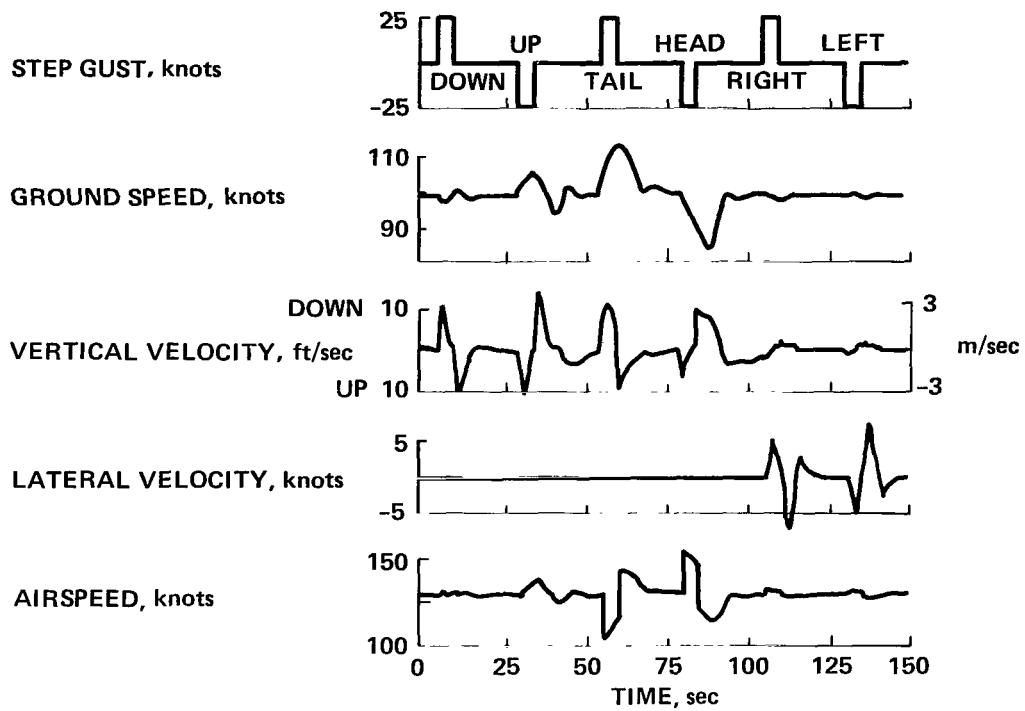
(a) Trajectory variables.
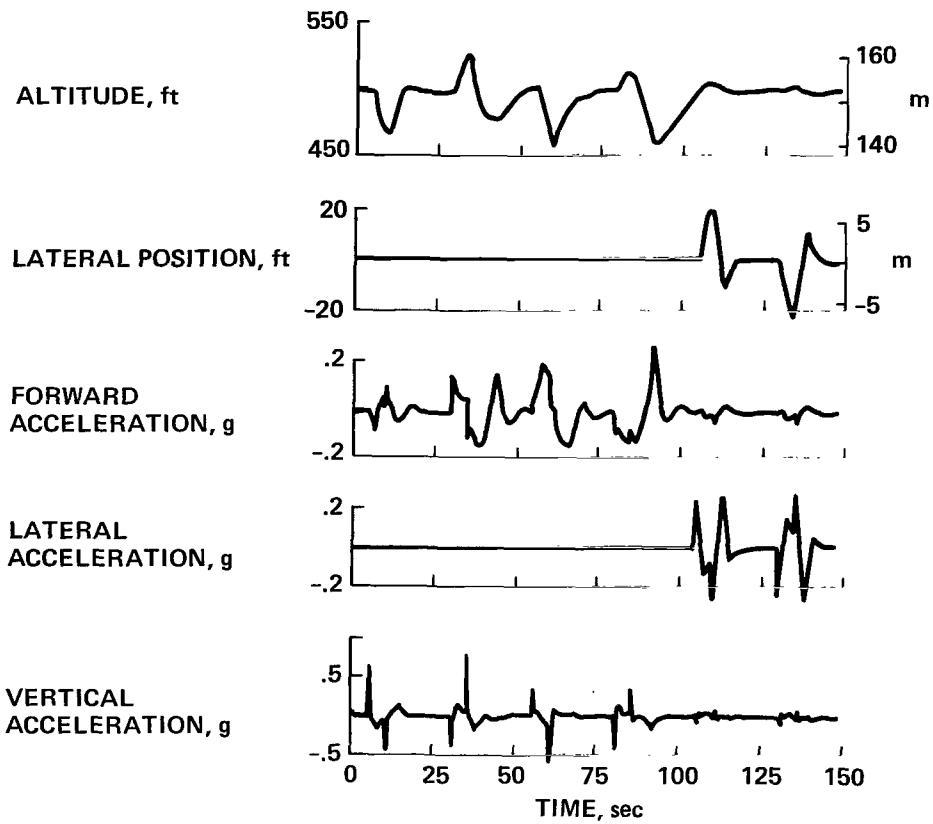
Figure 8.- Level run with step gust disturbances.

(a) Trajectory variables - Concluded.

Figure 8.- Level run with step gust disturbances - Continued.
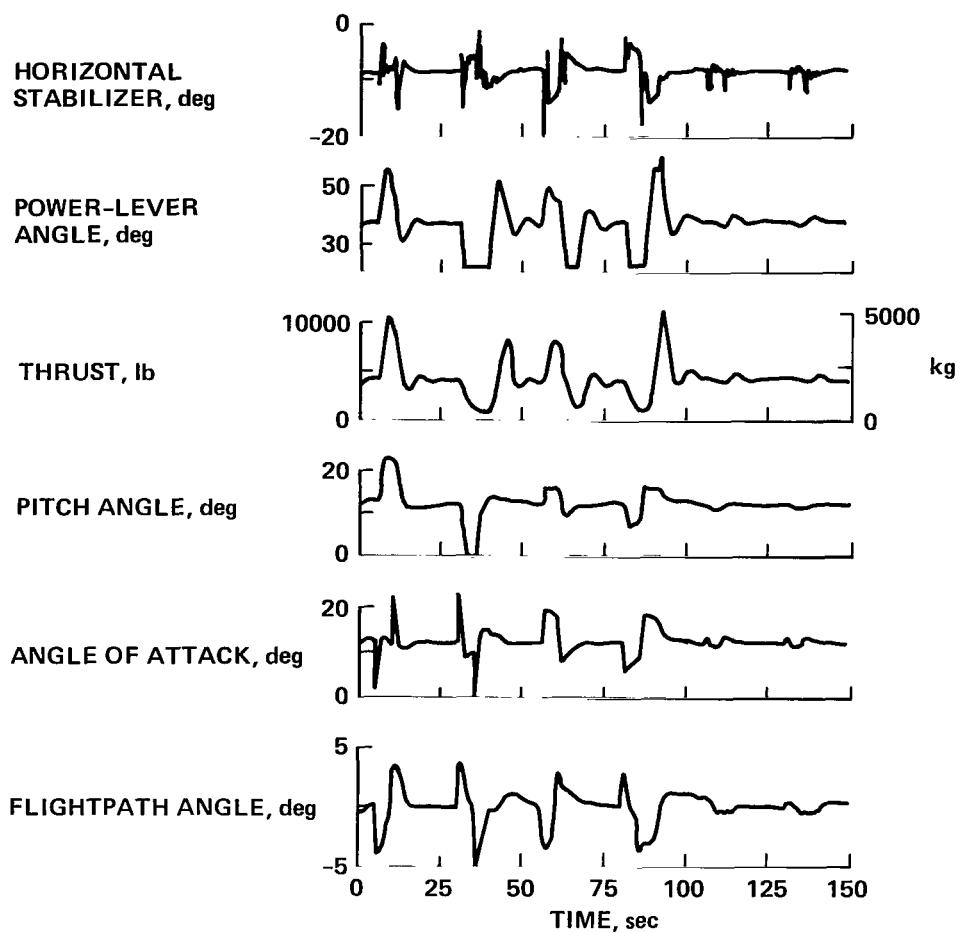
(b) Aircraft variables.

Figure 8.- Level run with step gust disturbances - Continued.
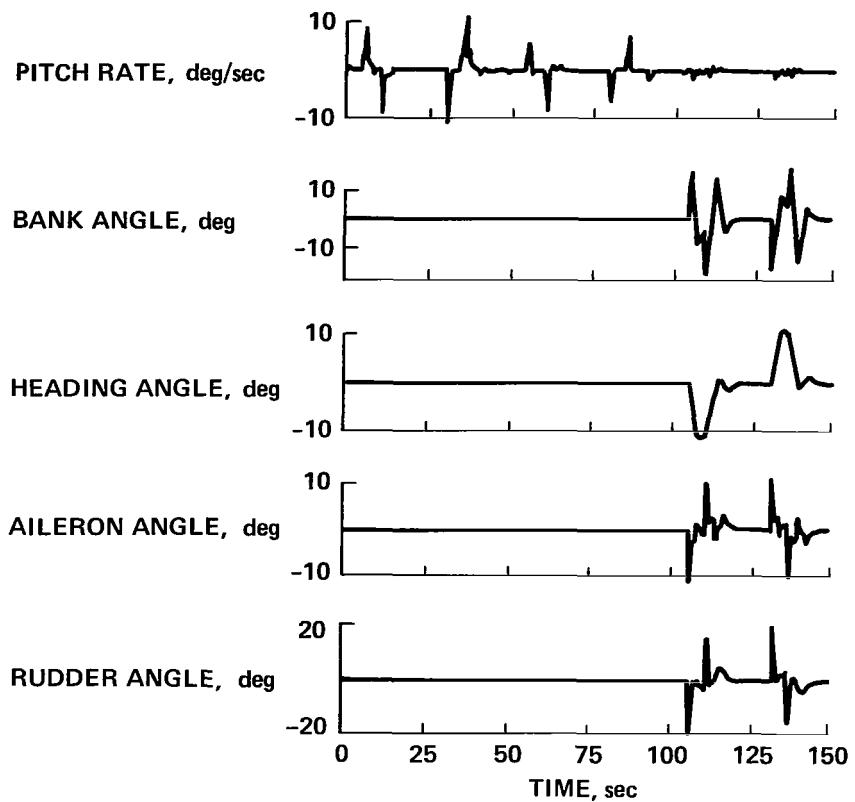
(b) Aircraft variables - Concluded.

Figure 8.- Level run with step gust disturbances - Continued.
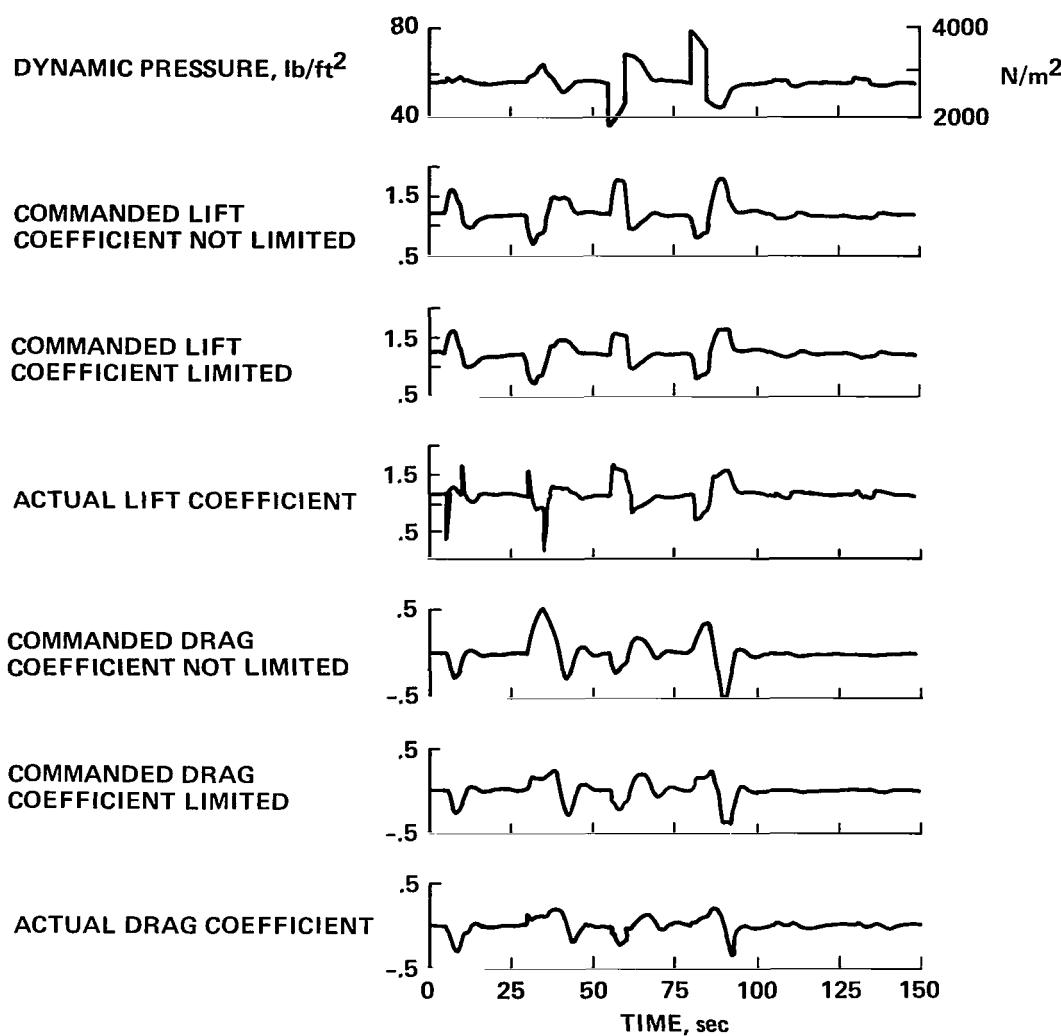
(c) Lift and drag coefficients.

Figure 8.- Level run with step gust disturbances - Continued.
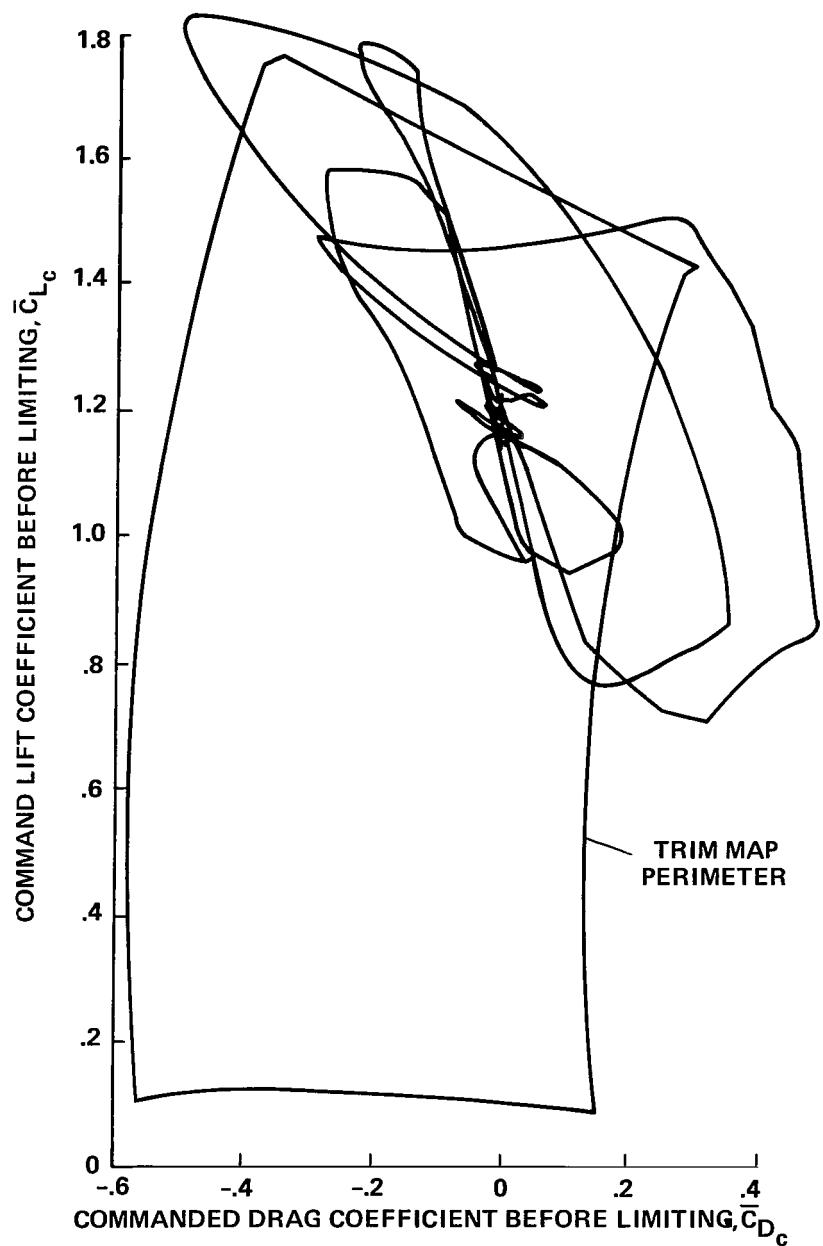
(d) Commanded lift vs drag coefficients, not limited.

Figure 8.- Level run with step gust disturbances - Continued.
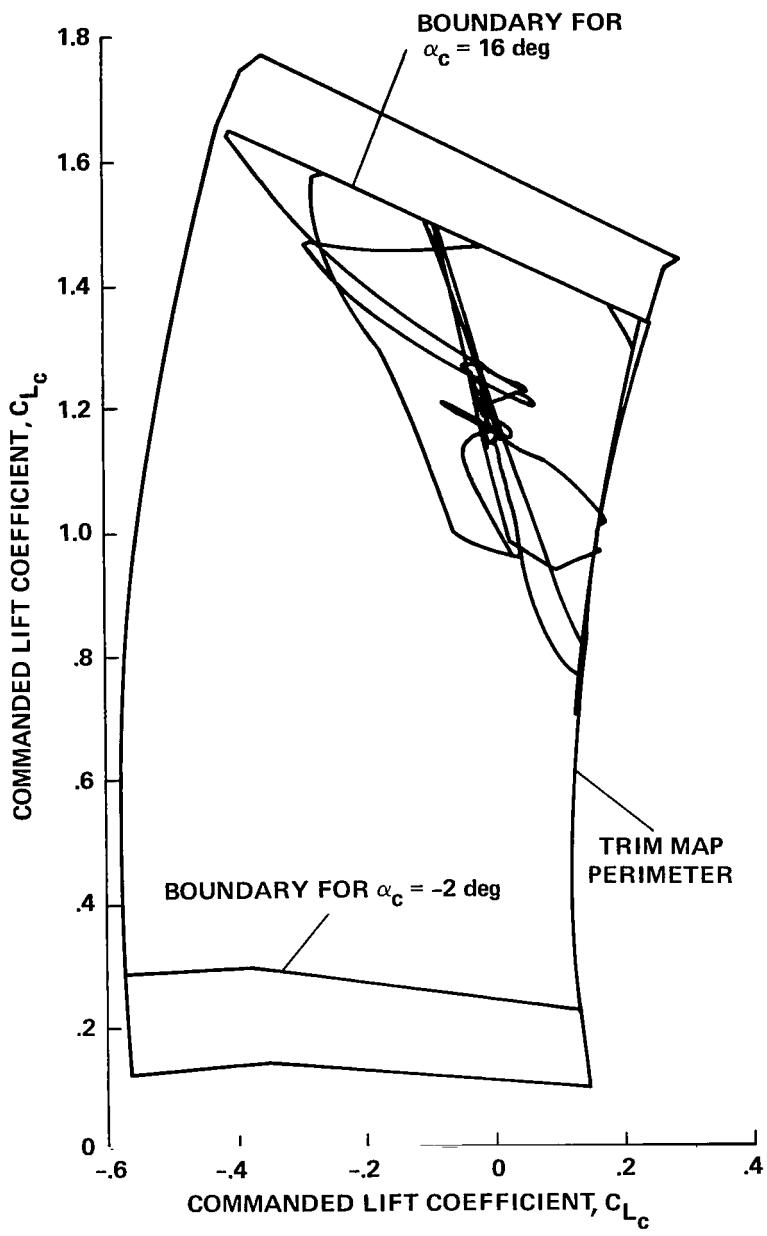
(e) Commanded lift vs drag coefficients.

Figure 8.- Level run with step gust disturbances - Continued.
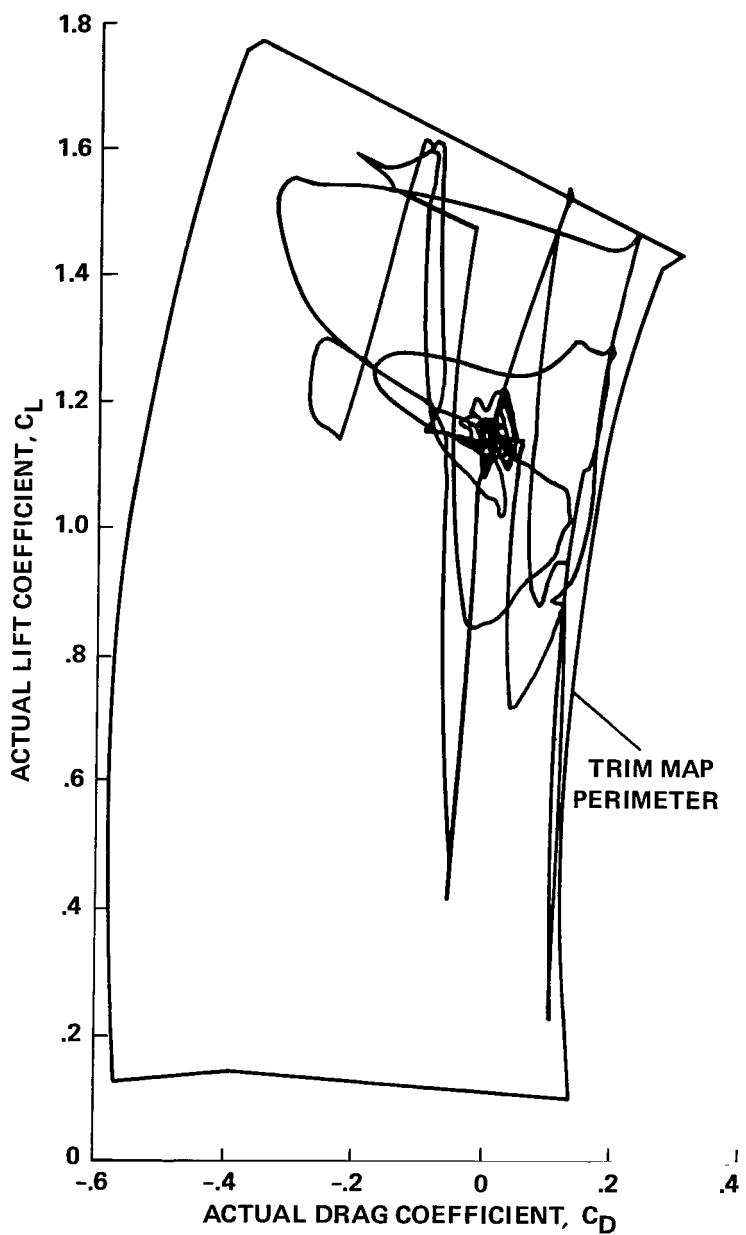
(f) Actual lift vs drag coefficients.

Figure 8.- Level run with step gust disturbances - Concluded.

VERTICAL PROFILE

HORIZONTAL PROFILE
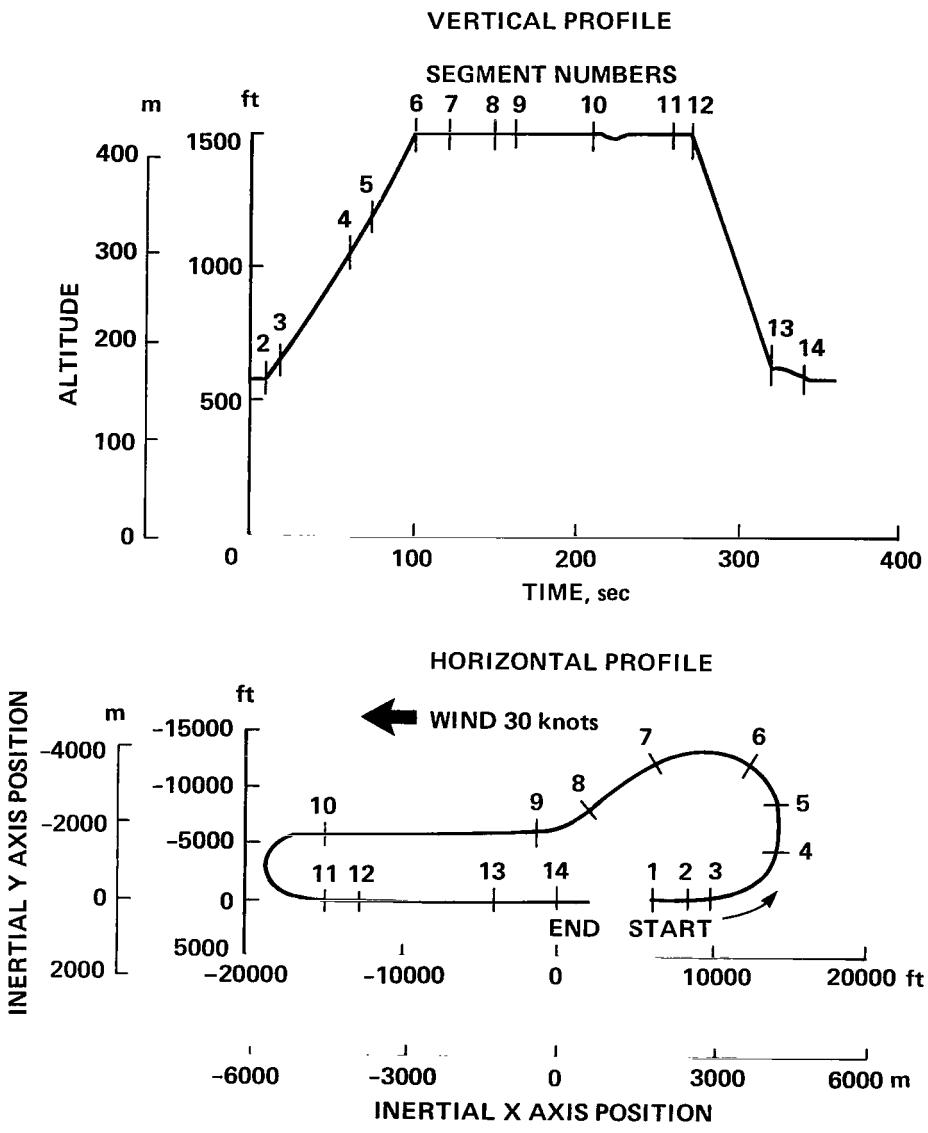
(a) Flight profiles.

Figure 9.- Closed-course trajectory.

ALTITUDE, ft

INERTIAL X AXIS POSITION, ft

INERTIAL Y AXIS POSITION, ft

VERTICAL VELOCITY, ft/sec

INERTIAL X AXIS VELOCITY, knots

INERTIAL Y AXIS VELOCITY, knots

AIRSPEED, knots

TIME, sec
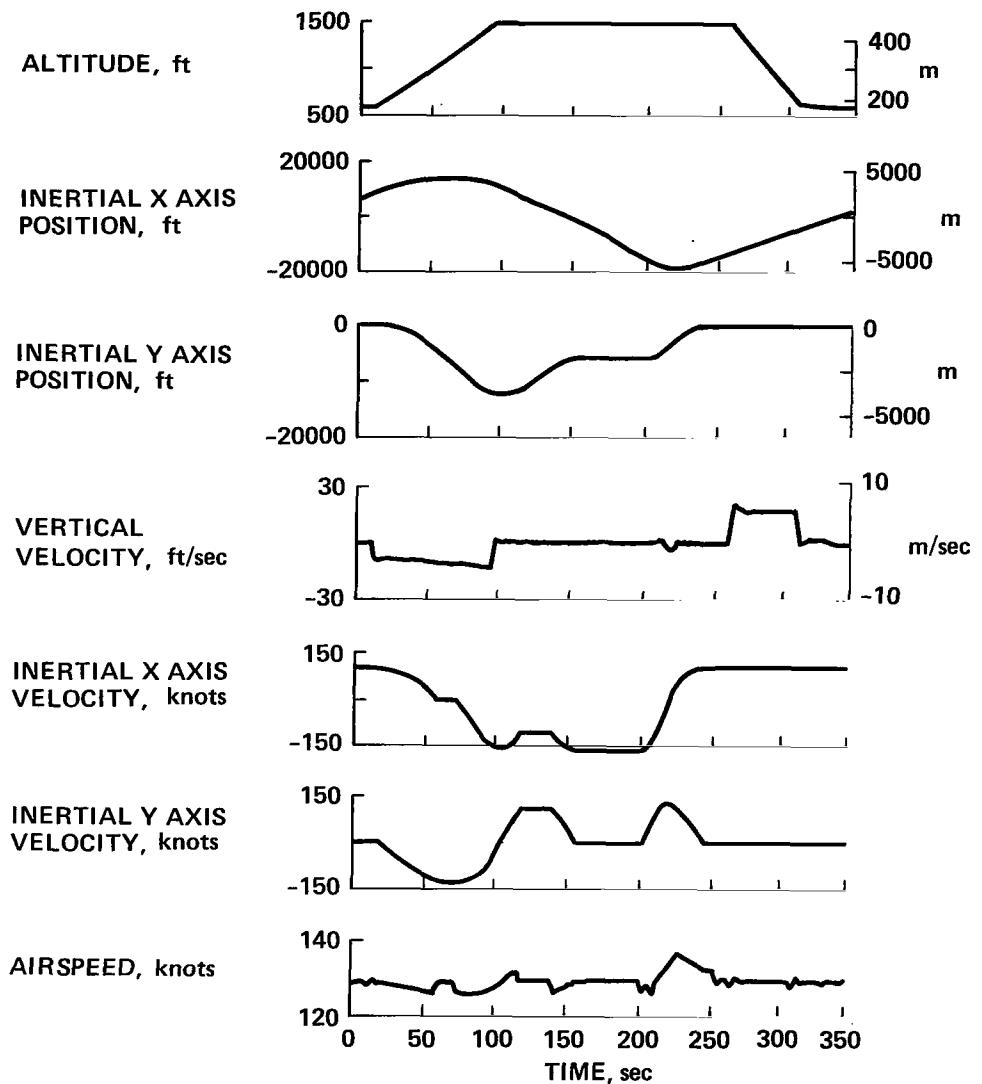
(b) Trajectory variables.

Figure 9.- Closed-course trajectory - Continued.
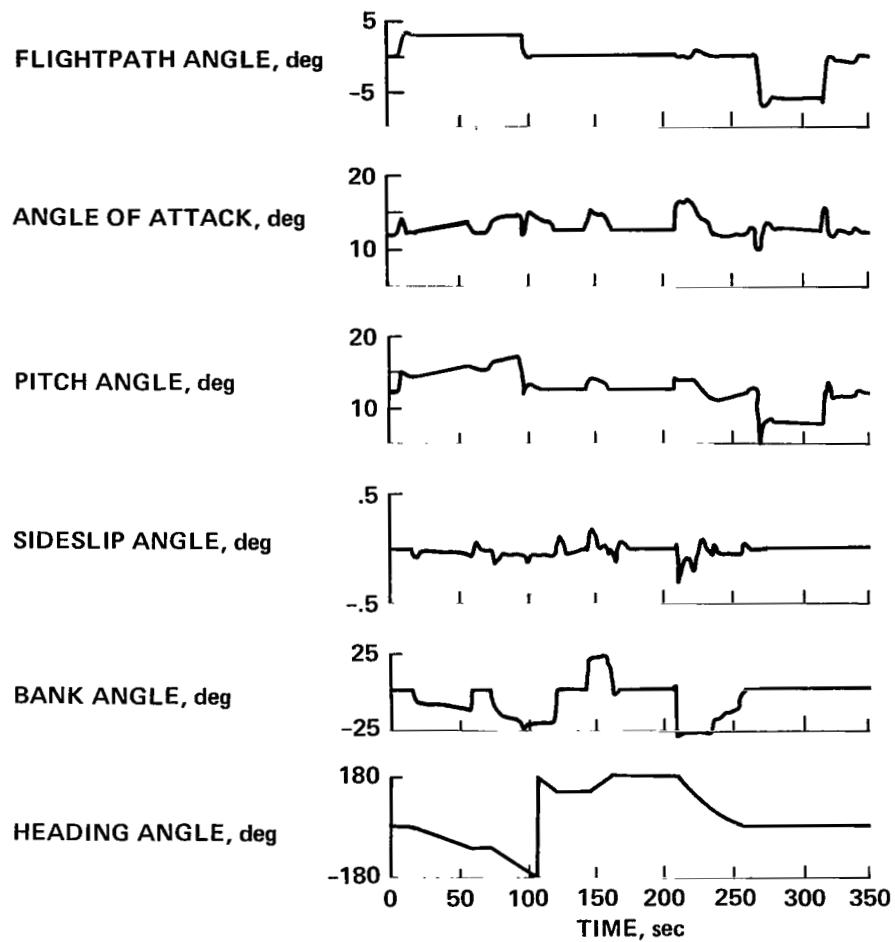
(c) Angle variables.

Figure 9.- Closed-course trajectory - Continued.

(d) Aircraft variables.

Figure 9.- Closed-course trajectory - Continued.

ROUGH INERTIAL Y AXIS POSITION ERROR, ft

SMOOTH INERTIAL Y AXIS POSITION ERROR, ft

ROUGH INERTIAL X AXIS POSITION ERROR, ft

SMOOTH INERTIAL X AXIS POSITION ERROR, ft

ROUGH INERTIAL Z AXIS POSITION ERROR, ft

SMOOTH INERTIAL Z AXIS POSITION ERROR, ft

TIME, sec
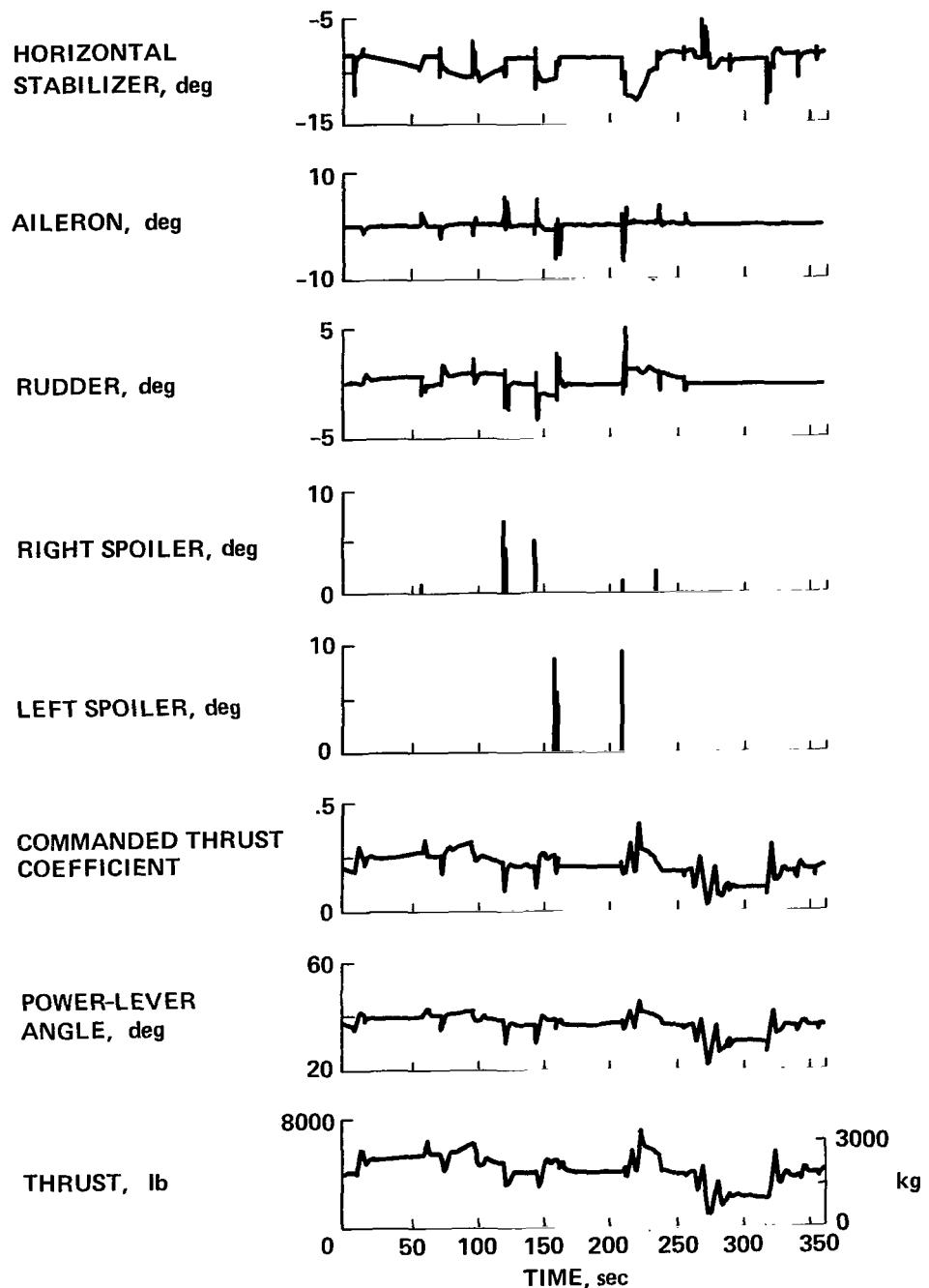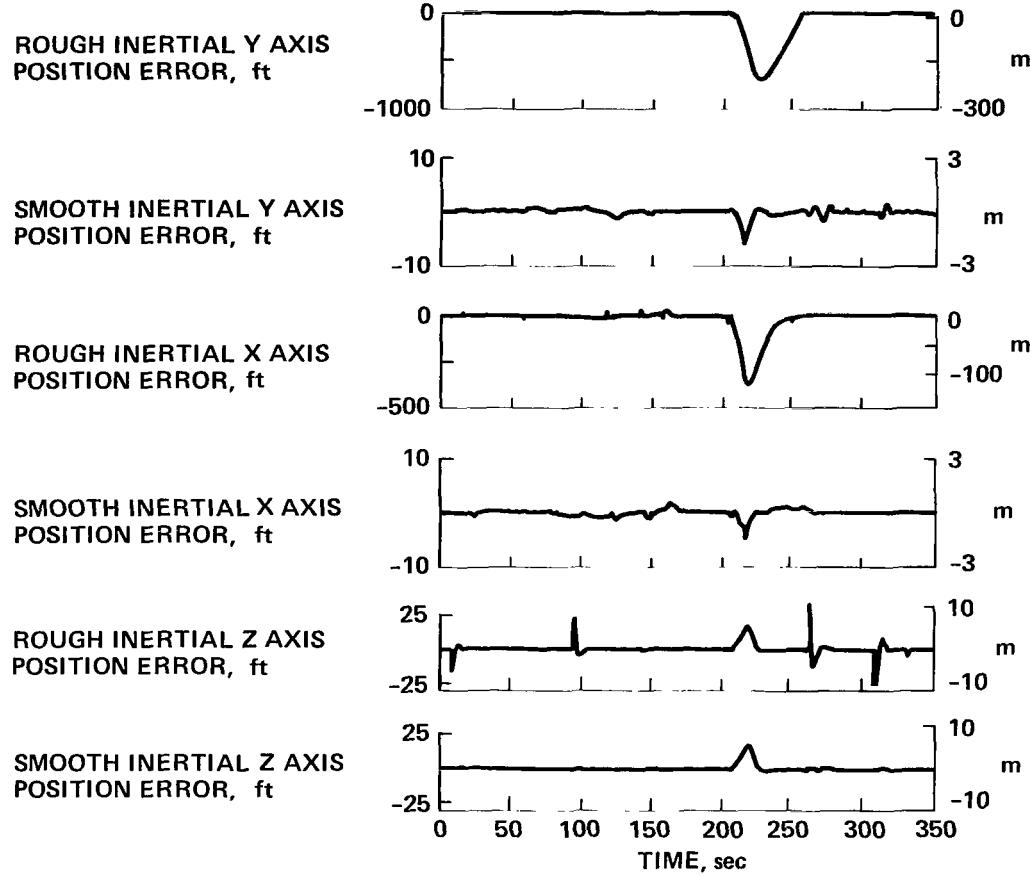
(e) Position errors.

Figure 9.- Closed-course trajectory - Continued.

75

INERTIAL Y AXIS POSITION

INERTIAL X AXIS POSITION

PARTIAL GROUND TRACK — COMMANDED AND EXECUTED
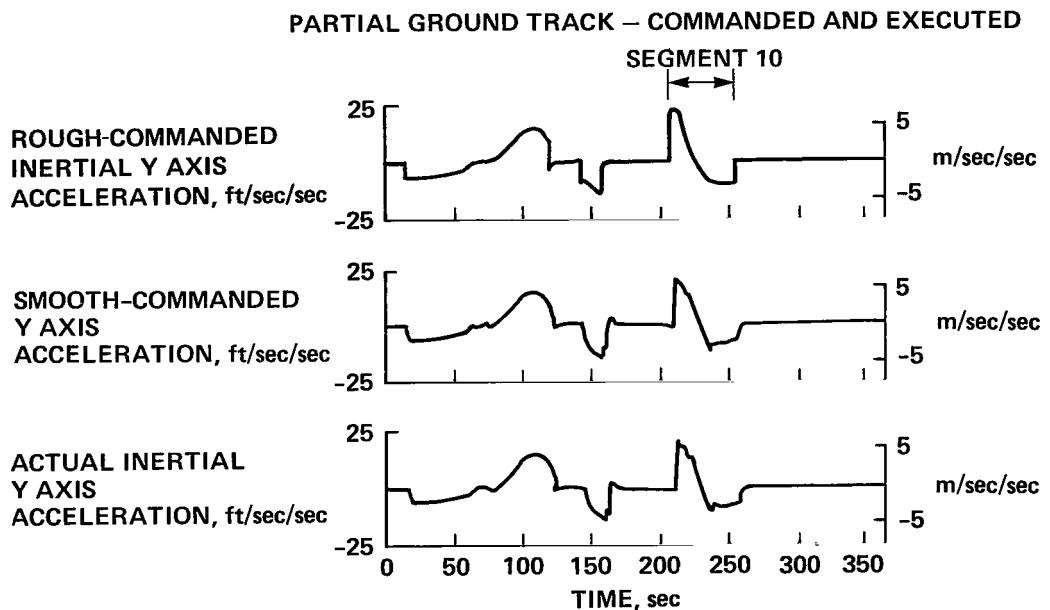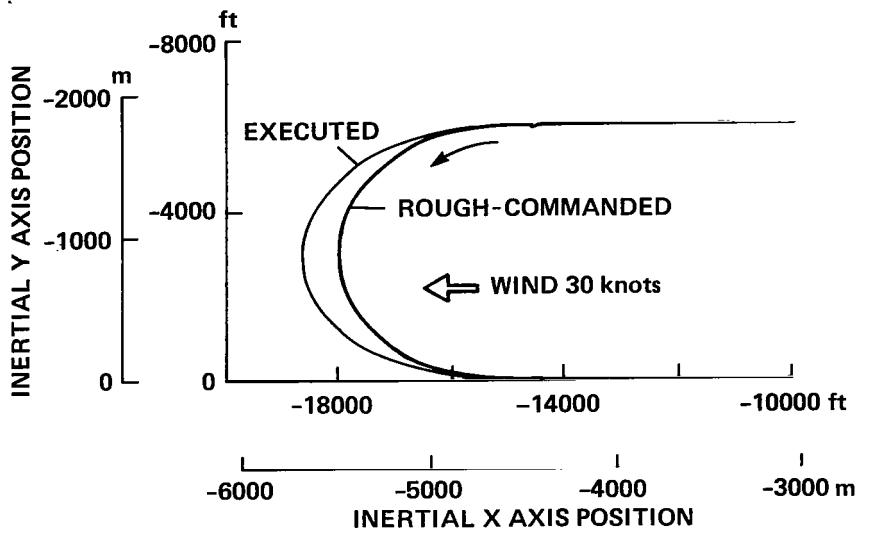
(f) Downwind turn details.

Figure 9.- Closed-course trajectory - Concluded.
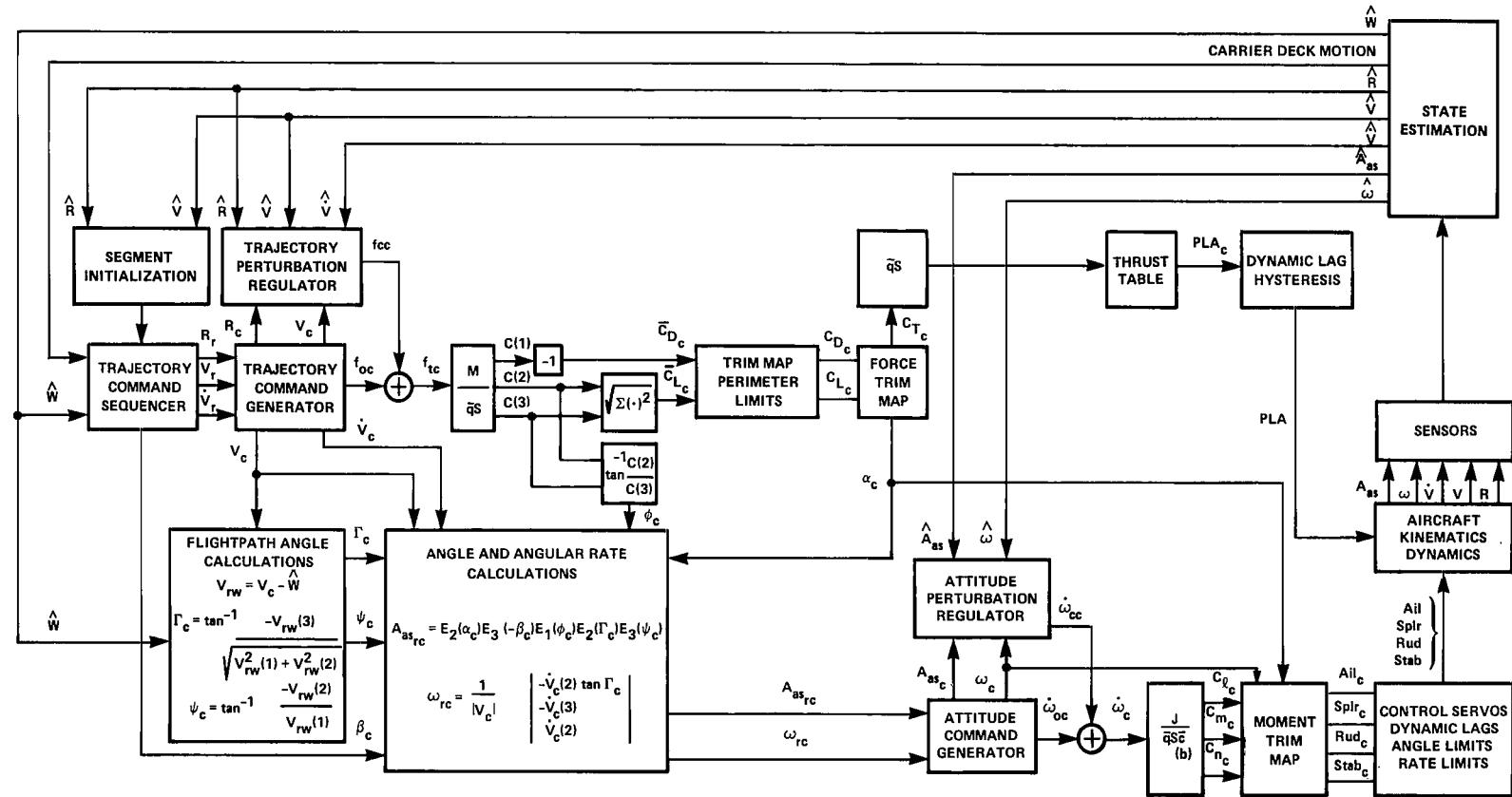
Figure 10.- TAFCOS simulation information flow.
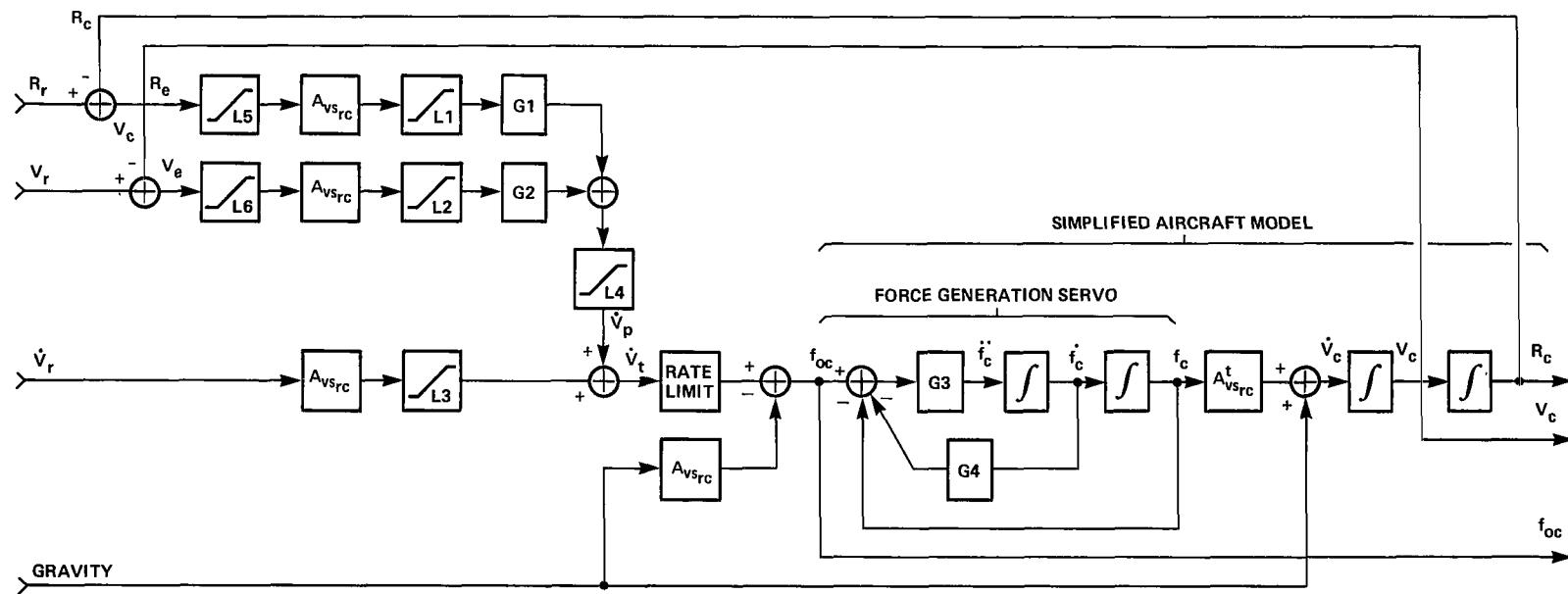
Figure 11.- Trajectory command generator conceptual diagram.
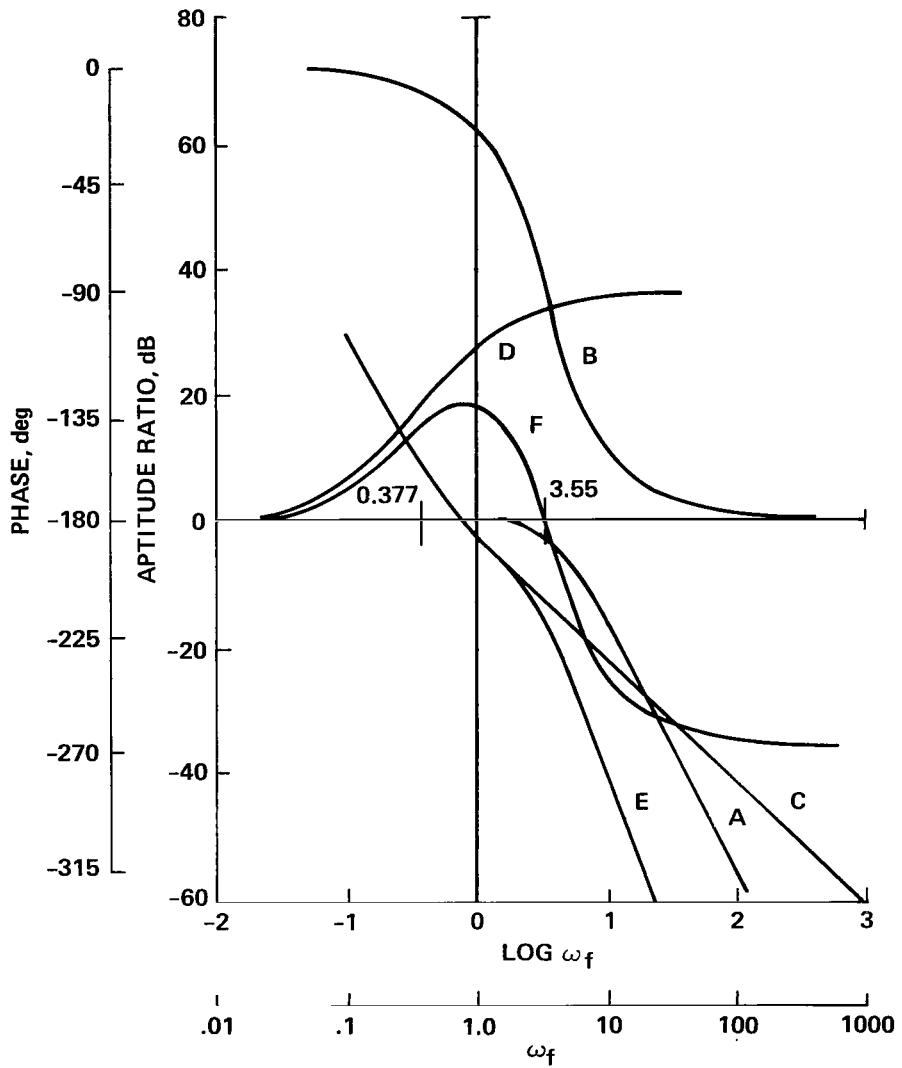
Figure 12.– Open-loop frequency response of trajectory-command-generator perturbation model.
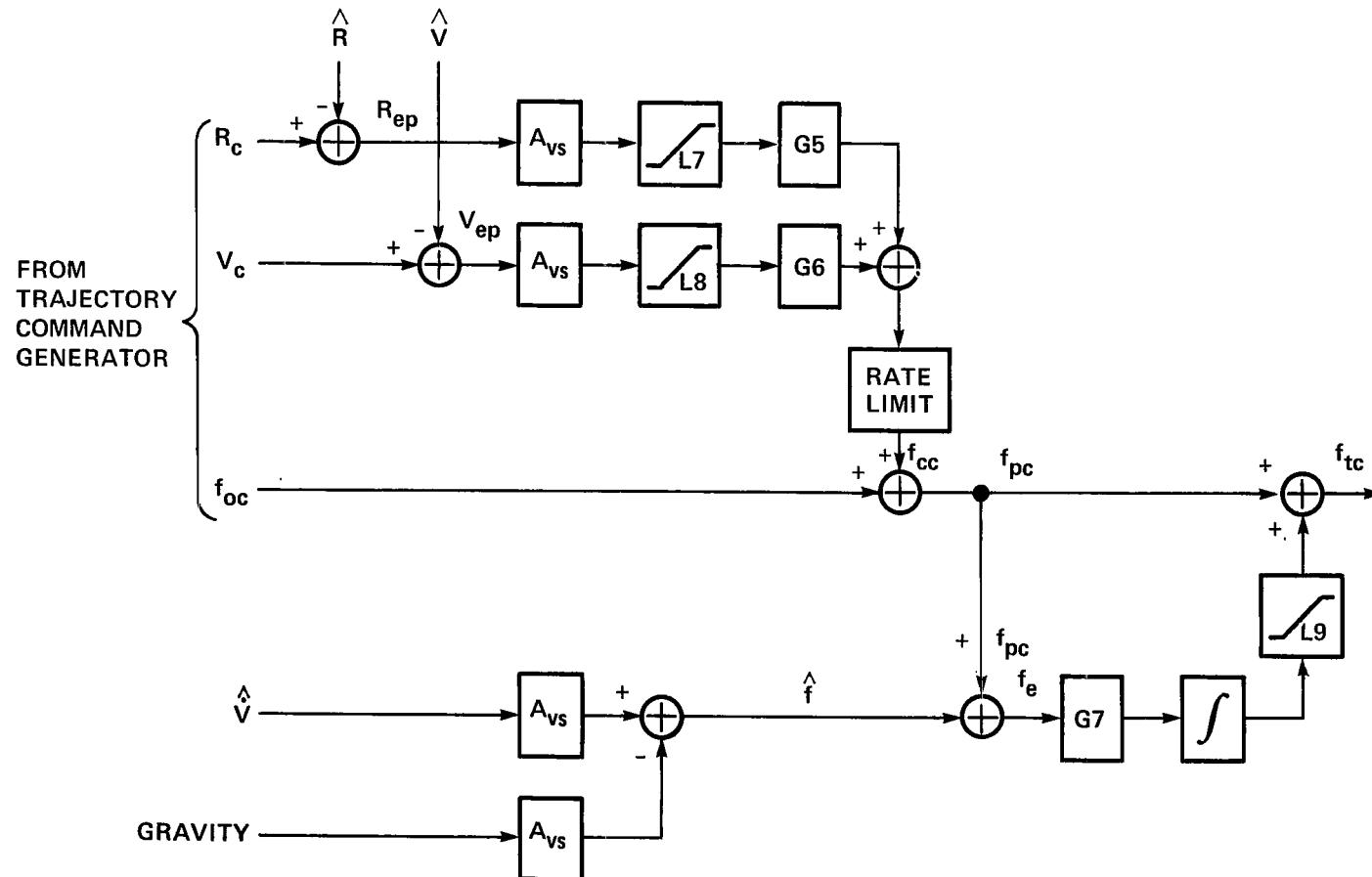
Figure 13.- Trajectory perturbation regulator
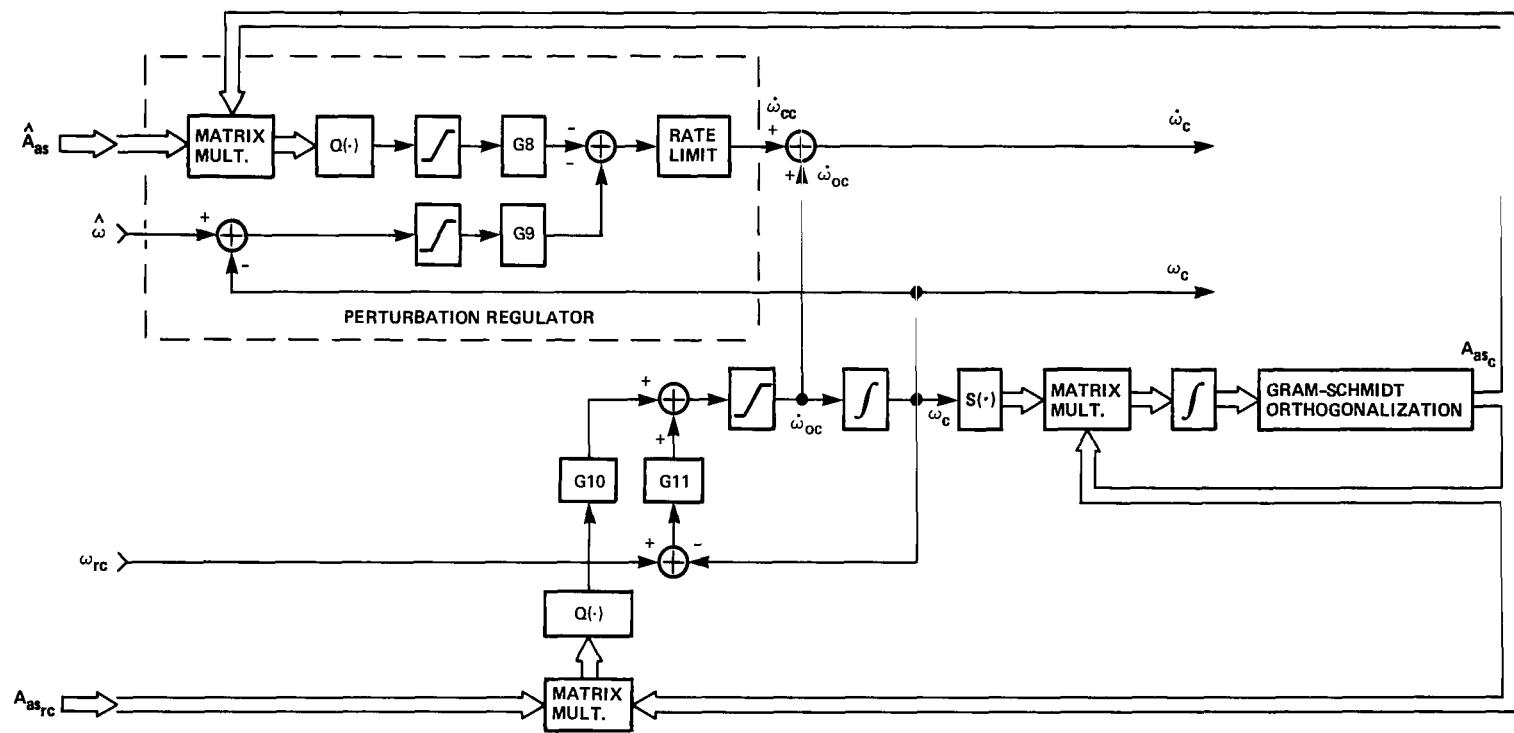
Figure 14.- Attitude command generator and perturbation regulator.
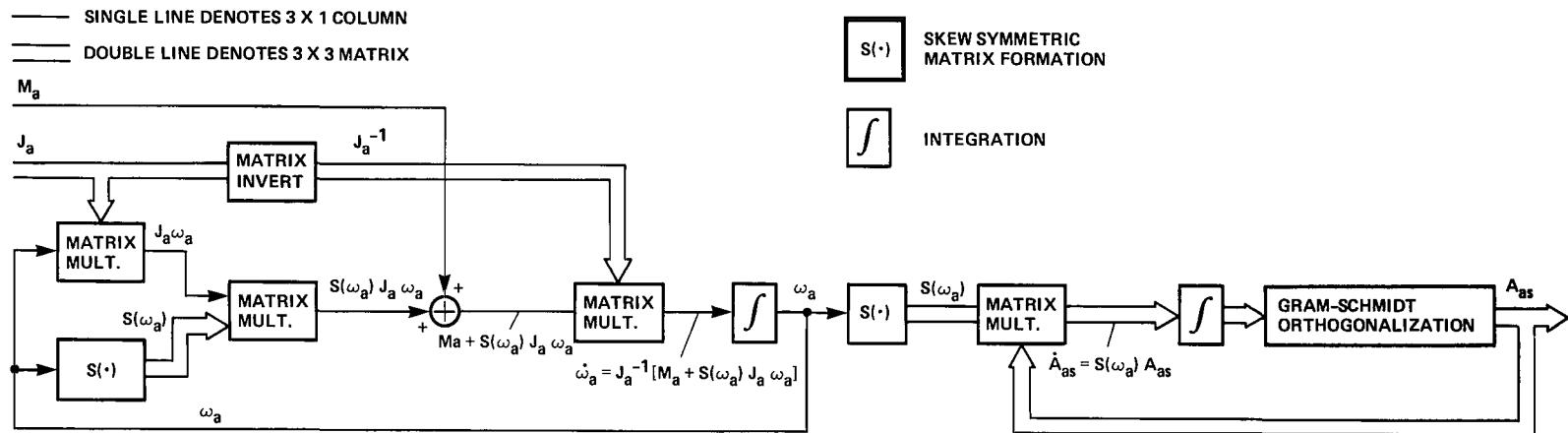
Figure 15.- Rotational dynamics in aircraft section of simulation.

1. Report No. NASA TP-1512	2. Government Accession No.	3. Recipient's Catalog No.
4. Title and Subtitle APPLICATION OF THE CONCEPT OF DYNAMIC TRIM CONTROL TO AUTOMATIC LANDING OF CARRIER AIRCRAFT		5. Report Date April 1980
		6. Performing Organization Code
7. Author(s) G. Allan Smith and George Meyer		8. Performing Organization Report No. A-7801
		10. Work Unit No. 505-11-41
9. Performing Organization Name and Address Ames Research Center, NASA Moffett Field, Calif. 94035		11. Contract or Grant No.
		13. Type of Report and Period Covered Technical Paper
12. Sponsoring Agency Name and Address National Aeronautics and Space Administration, Washington, D.C. 20546		14. Sponsoring Agency Code

15. Supplementary Notes

16. Abstract

The results of a simulation study of an alternative design concept for an automatic landing-control system are presented. The concept was applied on an A-7E aircraft approaching a Navy aircraft carrier.

In the alternative concept, the aircraft trajectory is directly controlled by commanding the aerodynamic and propulsive forces required rather than by a conventional autopilot that commands aircraft attitude to minimize trajectory errors. Furthermore, the dynamic trim concept allows a single configuration to function over the complete flight envelope without the gain scheduling or configuration switching that is employed in conventional systems based on perturbations about a number of different static trim points. The design concept is called a "total aircraft flight control system," or TAFCOS. TAFCOS is essentially an open-loop, feed-forward system that commands the proper instantaneous thrust, angle of attack, and roll angle to achieve the forces required to follow the desired trajectory. These dynamic trim conditions are determined by an inversion of the aircraft nonlinear force characteristics to calculate the required angle of attack, roll angle, and throttle setting.

An explanation of implementation details with an airborne digital computer is given. Results are presented that show two-to-one improvement in touchdown point dispersion over the presently operational automatic carrier-landing system. Further, results show excellent performance over the entire approach profile in the presence of severe gust disturbances.

17. Key Words (Suggested by Author(s)) Aircraft stability Control Autopilot	18. Distribution Statement Unclassified - Unlimited STAR Category — 08

19. Security Classif. (of this report) Unclassified	20. Security Classif. (of this page) Unclassified	21. No. of Pages 89	22. Price* $6.00

National Aeronautics and
Space Administration

Washington, D.C.
20546

THIRD-CLASS BULK RATE

U.S.MAIL

1   1 1U, A,   022980 S00903DS
DEPT OF THE AIR FORCE
AF WEAPONS LABORATORY
ATTN: TECHNICAL LIBRARY (SUL)
KIRTLAND AFB NM 87117

NASA